

State Higher Vocational School
in Tarnów



Hochschule Wismar



Leibniz-Institute of Atmospheric Physics e.V. at University of Rostock



Diploma Thesis

Development of radar beam configurations for meteor experiments with the atmospheric sounding radar MAARSY

Author: Rafał Gancarz

Supervisors: Dr hab. inż. Krzysztof Oprzędkiewicz (SHVS Tarnów)
Prof. Dr.-Ing. habil. Andreas Ahrens (HS Wismar)
M. Sc.-Ing. Toralf Renkwitz (IAP Kühlungsborn)

Kühlungsborn, 18th June 2010

Development of radar beam configurations for meteor experiments with the atmospheric sounding radar MAARSY

Objective

Development and optimization of an antenna radiation pattern with a so called “donut beam” shape to be used for meteor observation experiments with a VHF radar system with phased array antenna.

Mission statement

MAARSY the Middle Atmosphere Alomar Radar System is built in 2009/2010 on the northern Norwegian island Andøya (69.30°N, 16.04°E) by the *Leibniz-Institute of Atmospheric Physics e.V. at University of Rostock (IAP)*. The new powerful VHF radar (53.5 MHz) with a phased-array antenna is designed for exploring the polar atmosphere in the altitude range from 2 to 110 km. The almost circular antenna array with a diameter of 90 m consists of 433 three-element Yagi antennas arranged in a equilateral triangular lattice structure. Any antenna is connected to a 2 kW transceiver whose phase can be set independently while transmitting and receiving. Furthermore, any transceiver’s output power and frequency is adjustable. This arrangement allows the formation of antenna radiation patterns with different beamwidth and beam shape for a variety of monitoring tasks in the middle atmosphere. The installation and commissioning of the system in a first stage of 217 transceiver modules is made in the spring of 2010.

For the initial and final stage of the system different radiation patterns have to be developed and optimized for the various radar sounding experiments in the middle atmosphere. An axially symmetric radiation pattern with maximum radiated power at a zenith distance of about 60° and a beamwidth of about 30° (a so called “donut beam”) has to be designed for the location of meteor trail echoes of meteoroids burning up at altitudes between 70 and about 110 km.

The antenna simulation program NEC4.1 is available as tool. The obtained optimal settings of the transmitter modules (phase, power) will be tested during the commissioning of the first phase in May 2010.

Contents

1	Introduction	10
1.1	Motivation.....	10
1.2	General information about meteor observations	12
1.3	Meteor observations with the use of VHF radars	14
2	Theoretical introduction	17
2.1	Yagi-Uda antenna.....	17
2.2	Basic equations.....	18
2.3	Radiation pattern	20
2.4	Radiation pattern lobes	23
2.5	Field regions.....	25
2.6	Impedance	26
2.7	Bandwidth.....	27
2.8	Efficiency, Gain and Effective aperture (effective area).....	29
2.9	Numerical Electromagnetic Code (NEC).....	30
2.10	Phased array	31
3	Array studies	36
3.1	64-antennas array.....	36
3.2	MAARSY array – 4 rings	40
3.3	MAARSY array – groups	43
3.4	MAARSY array – 12 slices.....	46
3.5	MAARSY array – 18 slices.....	50
3.6	MAARSY array – 168 antennas, the actual state of the MAARSY radar	51
4	Summary	53
	References	55
	Appendix	56
	Declaration of Authorship	82

List of figures

1.1	Mean temperature structure of the Earth's atmosphere from a climatological model (CIRA86) for summer and winter solstice conditions at 70° N.....	11
1.2	Angular distribution of meteors on the date of 17 th of May 2010.	12
1.3	Meteor flux – 17.05.2010.....	13
1.4	Picture of the MAARSY array on Andøya/Norway.	15
1.5	Cross section of radiation pattern of the MAARSY array, with the main beam directed to $\theta=0^\circ$	15
1.6	Location of antennas groups and single antennas in the MAARSY array.....	16
2.1	Yagi antenna applied in the MAARSY array.....	17
2.2	Coordinate system.	18
2.3	Three-dimensional radiation pattern of a 3-element folded-dipole Yagi antenna used in the MAARSY array.	21
2.4	Cross sections of the radiation pattern for a 3-element folded-dipole Yagi antenna used in the MAARSY array.	22
2.5	Radiation pattern lobes.	23
2.6	Grating lobes.	24
2.7	Antenna array of 9 x 3-el Yagi on a squared grid structure with a spacing of 3.5λ and the cross section of the radiation pattern of this structure.	24
2.8	Field regions.....	26
2.9	Input impedance of the three-element folded-dipole Yagi antenna used in the MAARSY array.....	27
2.10	Bandwidth of 3-element folded-dipole YAGI antenna operating at frequency of 53.5MHz, used in the MAARSY array.....	28
2.11	Squared 9-antennas array structure.....	32
2.12	Two-dimensional plots of radiation pattern for the squared 9-antennas array structure as a function of a zenith angle.....	32
2.13	Top views of radiation patterns for the squared 9-antennas array structure, for a beam tilted to $\theta=0^\circ$ and tilted to $\theta=20^\circ$	33
2.14	Equilateral 9-antennas array structure.	33
2.15	Two-dimensional plots of the radiation pattern of the equilateral 9-antennas array structure as a function of a zenith angle.....	34
2.16	Top views of radiation patterns for the equilateral 9-antennas array structure, for a beam tilted to $\theta=0^\circ$ and tilted to $\theta=20^\circ$	35

3.1	64-antennas star structure – example 1	36
3.2	Top view of the radiation pattern of the 64-antenna star structure – example 1	37
3.3	64-antennas star structure – example 2	38
3.4	Top view of the radiation pattern of the 64-antenna star structure – example 2	39
3.5	Positions of the 433 Yagi antennas within the MAARSY array	40
3.6	MAARSY array divided into four rings	40
3.7	Top views of radiation patterns for five ways of the antenna excitations for the 4- <i>rings</i> MAARSY array	42
3.8	MAARSY array divided into 18 main groups consisting of 21 antennas each	43
3.9	MAARSY array with <i>green, orange</i> and <i>red</i> groups of selected antennas	44
3.10	Radiation patterns for 2 instances of excitation for models shown in figure 3.9 (a, b).....	44
3.11	MAARSY array with the outer ring fed.....	45
3.12	Radiation patterns for models shown in figure 3.11	46
3.13	MAARSY array divided into 12 slices with the same value of a zenith angle for every used antenna.....	47
3.14	Radiation patterns for the array structures shown in figure 3.13, for $\theta=30^\circ$	48
3.15	MAARSY array divided into 12 slices with two different values of zenith angle	49
3.16	Radiation patterns for the structures shown in figure 3.15 for different values of zenith angle	49
3.17	MAARSY array divided into 18 slices and its radiation pattern.....	50
3.18	MAARSY array - 168 out of 433 antennas.....	51
3.19	MAARSY array - 107 out of 168 antennas used.....	52
3.20	Radiation patterns for the structures shown in figure 3.19.....	52
A.1	Cross section plots for a 64-antenna star structure – antennas aligned perpendicular to arms.....	56
A.2	Cross section plots for a 64-antenna star structure – example 2a (feeding with equal phasing in each arm).....	57
A.3	Cross section plots for a 64-antenna star structure – example 2b (feeding with different phasing in each arm).....	58
A.4	Cross section plots for the radiation pattern for the MAARSY array divided into groups and 426 antennas selected – example 1	59
A.5	Cross section plots for the radiation pattern for the MAARSY array divided into groups and 426 antennas selected – example 2.....	60

A.6	Cross section plots for the radiation pattern for the MAARSY array divided into groups and 252 antennas selected.....	61
A.7	Cross section plots for the radiation pattern the MAARSY array divided into groups and 300 antennas selected.....	62
A.8	Cross section plots for the radiation pattern the MAARSY array divided into 12 slices and 426 antennas selected.....	63
A.9	Cross section plots for the radiation pattern the MAARSY array divided into 12 slices and 384 antennas selected.....	64
A.10	Cross section plots for the radiation pattern the MAARSY array divided into 12 slices and 312 antennas selected.....	65
A.11	Cross section plots for the radiation pattern the MAARSY array divided into 12 slices and 234 antennas selected.....	66
A.12	Cross section plots for the radiation pattern the MAARSY array divided into 12 slices and 2 values of a zenith angle in each slice applied – instance 1.....	67
A.13	Cross section plots for the radiation pattern the MAARSY array divided into 12 slices and 2 values of a zenith angle in each slice applied – instance 2.....	68
A.14	Cross section plots for the radiation pattern for the actual state of the MAARSY radar with 6 main beams generated	69
A.15	Cross section plots for the radiation pattern for the actual state of the MAARSY radar with 9 main beams generated	70

List of tables

2.1	Antennas excitations for a squared 9-antennas array, for a beam tilted to $\theta=0^\circ$ and tilted to $\theta=20^\circ$	33
2.2	Antennas excitations for an equilateral 9-antennas array, for a beam tilted to $\theta=0^\circ$ and tilted to $\theta=20^\circ$	34
3.1	64-antennas feeding – example 1.....	37
3.2	64-antennas feeding – example 2 a (the same phases in each arm).....	38
3.3	64-antennas feeding – example 2 b (different phases in each arm, reference arm (arm 1) is the one for value of $y=0$ and for negative x -values).....	39
3.4	Different configurations of feeding the <i>4-rings</i> MAARSY array.....	41
A.1	Zenith (θ) and azimuth (ϕ) angles for the structure shown in figure 3.6 – configuration 1.....	71
A.2	Zenith (θ) and azimuth (ϕ) angles for the array consisting of 426 antennas for the generation of 12 beams – example 1.....	72
A.3	Zenith (θ) and azimuth (ϕ) angles for the array consisting of 252 antennas for the generation of 12 beams.....	73
A.4	Zenith (θ) and azimuth (ϕ) angles for the array consisting of 300 antennas for the generation of 12 beams.....	73
A.5	Zenith (θ) and azimuth (ϕ) angles for the MAARSY array divided into 12 slices and 426 antennas selected.....	74
A.6	Zenith (θ) and azimuth (ϕ) angles for the MAARSY array divided into 12 slices and 384 antennas selected.....	75
A.7	Zenith (θ) and azimuth (ϕ) angles for the MAARSY array divided into 12 slices and 312 antennas selected.....	76
A.8	Zenith (θ) and azimuth (ϕ) angles for the MAARSY array divided into 12 slices and 234 antennas selected.....	77
A.9	Zenith (θ) and azimuth (ϕ) angles for the MAARSY array divided into 12 slices and 2 values of a zenith angle ($\theta_{\text{inner}}=20^\circ$, $\theta_{\text{outer}}=30^\circ$) in each slice applied.....	78
A.10	Zenith (θ) and azimuth (ϕ) angles for the MAARSY array divided into 12 slices and 2 values of a zenith angle ($\theta_{\text{inner}}=25^\circ$, $\theta_{\text{outer}}=35^\circ$) in each slice applied.....	79
A.11	Zenith (θ) and azimuth (ϕ) angles for the actual state of the MAARSY radar with 6 main beams generated.....	80
A.12	Zenith (θ) and azimuth (ϕ) angles for the actual state of the MAARSY radar with 9 main beams generated.....	80

List of symbols

Γ	reflection coefficient
λ	wavelength
ϕ	azimuth angle
θ	zenith angle
θ_3	half-power beamwidth
$\Phi(\theta, \phi)$	radiation intensity
η	radiation efficiency
η_a	aperture efficiency of the antenna
a	spacing of array element in direction of column
A	physical area of antenna's aperture
b	spacing of array element in direction of row
$A_e(\theta, \phi)$	effective area
D	the largest antenna dimension
D_{max}	maximum directivity for a planar aperture
$D(\theta, \phi)$	antenna directivity
$G(\theta, \phi)$	gain
P	power available to the antenna receiver
P_o	power accepted by antenna
P_r	power radiated by antenna
$P(\theta, \phi)$	power density
pos_c	position of element in column
pos_r	position of element in row
r	radius
V_{max}	maximum voltage measured at the feed point of an antenna
V_{min}	minimum voltage measured at the feed point of an antenna
W	power density of a plane wave
Z_l	impedance of the feeder toward the load
Z_s	impedance of the feeder toward the source

List of abbreviations

ALWIN	Alomar WIND radar
AMP	Antenna Modeling Program
CIRA86	COSPAR international reference atmosphere 1986
HPBW	Half-Power BeamWidth
IAP	Leibniz-Institute of Atmospheric Physics e.V. at University of Rostock
LIDAR	Light Detection and Ranging
MAARSY	Middle Atmosphere Alomar Radar System
MLT	Mesosphere Lower Thermosphere
MoM	Method of Moments (NEC)
MST	Mesosphere Stratosphere Troposphere
NEC	Numerical Electromagnetic Code
PMSE	Polar Mesosphere Summer Echoes
VHF	Very High Frequency
VSWR	Voltage Standing Wave Ratio

Chapter 1

Introduction

This chapter presents motivation for this thesis. It also includes a brief overview about meteor observations and basic information about the Middle Atmosphere Alomar Radar System (MAARSY).

In chapter 2 an introduction to the antenna theory is presented. Historical and principle facts relating the Yagi-Uda antenna are also included. In this part of the thesis, the general equations and plots are shown, which shall help to understand the functionality of antennas. Additionally chapter 2 gives an introduction for the Numerical Electromagnetic Code (NEC) and it contains a brief overview of the theory of phased antenna arrays with some examples.

Within chapter 3 various antenna array structures are presented and discussed. The first example is a small structure consisting of 64 antennas which are arranged in a star configuration. However the main focus in this section is put on the 433 antennas MAARSY array, where several different configurations are studied.

A summary is given in chapter 4, where the previously studied antenna array configurations are compared.

Additional antenna radiation patterns and phasing tables discussed in chapter 3 are presented in the appendix.

1.1 Motivation

This thesis contains potential improvements to an atmospheric radar system operated by the *Leibniz-Institute of Atmospheric Physics e.V. at University of Rostock (IAP)*. The atmosphere itself has a rather complex structure. The figure 1.1 shows the mean temperature structure of the Earth's atmosphere at 70° N and it is taken from [Sch07]. To understand the processes in the atmosphere in-situ measurements of parameters like temperature, pressure, composition and wind are important. In the altitudes higher than 40 km measurements can be performed by satellites, radars, lidars or rockets. This work will focus on the extension of the MAARSY radar to a meteor observation mode.

The objective of the meteor trail observations is the determination of wind fields. To classify the wind fields correctly, the beam generated by these meteor radars have to be broad, because meteors seams to arrive from different directions in the sky. The (IAP) studies the middle part of the atmosphere in the altitude range from 10 km to 100 km. The least understanding of the atmosphere is the MLT-region (Mesosphere Lower Thermosphere) which is located between

the altitude of 70 km and 100 km. In this region most of meteors start to ablate and create an ionized ambipolar plasma trails. This plasma trails can be detected by radars like the MAARSY. The MAARSY radar is operating at frequency of 53.5 MHz and it is located on the Norwegian island Andøya. This is the most advanced and powerful MST radar in the Europe. The new radar is characterized by a minimum half-power beamwidth of 3.6° and the maximum gain of 33.5 dB. More accurate descriptions of the MAARSY radar can be found in section 1.3. The main objective of this thesis is generating a radiation pattern with beamwidth of approximately 30 degrees and maximum power for the MAARSY radar. Figure 1.2 shows the angular distribution of selected meteors on the date of 17th of May 2010. Red circle in the center is the minimal beamwidth of the MAARSY radar when the main lobe is pointed directly to the zenith. The area between the two green circles is the beamwidth with should be achieved to observe the meteor trails effectively. It can be seen that with a beamwidth of 3.6° only a few meteors can be detected. Efforts of generating the radiation pattern with the beamwidth of approximately 30° and power radiated up to off-zenith angle of about 60° (“donut beam”) are discussed in the chapter 3.

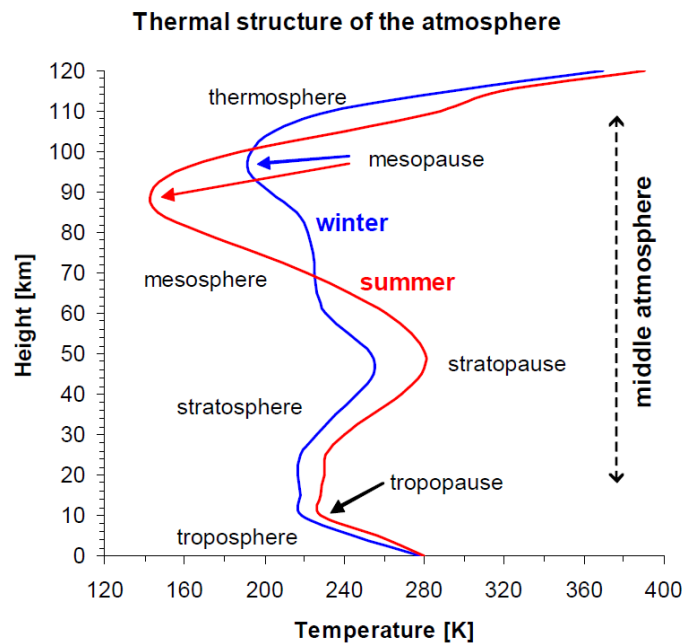


Figure 1.1. Mean temperature structure of the Earth’s atmosphere from a climatological model (CIRA86) for summer and winter solstice conditions at 70° N.

Other IAPs radars located on the Norwegian island Andøya are the Saura-MF radar and the Meteorradar (SKiYMET). Saura-MF is a narrow beam radar operating at frequency of 3.17 MHz. It was installed in July 2002. The half power beamwidth (HPBW) of the Saura-MF radar is 6.4 degree, its peak power is 116 kW and the range of height for atmospheric observations is between 50 and 94 km. The meteorradar (SKiYMET) is almost in continuous operation since

October 2001. The SKiYMET system consists of a one antenna for transmission and 5 interferometer antennas for reception arranged in the form of an asymmetric cross, with arms of

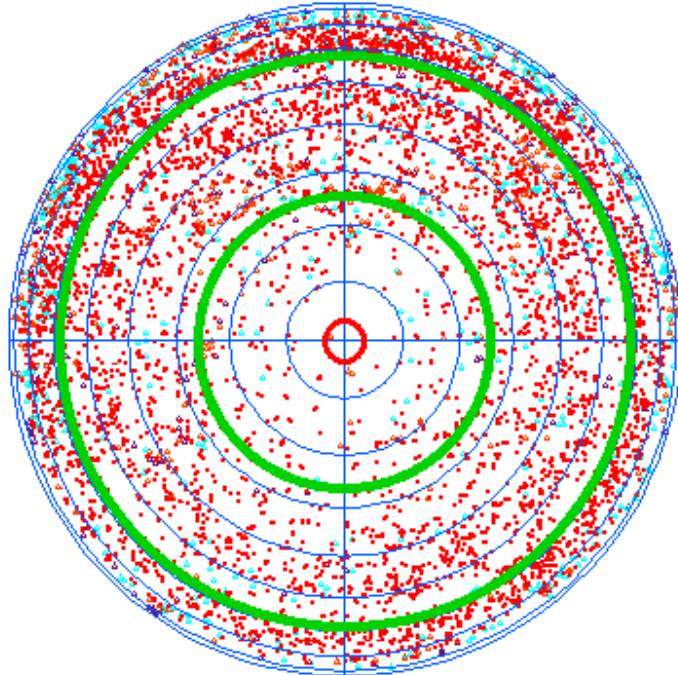


Figure 1.2. Angular distribution of meteors on the date of 17th of May 2010.

lengths of either 2 wavelengths or 2.5 wavelengths. This radar is operating at the frequency of 32.55 MHz and the output power has been at least 12 kW. Data obtained from the use of the meteor radar are the radial plasma drift, the decay time of the rapidly diffusion trails and an accurate determination of the trail in the sky. The radial wind drift speeds are used to derive the wind field and the decay time is suitable to estimate the temperature at 90 km altitude. The intention is to use also the MAARSY radar for meteor trail observations as it is operating at a different frequency than the SKiYMET radar.

1.2. General information about meteor observations

In the history of meteor studies, purposes of meteor trail observations were to get information about the meteors and about the atmosphere in which they burn up. In the 1980s and 1990s, the technique was poor comparably to nowadays. Furthermore the photographic film or old and slow computers with primitive algorithms were used, what often brought wrong results. Today very fast computers with large memory resources are used and meteor observations give more reliable results. Examinations which took hours in the past, can now be done almost immediately. New algorithms are now much more advanced and allow to detect real meteors

and reject signals, which are not coming from meteor trails and were false detected in the past.

The parameters which describe meteors and their plasma trails are:

- location of the meteor in the sky
- speed of the meteor entering to the atmosphere
- decay time of the plasma
- radial drift velocity

Another important parameters:

Meteor flux – it is one of the most easy parameter to measure. The method of measuring relies on counting the occurrences of meteors. After that process it is necessary to make certain adjustment to prepare the results for astronomy purposes. Usually the number of meteors observed each day is between 6000 and 18000, depending on time of a year. This number can be much bigger during meteor-shower. Figure 1.3 shows the meteor flux observed on 17th of May 2010 and it is taken from *The Leibniz-Institute of Atmospheric Physics (IAP)* website.

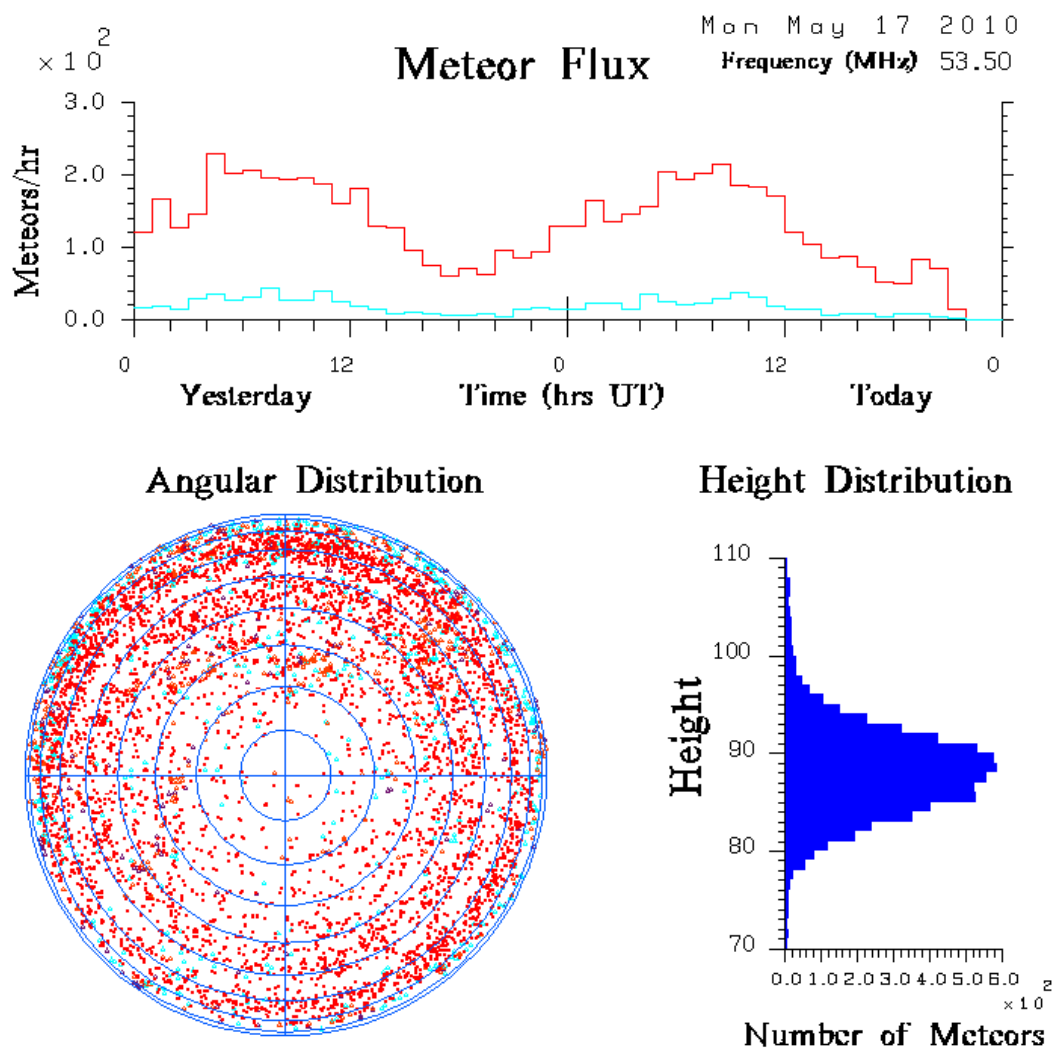


Figure 1.3. Meteor flux – 17.05.2010.

Upper middle-atmosphere winds – this is one of the most important parameters of radio-meteor research. To obtain it, it is necessary to measure the radial velocities of all detected meteors and combining them in all-sky manner.

Radiant location – meteors may come from different locations in the sky. The transmitted radar signal is scattered at the plasma trail produced by meteors during their entering into the atmosphere. This trail is perpendicular to the vector of the radar, which is pointing to the trail. It can be said then, that there is a circle in the sky and the radar is its center. Thus, the radiant has to be somewhere on the another circle, which is aligned perpendicularly to the vector from the radar. If more meteors will be considered like that, there will be circle of possible radiant for each of them. All those circles can be plotted in a celestial coordinates. If meteors were entering the atmosphere from a single source, than their circles cross at some point, which is considered as the radiant source.

Meteor entrance speed – speed of entering the meteor into the atmosphere is usually between 10 and $72 \frac{km}{s}$.

1.3. Meteor observations with the use of VHF radars

The *Leibniz-Institute of Atmospheric Physics e.V. at University of Rostock* (IAP) is installing a new powerful VHF radar (Figure 1.4) on the North-Norwegian island Andøya in 2009/2010. The new radar is replacing the existing ALWIN radar, which has been exploited continuously for over 10 years.

The purpose of the new system is the research of horizontal structures of Polar Mesosphere Summer Echoes (PMSE) caused by mesospheric ice clouds. Three dimensional structures of wind fields and turbulent parameters determined from the radar data will be exploited to run precise comparison of detected PMSE distribution with wind and turbulence variations caused by wave activity.

MAARSY is a monostatic radar with an active phased array antenna. The radar is operating at the frequency of 53.5 MHz with the maximum output power of 800 kW. The system is assembled of an active phased array antenna projected by IAP, consisting of 433 Yagi antennas and same number of transceivers. The radar equipment was designed and produced by Genesis Software Pty Ltd. An almost circular array with a diameter of approximately 90m has a very symmetric radiation pattern with a maximum gain of 33.5 dBi and a half power beamwidth of approximately 3.6°. First side lobes are attenuated by 17 dB to the main lobe (Figure 1.5). The beam can be steered down to an off-zenith angle up to 30° without evaluating grating lobes, due to the equilateral triangle grid structure.



Figure 1.4. Picture of the MAARSY array on Andøya/Norway.

The MAARSY array (Figure 1.6) consists of 61 subarrays, where 55 of them are identical hexagons created of 7 antennas each. Remaining 6 subarrays are located on the circumference of the array, giving an almost circular structure. Those 6 groups contain 8 antennas each.

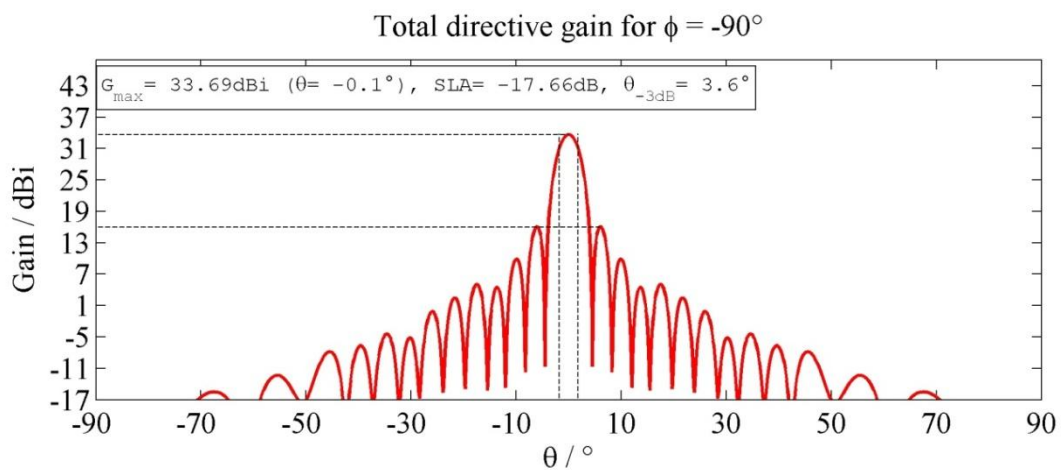


Figure 1.5. Cross section of radiation pattern of the MAARSY array, with the main beam directed to $\theta=0^\circ$.

The installation of the antenna array, situation and connection cables between each of the 433 antennas and the 6 containers with transceivers and all connections between containers and the radar control house was completed in August 2009. It is planned to observe the 2011 PMSE season with full power, after finalizing MAARSY extension in spring 2011. [LSRR10].

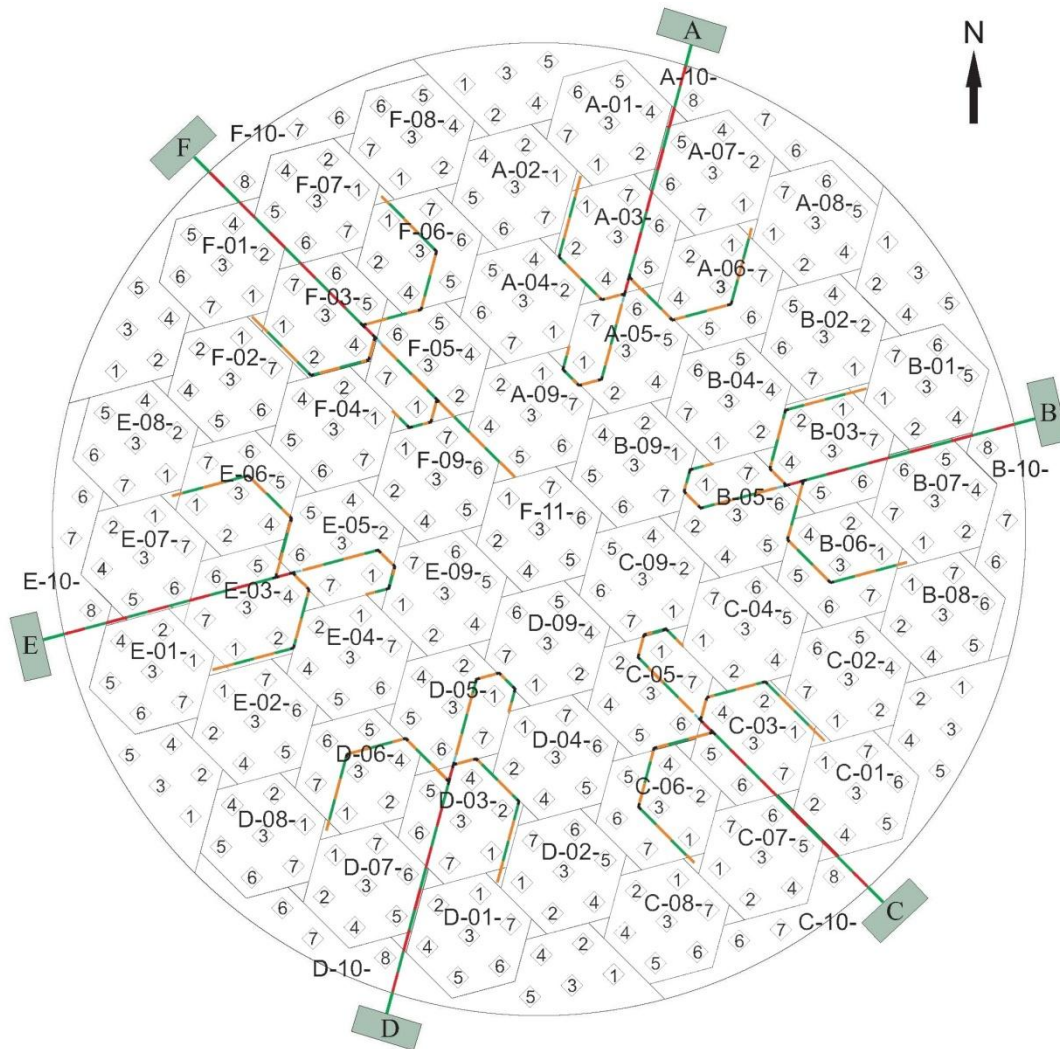


Figure 1.6. Location of antennas groups and single antennas in the MAARSY array.

Chapter 2

Theoretical introduction

2.1. Yagi-Uda Antenna

In the twenties of the twentieth century Shintaro Uda, professor at the Royal University of Tohoku developed in collaboration with engineer Hidetsugu Yagi, an employee of the university, a new type of directional antenna called the wave channel. Although the main originator and the designer of the antenna was Professor Uda, Yagi Hidetsugu, who spoke English language, published information about this invention in the Western press in 1928. Therefore it was his name combined to this type of antenna.

In February 1926 the antenna was patented in Japan and the U.S. patent was issued in May 1932. Yagi-Uda antennas were widely used in amateur and commercial communications, digital communications, television and radio .

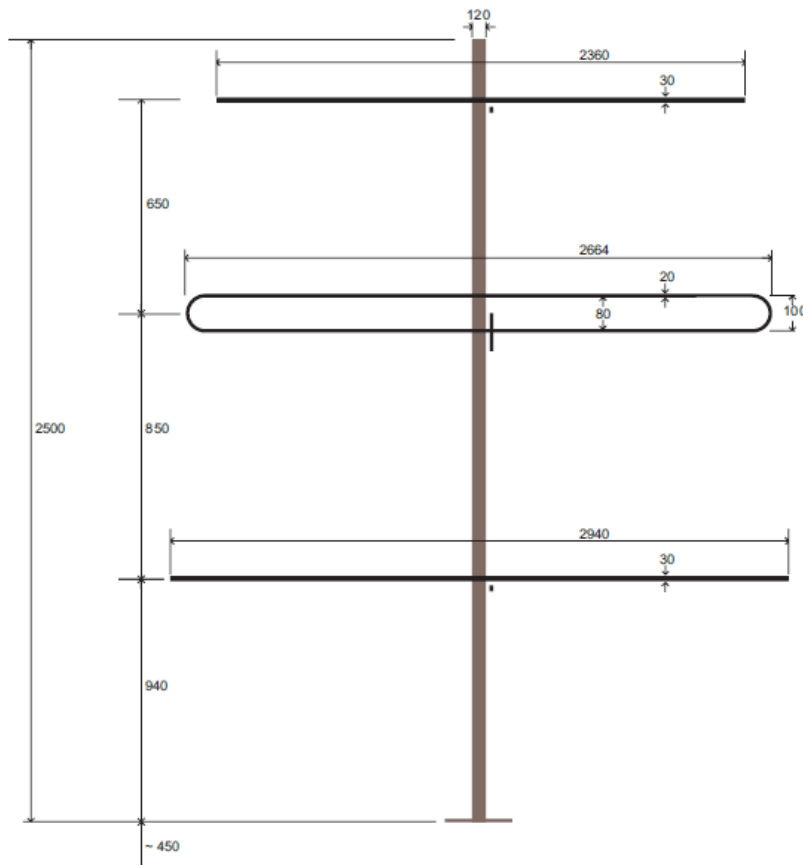


Figure 2.1. Yagi antenna applied in the MAARSY array.

A Yagi-Uda antenna is generally composed of many elements, has the directional and polarization characteristics consistent with the settings of its components (horizontal or vertical). The antenna consists of a single 'feed' or 'driven' element, typically a dipole or a folded dipole with a length of approximately half wavelength. The other antenna elements are not connected, so they are called passive elements. The most simple Yagi structure consists of 2 elements, a dipole and a reflector. In case, the antenna is actively used for transmitting, the elements along the path of main propagation are shorter than the length of the dipole and are called directors. The elements opposite to the directors are longer than the dipole and called reflectors. The number of directors affects the directionality and the energy gain of the antenna (the more directors, the greater the profit and greater directionality, while the beam gets narrower).

The first use of Yagi antennas took place during the II World War in devices such as radar installed on aircrafts [Bem73], [SMO⁺06].

These antennas typically operate in the HF to UHF bands (about 3 MHz to 3 GHz), although their bandwidth is typically small, on the order of a few percent of the center frequency. The Yagi antennas can be seen often, as they have been placed on top of the roofs for instance as a radio or television reception. Yagi antenna applied in the MAARSY array is shown in figure 2.1.

2.2. Basic equations

The antenna is located at the origin of the coordinate system, which is shown in figure 2.2.

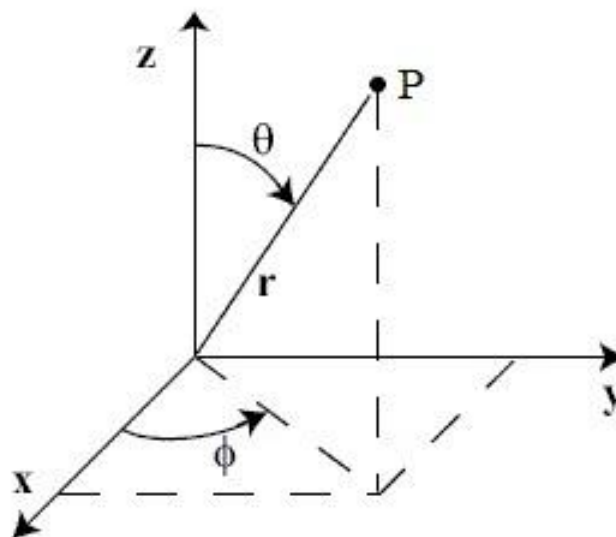


Figure 2.2. Coordinate system.

Assume the considered antenna is transmitting and:

P_o – power accepted by antenna (watts)

P_r – power radiated by antenna (watts)

η – radiation efficiency

r – radius

then:

$$\eta = \frac{P_r}{P_o} \quad (2.1)$$

The total power radiated from the antenna is given by:

$$P_r = \int_0^{2\pi} \int_0^\pi \Phi(\theta, \phi) \sin\theta d\theta d\phi \quad (2.2)$$

where:

$\Phi(\theta, \phi)$ – radiation intensity

The average radiation intensity is:

$$\Phi_{avg} = \frac{P_r}{4\pi} \quad (2.3)$$

Antenna directivity $D(\theta, \phi)$ define ability of an antenna to concentrate its radiated power to specified direction and it is given by:

$$D(\theta, \phi) = \frac{\Phi(\theta, \phi)}{\Phi_{avg}} = \frac{\Phi(\theta, \phi)}{\frac{P_r}{4\pi}} \quad (2.4)$$

The gain of antenna $G(\theta, \phi)$ is related to previous parameters and it appears as:

$$G(\theta, \phi) = \eta D(\theta, \phi) = \frac{\eta \Phi(\theta, \phi)}{\frac{P_r}{4\pi}} \quad (2.5)$$

what results with equation 2.1 to:

$$G(\theta, \phi) = \frac{\Phi(\theta, \phi)}{\frac{P_o}{4\pi}} \quad (2.6)$$

Another parameter called the power density $P(\theta, \phi)$ in $\frac{W}{m^2}$ is related to the radiation intensity as follows:

$$P(\theta, \phi) = \frac{\Phi(\theta, \phi) \Delta\theta \Delta\phi}{(r\Delta\theta)(r\Delta\phi)} = \frac{\Phi(\theta, \phi)}{r^2} \quad (2.7)$$

Result of substituting equation (2.6) to (2.7) is:

$$P(\theta, \phi) = G(\theta, \phi) \frac{P_o}{4\pi r^2} \quad (2.8)$$

An effective area $A_e(\theta, \phi)$ measured in m^2 is given as:

$$A_e(\theta, \phi) = \frac{\lambda^2}{4\pi} G(\theta, \phi) \quad (2.9)$$

When:

η_a —aperture efficiency of the antenna

A – physical area of antenna’s aperture (m²)

then:

$$\eta_a = \frac{A_e}{A} \quad (2.10)$$

Conclusion of the comparison of the equations 2.8 and 2.9 is:

$$G = \eta_a \frac{4\pi}{\lambda^2} A \quad (2.11)$$

Below, the dependence of the power radiated from a transmitting antenna and the power absorbed by the receiving antenna is considered. Both antennas are situated in the far field of each other. Receive power is then:

$$P_r = P A_e \quad (2.12)$$

and substituted with equation (2.8) and (2.9) gives:

$$P_r = \frac{G_t P_t}{4\pi r^2} \frac{\lambda^2 G_r}{4\pi} = \left(\frac{\lambda}{4\pi R} \right)^2 G_t G_r P_t \quad (2.13)$$

More information can be found in [Bal05], [Joh93], [Stu81], [Szo01], [Zie01].

2.3. Radiation pattern

The radiation pattern or antenna pattern describes the relative strength of the radiated field in various directions from the antenna, at a constant distance. The radiation pattern is equal for transmit and receive mode, since it also describes the receiving properties of the antenna. The radiation pattern is three-dimensional, but usually the measured radiation patterns are a two-dimensional slices of the three-dimensional pattern, in the horizontal or vertical planes. [Bal05], [Bem73], [Joh93], [RMOK82].

Figure 2.3 shows a 3-dimensional radiation pattern of a three-element folded-dipole Yagi antenna. The antenna in the picture 2.3 is aligned to azimuth angle $\phi=45^\circ$.

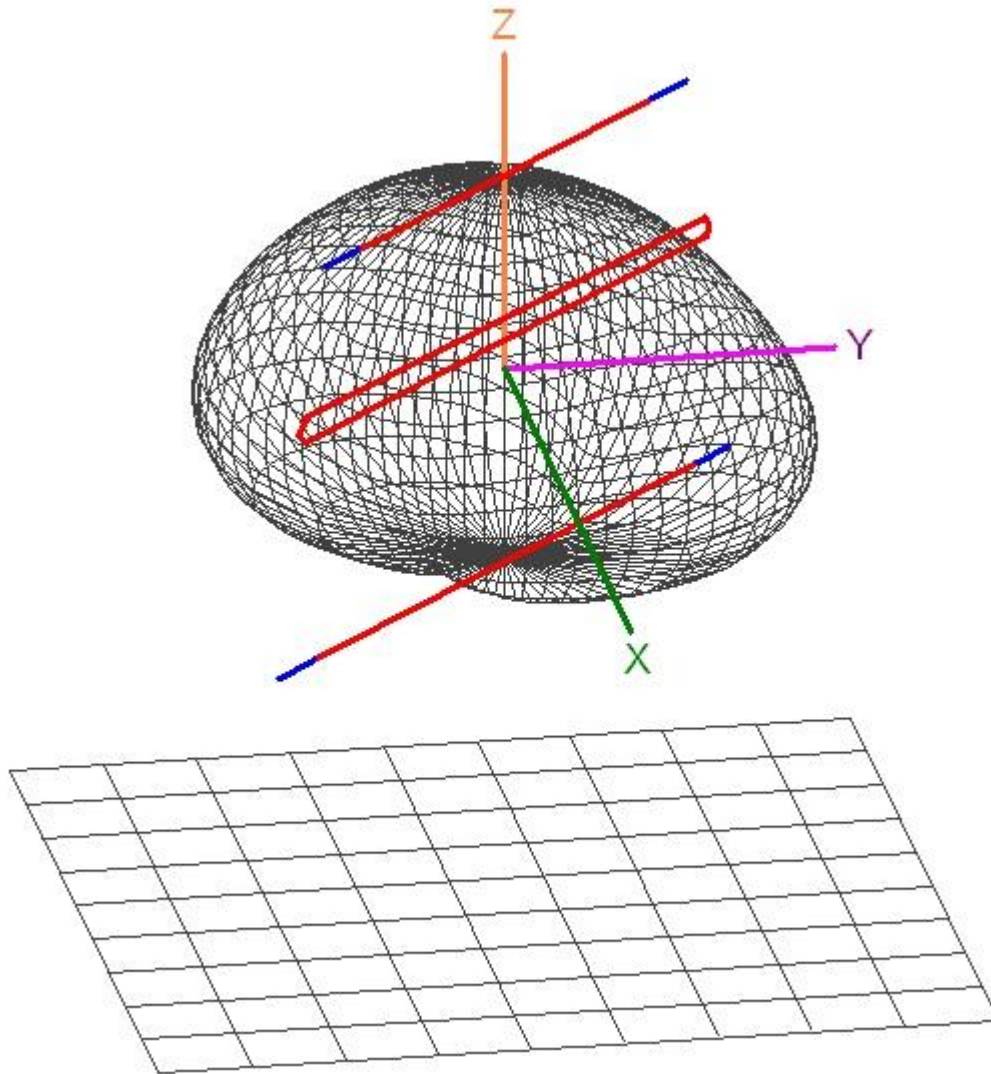


Figure 2.3. Three-dimensional radiation pattern of a 3-element folded-dipole Yagi antenna used in the MAARSY array.

For this antenna the maximum of the radiation pattern can be seen at a zenith angle of $\theta=0^\circ$. The half-power beamwidth for the azimuth angle $\phi=-45^\circ$ is 72 degrees and the HPBW for the azimuth angle $\phi=45^\circ$ is 145 degrees. These plots are useful for visualizing in which directions the antenna radiates. In the figure 2.4 the same radiation pattern as cross sections is shown.

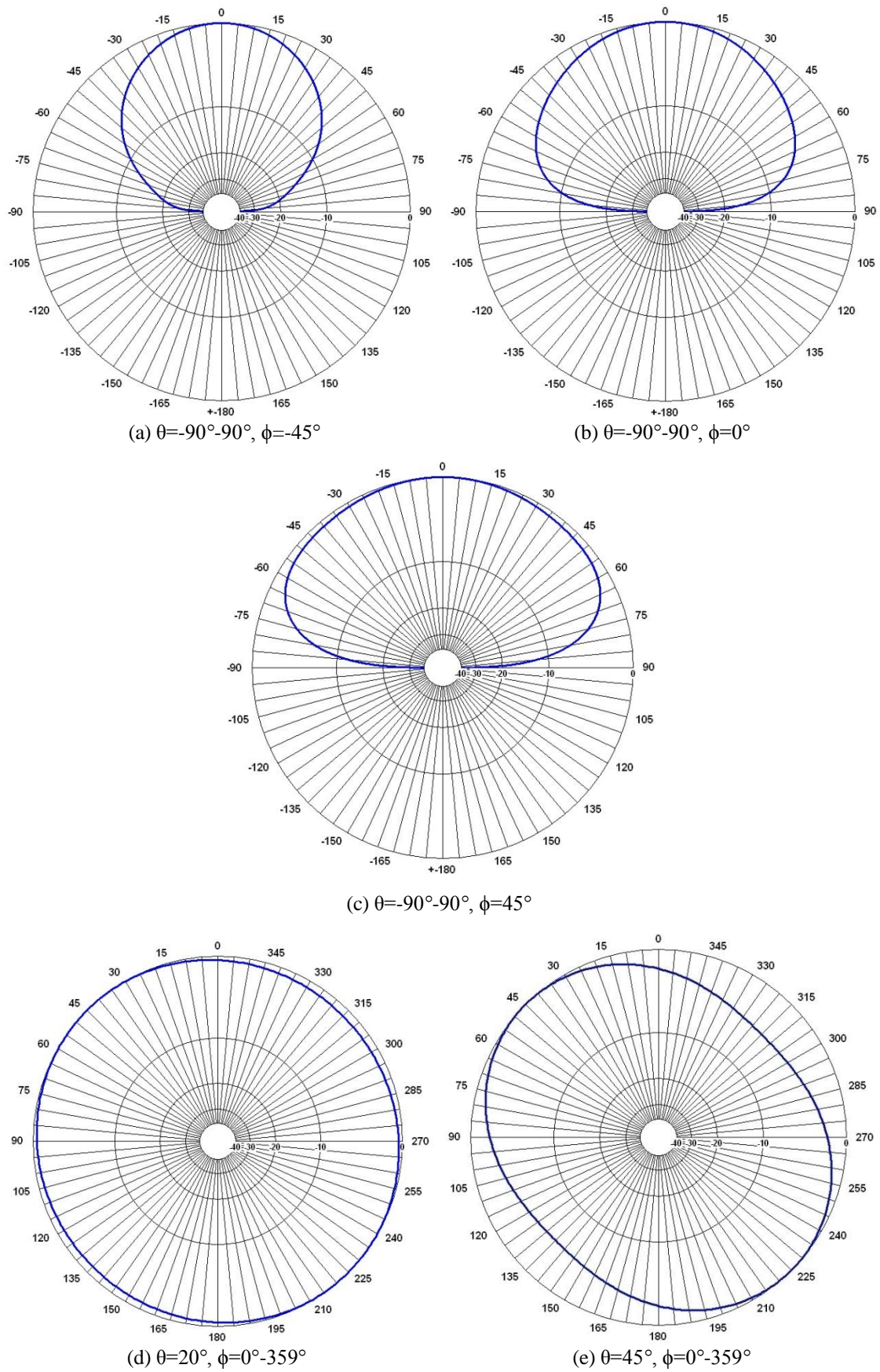


Figure 2.4. Cross sections of the radiation pattern for a 3-element folded-dipole Yagi antenna used in the MAARSY array.

Figures 2.4 (a, b, c) represent plots of the radiation pattern as a function of the zenith angle for three fixed azimuthal angles ($\phi=-45^\circ$, $\phi=0^\circ$, $\phi=45^\circ$) while figures 2.4 (d, e) are functions of the azimuthal angle for two fixed zenith angles ($\theta=20^\circ$, $\theta=45^\circ$).

The radiation pattern is called "isotropic" if it is equal in every direction. Such antennas do not exist in real world, but this model is typically used to compare with real antennas. There are also antennas described as "omnidirectional", what means that radiation patterns of those antennas are isotropic in a single plane. Third category are "directional" antennas, which prefer a distinct direction of radiation.

2.4. Radiation pattern lobes

In a radiation pattern we can distinguish different parts of the pattern called lobes, what is shown in figure 2.5.

First of them is *major lobe (main beam)*, which is described as the lobe pointing to direction of the maximum radiation. In figure (2.5) the major lobe is directed to zenith angle $\theta=0^\circ$. Some antennas may have more than one major lobe (for example split-beam antennas).

A *side lobe* is a smaller beam pointing to any other direction than the main lobe. Side lobes are the sum of all lobes beside the main lobe and they should be reduced to as low level as possible.

Back lobes are a subgroup of side lobes which are pointing to the rear side of the antenna.

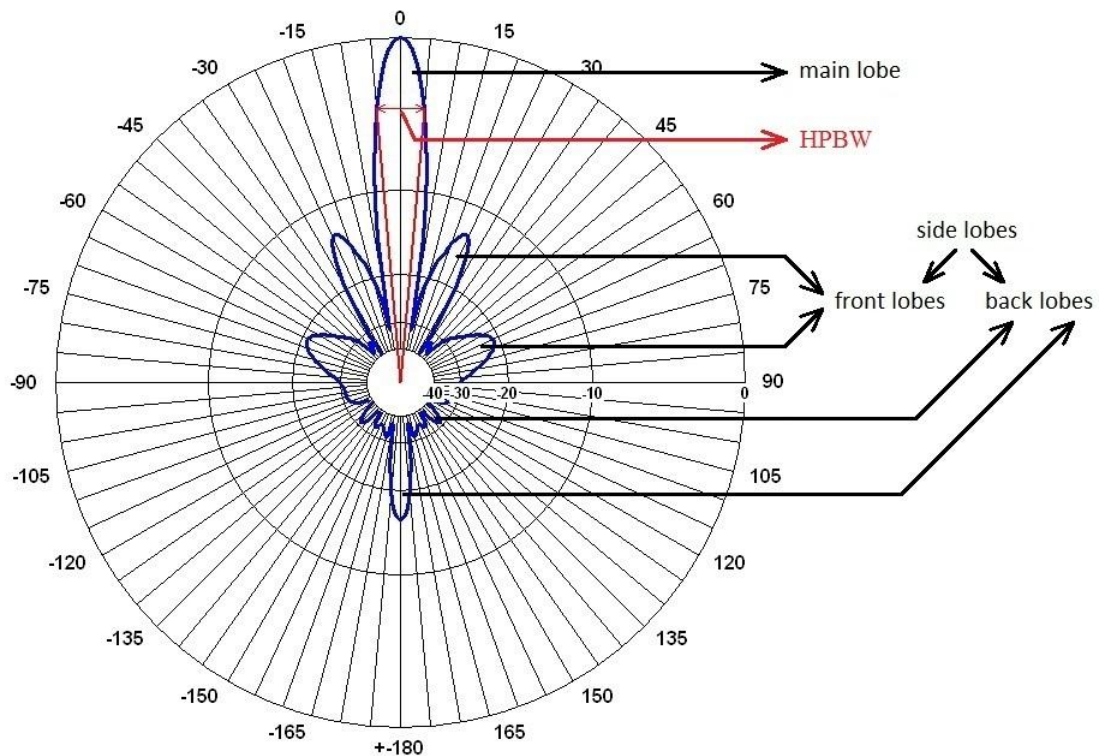


Figure 2.5. Radiation pattern lobes.

Another important parameter is the so called *Half Power Beamwidth* (HPBW). It is the angular separation between the points in major lobe, having a magnitude 50% or 3 dB smaller than its peak value. In this case the HPBW is 10° .

There are also another lobes in radiation pattern called *grating lobes*. In fact they are side lobes which becoming much larger in amplitude, due to the aliasing effect. It happens for antenna arrays, where the spacing between elements is greater than half of a wavelength. The grating lobes are almost identical to the major lobe. In the case when there are grating lobes in the radiation pattern, other side lobes should be considered as lobes occur in space between main lobe and grating lobes. [Bal05], [Han09], [Pie93], [Stu81]. An example of a radiation pattern with grating lobes is shown in figure 2.6.

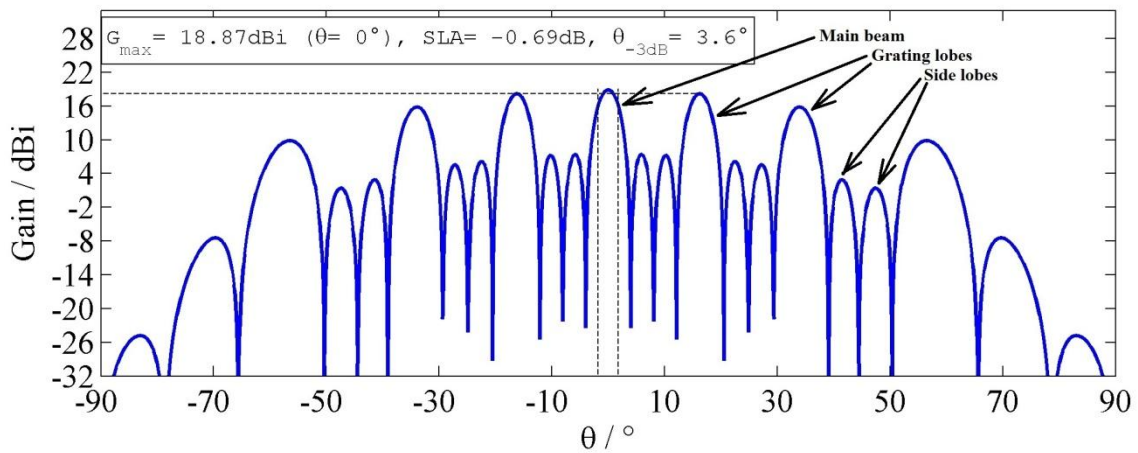


Figure 2.6. Grating lobes.

As an example to evaluate grating lobes, a 9-antennas squared structure with a spacing between elements greater than 3.5λ is used.

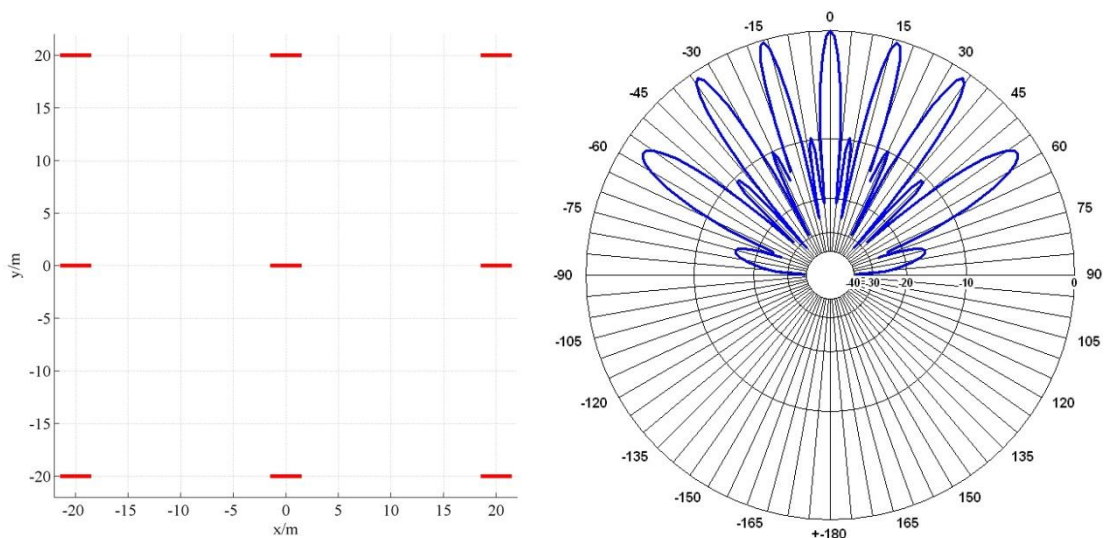


Figure 2.7. Antenna array of 9 x 3-el Yagi on a squared grid structure with a spacing of 3.5λ and the cross section of the radiation pattern of this structure.

2.5. Field regions

The space surrounding the antenna can be divided into three regions:

- Reactive near-field
- Radiating near-field (Fresnel region)
- Far-field (Fraunhofer region)

Reactive near-field is the region closely surrounding the antenna. In this portion of space, reactive fields predominate. This region boundary is given as:

$$R < 0.62 \sqrt{\frac{D^3}{\lambda}} \quad (2.14)$$

where D is the largest antenna dimension and λ is the wavelength.

Radiating near field (Fresnel region) is the region of field between reactive near-field and far-field. In this region reactive fields do not dominate anymore and radiating fields begin to emerge. Angular field distribution in Fresnel region depends on the distance from the antenna. In case when the wavelength is very large, compared to the maximum antenna dimension, this region may not exist. Radiating near-field region is given by:

$$0.62 \sqrt{\frac{D^3}{\lambda}} < R < \frac{2D^2}{\lambda} \quad (2.15)$$

Far-field (Fraunhofer region) is the region far from the antenna, wherein the distance from the antenna has no influence to the radiation pattern. This region is dominated by radiated fields. [Bal05], [Joh93], [Orf04], [RMOK82]. The region of far-field is given by:

$$R > \frac{2D^2}{\lambda} \quad (2.16)$$

Field regions are shown in figure 2.8.

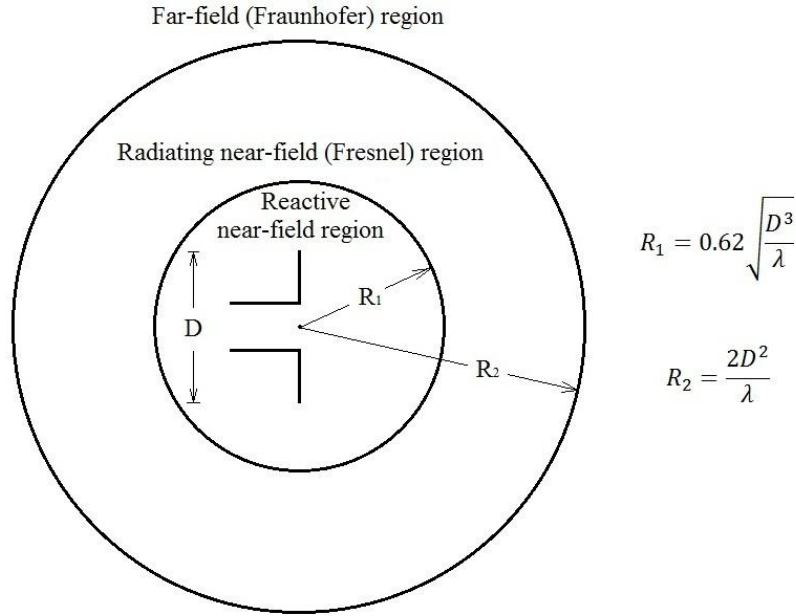


Figure 2.8. Field regions.

Values of R_1 and R_2 for the MAARSY array are equal:

$$R_1 = 0.62 \sqrt{\frac{D^3}{\lambda}} = 0.62 \sqrt{\frac{90^3}{5,60360}} = 223,6258 \text{ m}$$

$$R_2 = \frac{2D^2}{\lambda} = \frac{2 \cdot 90^2}{5,60360} = 2891,0 \text{ m}$$

2.6. Impedance

An antenna system consists of different parts (antenna, feed line, free space) and electromagnetic waves travel through all of those components. Some part of the waves energy can be reflected at each part of the system. As a result of that, a voltage standing wave in the feed line is formed. The maximum voltage to minimum voltage ratio is called the voltage standing wave ratio (VSWR). The minimum value of VSWR is theoretically 1, but in real it is difficult to obtain. However, if VSWR is lower than 1.5, it is acceptable in most cases. To minimize VSWR value, impedance matching at each interface is used. The VSWR can be calculated by:

$$VSWR = \frac{V_{max}}{V_{min}} \quad (2.17)$$

or:

$$VSWR = \frac{1+|\Gamma|}{1-|\Gamma|} \quad (2.18)$$

where Γ is a reflection coefficient and it is defined as:

$$\Gamma = \frac{Z_l - Z_s}{Z_l + Z_s} \quad (2.19)$$

Values of V_{max} and V_{min} are the maximum and minimum voltage measured at the feed point of an antenna or on the transmission line. Z_s is the impedance of the feeder toward the source and Z_l is the impedance toward the load, which in this case is the antenna impedance.

Figure 2.9 shows an impedance of the three-element folded-dipole Yagi antenna used in the MAARSY array.

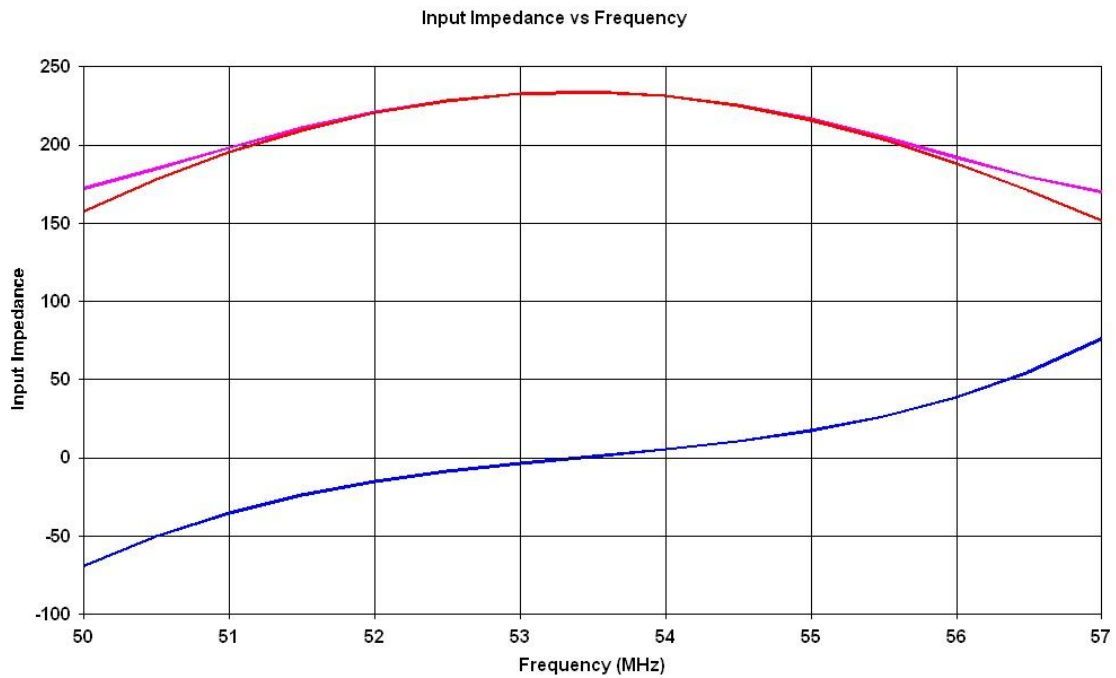


Figure 2.9. Input impedance of the three-element folded-dipole Yagi antenna used in the MAARSY array.

In figure 2.9 lines marked in blue, red and pink respectively represent:

- imaginary impedance
- real impedance
- magnitude impedance

2.7. Bandwidth

Another fundamental antenna parameter is bandwidth. It describes the range of frequencies, within the antenna can properly receive and transmit energy. Very often bandwidth is a decisive parameter used to choose a proper antenna. Many types of antennas have very narrow bandwidth and they cannot be used for wideband operation systems. [Bal05], [RMOK82], [Szo01].

The bandwidth can be considered as the range of frequencies where the characteristics of an antenna is satisfactory or aside of the center frequency, where the antenna characteristics are within an acceptable value of those at the center frequency. When we consider broadband antennas, their bandwidth is generally given as the ratio of the upper-to-lower acceptable frequency. If we have a 5:1 bandwidth, that means that upper frequency is 5 times greater than lower one. However, if the antenna we consider is narrowband, its bandwidth is represented as a percent of a frequency difference: $\frac{\text{upper frequency} - \text{lower frequency}}{\text{center frequency}}$. For instance, a 5% bandwidth means that the acceptable frequency difference is 5% of the center frequency of the bandwidth. [Bal05].

Antenna bandwidth is also quoted in terms of VSWR (Voltage Standing Wave Ratio). As an example, an antenna can be described as operating at 100-400 MHz with a VSWR<1.5. It means that the reflection coefficient (equation 2.19) is less than 0.2 in the whole range of operating frequency. Hence, only 4% of power delivered to the antenna is reflected back to the transmitter.

Figure 2.10 shows the bandwidth of the 3-element folded-dipole YAGI antenna used in the MAARSY array. For this antenna the VSWR is lower than 1.5 in range from ~50.2 MHz to ~56.7 MHz.

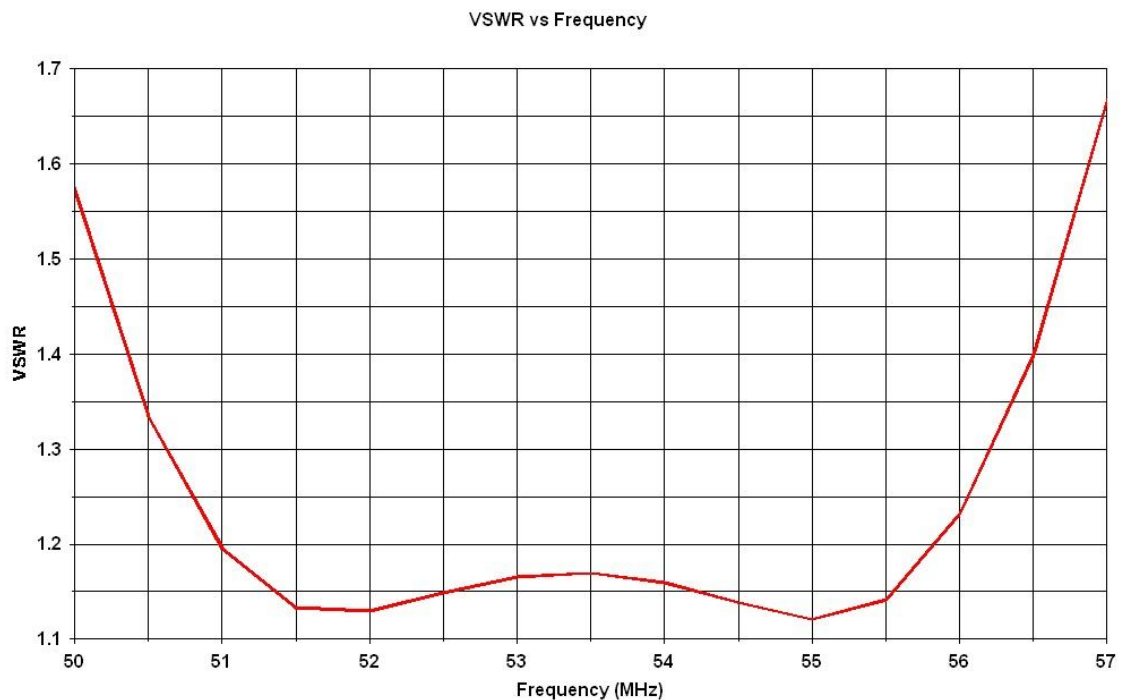


Figure 2.10. Bandwidth of 3-element folded-dipole YAGI antenna operating at frequency of 53.5MHz, used in the MAARSY array.

2.8. Efficiency, Gain and effective aperture (effective area)

Antenna *efficiency* is the relation between power delivered to the antenna and power transmitted by it and it is given as equation (2.1).

Obviously a high efficiency antenna is achieved, if the greater part of power delivered to the antenna is radiated by it and a low efficiency antenna respectively, if most of the power sent to the antenna is lost.

Antenna losses are mainly related to conduction losses due to the finite conduction of the antenna and dielectric losses. Sometimes antenna efficiency can become worse because of mismatch of antenna and the transmission line respectively. [Bal05], [RMOK82].

The *gain* of an antenna is often quoted referring to a hypothetical antenna that radiates equally in all directions (isotropic). When the gain is measured in decibels, it is called dBi. To have a high gain, the antenna must have at least one narrow beam and also must be physically large. The antenna gain can be also measured in dBd, which is the gain in decibels compared to the maximum intensity direction of a half wave dipole. It is important not to mislead dBi and dBd, because the value of dBi is 2.15 dB higher than dBd. The reason is that a dipole has 2.15 dB gain compared to an isotropic antenna. Gain also depends on the number of elements and their arrangement. [Bal05], [Han09], [RMOK82], [Szo01].

Sometimes the gain of a real antenna can reach a value of 40 or 50 dB e.g. for very large dish antennas. When the antenna is electrically small (relative to the wavelength), it can be really inefficient and its gain can be even lower than -10 dB.

The *effective aperture* is another useful parameter used to calculate the power of an antenna and its effective area. Assume that a plane wave polarized same as receiving antenna is incident upon the antenna. Also assume that the wave is coming towards the maximum of directivity. The effective aperture parameter define how much of energy will be captured and delivered by the antenna. [Bal05], [Han09], [Orf04], [Szo01].

$$P = A_e W \quad (2.20)$$

where: W is the power density of a plane wave ($\frac{W}{m^2}$),

P is the power available to the antenna receiver

Relation between an effective aperture and the gain is given by equation (2.9).

2.9. Numerical Electromagnetic Code (NEC)

The Numerical Electromagnetic Code (NEC) is an advanced version of the Antenna Modeling Program (AMP) and it has been developed by the Lawrence Livermore Laboratory. NEC is used for the analysis of the electromagnetic response of antennas. This software bases on the Method of Moments (MoM) code. NEC bases on the numerical solution of integral equations for the currents induced on the texture by sources or incident fields. This code allows modeling a wide range of structures. Model created in NEC may include different kinds of ground like perfectly reflecting ground, finitely conducting ground or free space. It can also contain non-radiating networks and transmission lines and perfect or imperfect conductors. [BP81], [Ceb99], [NS98]. A list of the most frequently used commands for generating antenna models as described in chapter 3 is presented below:

- Comment cards:
 - CM – Enter Comment
 - CE – End Comment
- Structure geometry input cards:
 - GA – Wire Arc Specification
 - GE – End Geometry Input
 - GM – Coordinate Transformation
 - GS – Scale Structure Dimensions
 - GW – Generate Wire
- Program control cards:
 - EN – End of Run
 - EX – Excitation
 - FR – Frequency Specification
 - GN – Ground Parameters
 - RP – Radiation Pattern

After the generation of the NEC antenna model it is possible to view the antenna structure using three dimensional preview of the antenna. It can be rotated, zoomed, panned and it is also possible to see axis, ground and all segments, sources and loads. When the model is already analyzed, user can look at rectangular, polar, Smith Chart and three dimensional plots. All of them are very helpful to understand how the antenna is radiating. 3-d pattern plots can be edited same as 3-d preview of the antenna.

2.10. Phased array

Very often a single antenna is not sufficient for specific objectives. The reason may be too low gain achievable with a single antenna. Therefore antenna arrays are often used to increase the gain. Moreover with the application of the antenna array not only the gain varies but the beamwidth, which value decreases with increasing the number of antennas in the array. These dependences are given by equations:

$$D_{max} = 4\pi \frac{A}{\lambda^2} \quad (2.21)$$

and

$$\theta_3 = \arcsin\left(0.886 \cdot \frac{\lambda}{D}\right) \quad (2.22)$$

where:

D_{max} – maximum directivity for a planar aperture

θ_3 – half-power beamwidth

λ – wavelength

D – aperture length

However the gain and the beamwidth are not the only reasons of using antenna arrays. Namely, it is sometimes necessary to point the main beam of the radiation pattern of an antenna array into a direction different than $\theta=0^\circ$, $\phi=0^\circ$. To generate an off-broadside beam where it is unfeasible to move or tilt the antenna structure mechanically, the antennas can however be fed separately with specific phase or time-delay. It is also possible to change the shape of radiation pattern with the use of a variable amplitude. When phase offset is used, the main beam is always moved to the direction of more negatively phased antennas. Magnitude of the phase offset depends on the structure of the antenna array. Basic equation for calculating the phase offset of a single element in an array is given by:

$$\Psi [^\circ] = -360^\circ \cdot \left[(pos_c - 1) \cdot \frac{a}{\lambda} \cdot \sin(\theta) \cos(\phi) + (pos_r - 1) \cdot \frac{b}{\lambda} \cdot \cos(\theta) \sin(\phi) \right] \quad (2.23)$$

where: θ – zenith angle

ϕ – azimuth angle

a – spacing of array element in direction of column

b – spacing of array element in direction of row

pos_c – position of element in column

pos_r – position of element in row

To count pos_c and pos_r properly, it is necessary to define a reference element in the array. [Han09], [Mai94], [Orf04], [Ren08], [Stu81].

There are two examples of phased arrays shown in this section. Both of them are models with an array composed of 9 antennas. First of them is for a squared grid structure, where both spacings (a and b) are equal and their magnitude is 4 m. In the second example the structure is equilateral with spacings of:

$$a = 4 \text{ m and } b = \frac{\sqrt{3}}{2} \cdot a = 3.4641 \text{ m.}$$

Example 1:

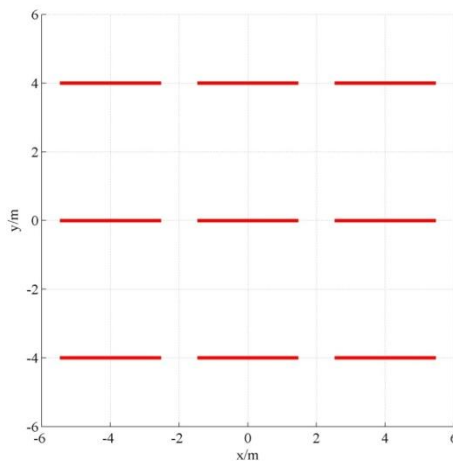


Figure 2.11. Squared 9-antennas array structure.

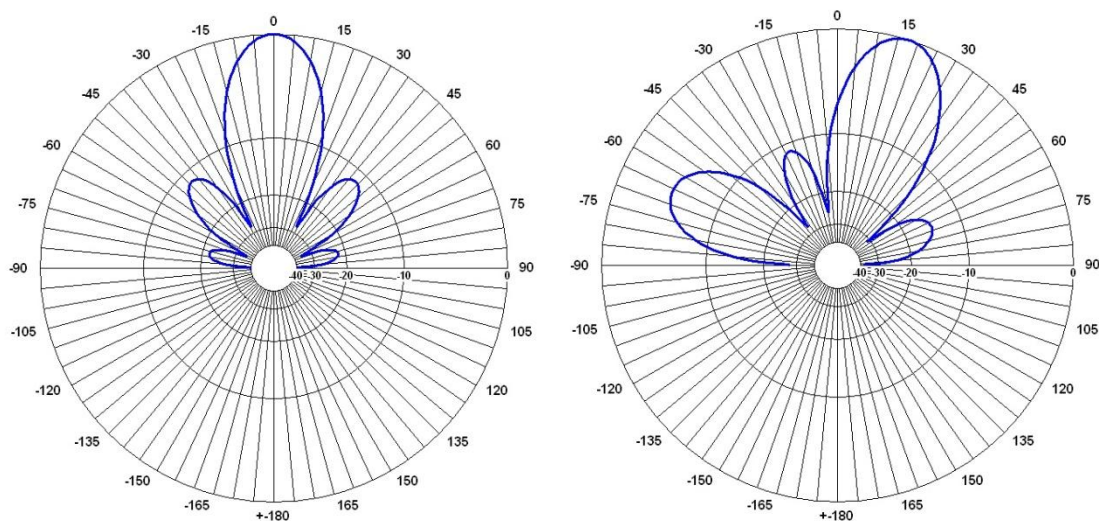


Figure 2.12. Two-dimensional plots of radiation pattern for the squared 9-antennas array structure as a function of a zenith angle.

Two 2-dimensional plots shown in figure 2.12 present the radiation pattern of the squared structure as a function of the zenith angle. On the left picture the main beam is pointed directly to zenith and in the right plot the major lobe is shifted to a zenith angle of $\theta=20^\circ$.

Phases in columns and rows for zenith angles $\theta=0^\circ$ and $\theta=20^\circ$ are shown in table 2.1.

		$\theta=0^\circ$					$\theta=20^\circ$		
		column					column		
		1	2	3			1	2	3
row	1	0°	0°	0°	row	1	0°	0°	0°
	2	0°	0°	0°		2	-87.89°	-87.89°	-87.89°
	3	0°	0°	0°		3	-175.78°	-175.78°	-175.78°

Table 2.1. Antennas excitations for a squared 9-antennas array, for a beam tilted to $\theta=0^\circ$ and tilted to $\theta=20^\circ$.

In the figure 2.13 radiation patterns in top views are presented. Left plot is for $\theta=0^\circ$ and the right one for $\theta=20^\circ$.

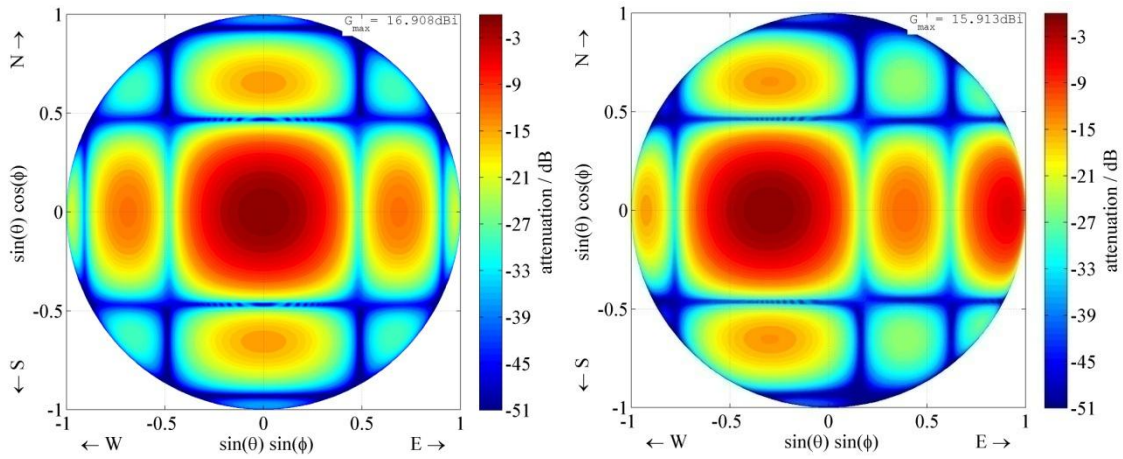


Figure 2.13. Top views of radiation patterns for the squared 9-antennas array structure, for a beam tilted to $\theta=0^\circ$ and tilted to $\theta=20^\circ$.

Example 2:

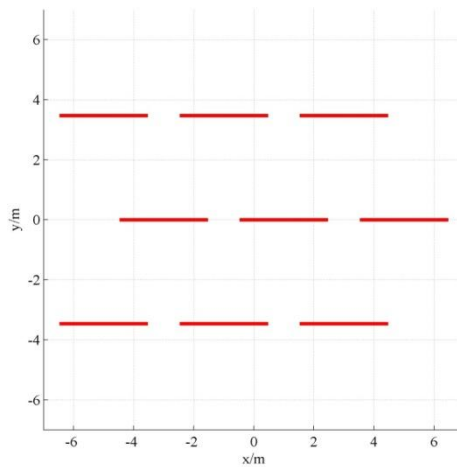


Figure 2.14. Equilateral 9-antennas array structure.

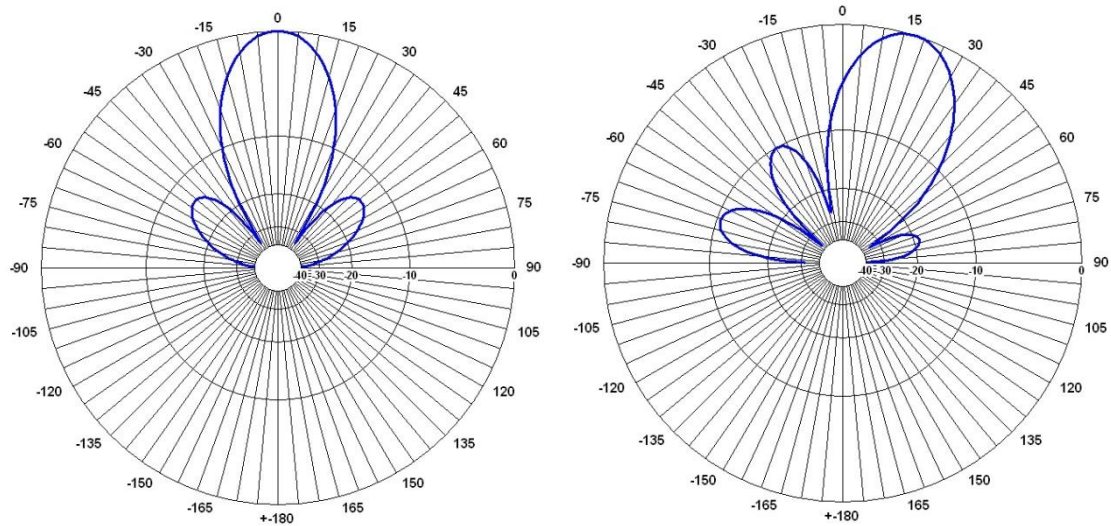


Figure 2.15. Two-dimensional plots of the radiation pattern of the equilateral 9-antennas array structure as a function of a zenith angle.

Figure 2.15 shows 2-dimensional plots of the radiation pattern for the equilateral structure as a function of the zenith angle. Left picture is for $\theta=0^\circ$, right one for $\theta=20^\circ$.

Comparing the figures 2.12 and 2.15 it can be seen that in case of the square structure a grating lobe is formed for the zenith angle of 65° and in the case of the equilateral structure this phenomenon does not occur yet. It appears that the equilateral structure gives more promising results than the square structure for the same geometry conditions.

Phases in columns and rows for the generation of maximum gain at two zenith angles ($\theta=0^\circ$, $\theta=20^\circ$) are shown in table 2.2.

		$\theta=0^\circ$					$\theta=20^\circ$		
		column					column		
		1	2	3			1	2	3
row	1	0°	0°	0°	row	1	0°	0°	0°
	2	0°	0°	0°		2	-76.12°	-76.12°	-76.12°
	3	0°	0°	0°		3	-152.23°	-152.23°	-152.23°

Table 2.2. Antennas excitations for an equilateral 9-antennas array, for a beam tilted to $\theta=0^\circ$ and tilted to $\theta=20^\circ$.

Top views of the radiation patterns for different phases of excitations are presented in figure 2.16. The left picture is for the beam pointed directly to zenith and the right one for zenith off-set equal 20° .

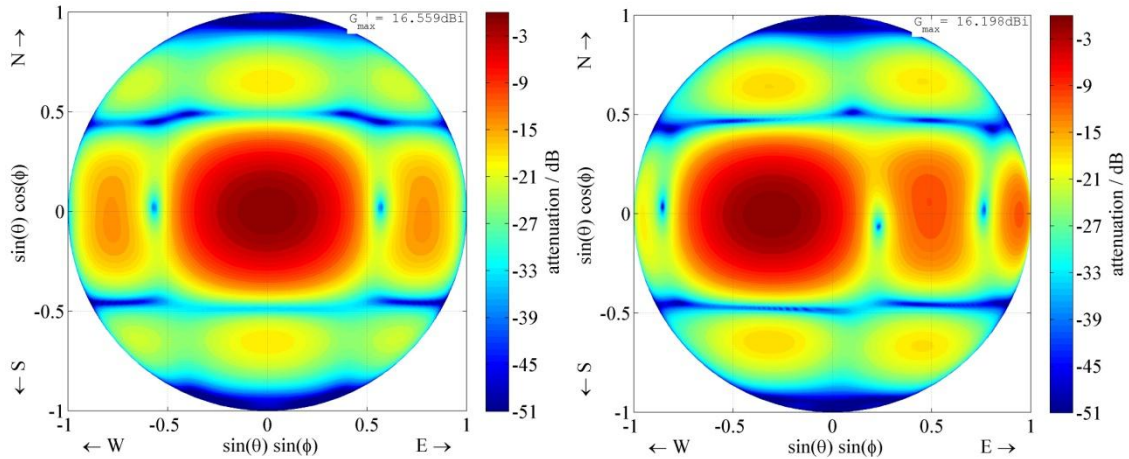


Figure 2.16. Top views of radiation patterns for the equilateral 9-antennas array structure, for a beam tilted to $\theta=0^\circ$ and tilted to $\theta=20^\circ$.

As a final conclusion of this section it can be said that the equilateral grid structure is more advantageous than the squared grid structure. The main reason of this is the greater resistance of the equilateral structure to the formation of grating lobes. Therefore the main beam of the radiation pattern of an equilateral structure can be shifted to a greater off-zenith angle than in a squared structure without the formation of unwanted grating lobes [Ren08].

Chapter 3

Array studies

Within this thesis approximately 200 models of different antennas array were created. The majority of this models brought unsatisfactory results. Some of those which were promising are described in the following chapter. The most attention has been paid for structures made for the MAARSY array, as it is the final objective to find a configuration for this antenna array. Some of remaining results, which also looked promising are in appendix and the rest of files with structures and their results are on the attached disc.

3.1. 64-antennas array

Two examples of a 64-antennas array are presented in figures 3.1 and 3.3. Their structure has a star shape with eight arms, consisting of 8 antennas each.

In the first example antennas are arranged parallel to each other in each arm and the angle between antennas in different arms is equal to the angle between those arms. The spacing between the nearest antennas is 4m. (Figure 3.1)

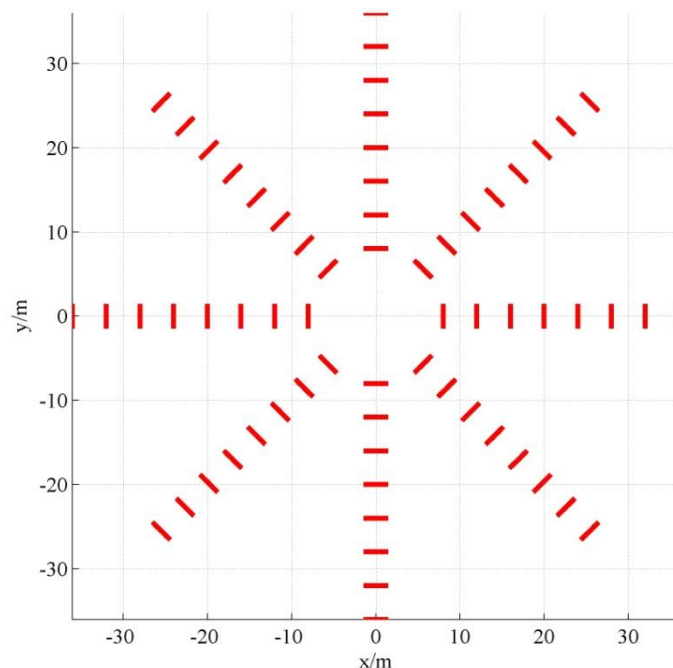


Figure 3.1. 64-antennas star structure – example 1.

Dipoles are fed with different phasing to generate a beam tilted to the off-zenith angle $\theta=35^\circ$ along each arm. Phases of the excitations starting from the most center antennas are presented in table 3.1.

	Arm 1	Arm 2	Arm 3	Arm 4	Arm 5	Arm 6	Arm 7	Arm 8
Ant.1	0.0°	0.0°	0.0°	0.0°	0.0°	0.0°	0.0°	0.0°
Ant.2	-147.4°	-147.4°	-147.4°	-147.4°	-147.4°	-147.4°	-147.4°	-147.4°
Ant.3	-294.8°	-294.8°	-294.8°	-294.8°	-294.8°	-294.8°	-294.8°	-294.8°
Ant.4	-442.2°	-442.2°	-442.2°	-442.2°	-442.2°	-442.2°	-442.2°	-442.2°
Ant.5	-589.6°	-589.6°	-589.6°	-589.6°	-589.6°	-589.6°	-589.6°	-589.6°
Ant.6	-737.0°	-737.0°	-737.0°	-737.0°	-737.0°	-737.0°	-737.0°	-737.0°
Ant.7	-884.4°	-884.4°	-884.4°	-884.4°	-884.4°	-884.4°	-884.4°	-884.4°
Ant.8	-1031.8°	-1031.8°	-1031.8°	-1031.8°	-1031.8°	-1031.8°	-1031.8°	-1031.8°

Table 3.1. 64-antennas feeding – example 1.

Three cross sections of the radiation pattern of this structure with such excitations are shown in figure A.1 in the appendix. All of those cross section plots are almost equal. The reason of that situation is that all three azimuth angles (ϕ), the plots are for, are containing one of the arms of the antenna structure. The maximum of the total directive gain appears for the zenith angle of about 39°. It is not the angle which was expected, but for $\theta=35^\circ$ the attenuation is not significant, therefore the pattern of this model is nevertheless satisfactory. The reason of the largest total gain occurring at the angle different than intended, is mutual coupling between antennas. For example the structure with antennas situated in one line, the maximum gain exists for zenith angle where it was intended. Figure 3.2 represents radiation pattern in top view.

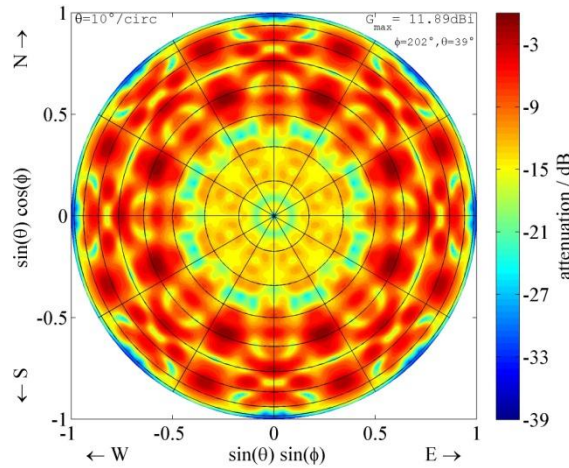


Figure 3.2. Top view of the radiation pattern of the 64-antenna star structure – example 1.

In this picture, it clearly can be seen, that the radiation pattern is symmetrical and that eight peak values of its gain appears at a zenith angle of approximately 39° and azimuth angle situated almost exactly in half way between arms of the star structure. The cause why the maximum values of gain do not turn up along the arms of star is again the mutual coupling between antennas. This radiation pattern has the shape of a ring in the range from $\theta=30^\circ$ to $\theta=75^\circ$.

Second example of eight-arms star structure is similar to first one, with just one difference. In this case, all antennas are parallel to each other, independently of their position in the array (Figure 3.3).

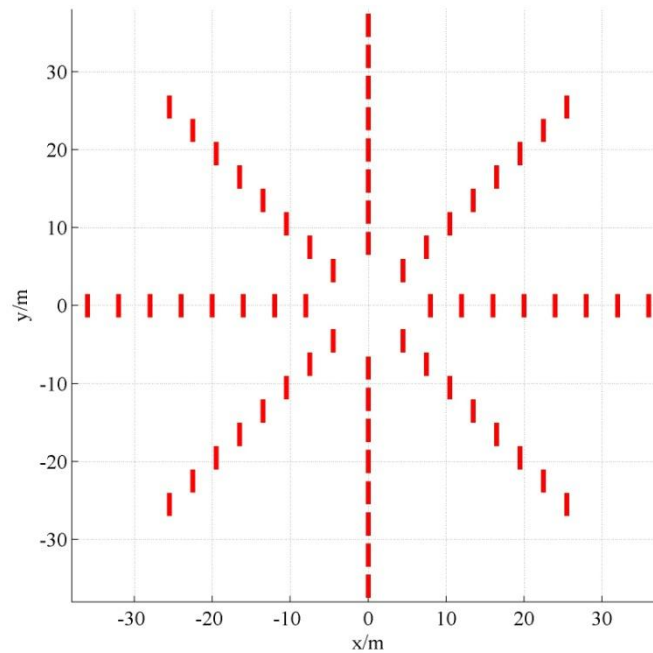


Figure 3.3. 64-antennas star structure – example 2.

The spacing between the antennas is 4m in each arm as it was also in the previous array. Phasing of the excitations are chosen to tilt the beam again to 35° off-zenith along each arm. There are two ways of feeding the dipoles of the antennas in this structure. First is using the same phases for each arm. The second method relies on feeding the antennas with adding to their phases the negative value of angle which the considered arm is shifted to. Tables 3.2 and 3.3 show the phases of excitations for both versions of feeding. Phases are starting from the most center antennas of the array.

	Arm 1	Arm 2	Arm 3	Arm 4	Arm 5	Arm 6	Arm 7	Arm 8
Ant.1	0.0°	0.0°	0.0°	0.0°	0.0°	0.0°	0.0°	0.0°
Ant.2	-147.4°	-147.4°	-147.4°	-147.4°	-147.4°	-147.4°	-147.4°	-147.4°
Ant.3	-294.8°	-294.8°	-294.8°	-294.8°	-294.8°	-294.8°	-294.8°	-294.8°
Ant.4	-442.2°	-442.2°	-442.2°	-442.2°	-442.2°	-442.2°	-442.2°	-442.2°
Ant.5	-589.6°	-589.6°	-589.6°	-589.6°	-589.6°	-589.6°	-589.6°	-589.6°
Ant.6	-737.0°	-737.0°	-737.0°	-737.0°	-737.0°	-737.0°	-737.0°	-737.0°
Ant.7	-884.4°	-884.4°	-884.4°	-884.4°	-884.4°	-884.4°	-884.4°	-884.4°
Ant.8	-1031.8°	-1031.8°	-1031.8°	-1031.8°	-1031.8°	-1031.8°	-1031.8°	-1031.8°

Table 3.2. 64-antennas feeding – example 2 a (the same phases in each arm).

Figures A.2 and A.3 in the appendix show the cross sections of the radiation pattern for these two different methods of excitation. Difference between them, for those two methods of feeding is not very big. However choosing first way brings a more symmetrical result and the magnitudes for the main peaks of the radiation pattern are greater. Figure 3.4 shows the top views of the radiation patterns for both methods of feeding.

	Arm 1	Arm 2	Arm 3	Arm 4	Arm 5	Arm 6	Arm 7	Arm 8
Ant.1	0.0°	-45.0°	-90.0°	-135.0°	-180.0°	-225.0°	-270.0°	-315.0°
Ant.2	-147.4°	-192.4°	-237.4°	-282.4°	-327.4°	-372.4°	-417.4°	-462.4°
Ant.3	-294.8°	-339.8°	-384.8°	-429.8°	-474.8°	-519.8°	-564.8°	-609.8°
Ant.4	-442.2°	-487.2°	-532.2°	-577.2°	-622.2°	-667.2°	-712.2°	-757.2°
Ant.5	-589.6°	-634.6°	-679.6°	-724.6°	-769.6°	-814.6°	-859.6°	-904.6°
Ant.6	-737.0°	-782.0°	-827.0°	-872.0°	-917.0°	-962.0°	-1007.0°	-1052.0°
Ant.7	-884.4°	-929.4°	-974.4°	-1019.4°	-1064.4°	-1109.4°	-1154.4°	-1199.4°
Ant.8	-1031.8°	-1076.8°	-1121.8°	-1166.8°	-1211.8°	-1256.8°	-1301.8°	-1346.8°

Table 3.3. 64-antennas feeding – example 2 b (different phases in each arm, reference arm (arm 1) is the one for value of $y=0$ and for negative x -values).

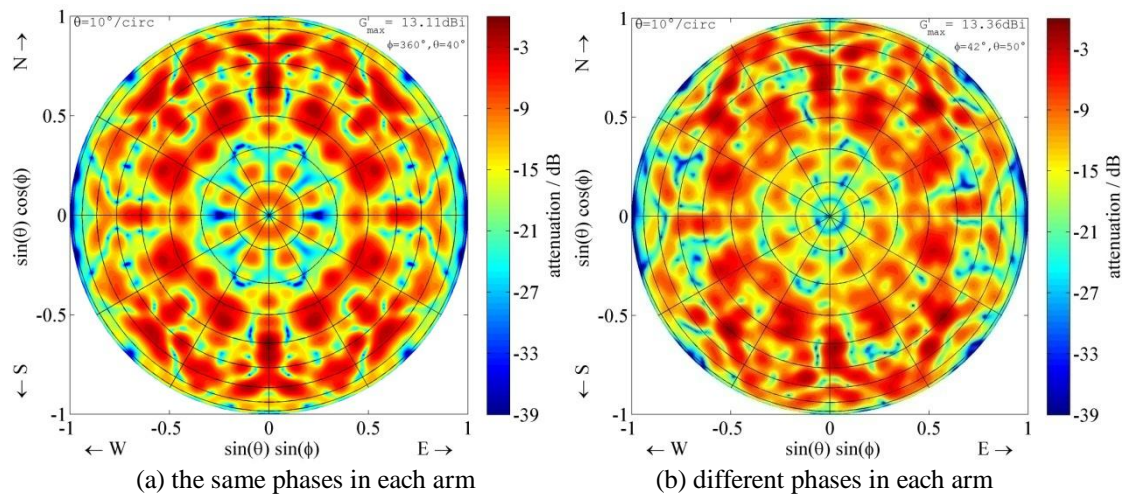


Figure 3.4. Top view of the radiation pattern of the 64-antenna star structure – example 2.

Comparing all three top view plots of 64-antennas star arrays, it can be assumed that the radiation pattern is more symmetric when the antennas are situated perpendicularly to the line along each arm of the star. Such model could be used for any meteor trail observations, but the objective of this thesis is to find a solution for the MAARSY array, where all of 433 antennas are situated parallel to each other. However it is always necessary to remember about the influence of mutual coupling between the antennas for every structure.

3.2. MAARSY array – 4 rings

In the next sections different attempts of generating a useful beam for meteor observation using the MAARSY array will be considered. The arrangement of the antennas in this array is described in section 1.3 of this thesis. Figure 3.5 represents the structure of the MAARSY array with its dimensions.

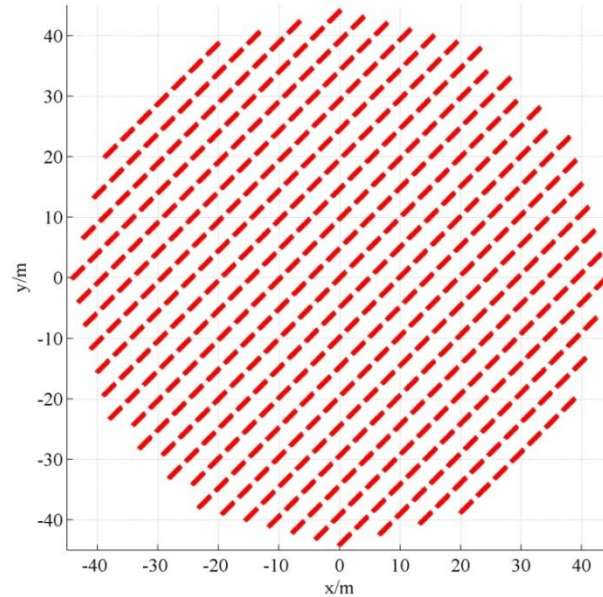


Figure 3.5. Positions of the 433 Yagi antennas within the MAARSY array.

The purpose of the following example was to make four rings with different phasing in each ring. In the figure 3.6 those four rings are shown and in table A.1 in the appendix, zenith and azimuth angles for each antenna can be found. Every antenna is fed in this case. Phase offset for each antenna is calculated using equation 2.23.

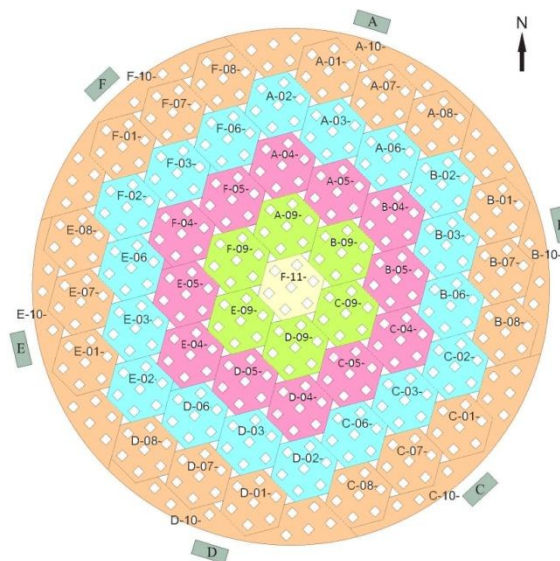


Figure 3.6. MAARSY array divided into four rings.

During further considerations, rings will be called:

- green
- blue
- center subarray
- pink
- orange

The rings with their associated antennas are shown in figure 3.6.

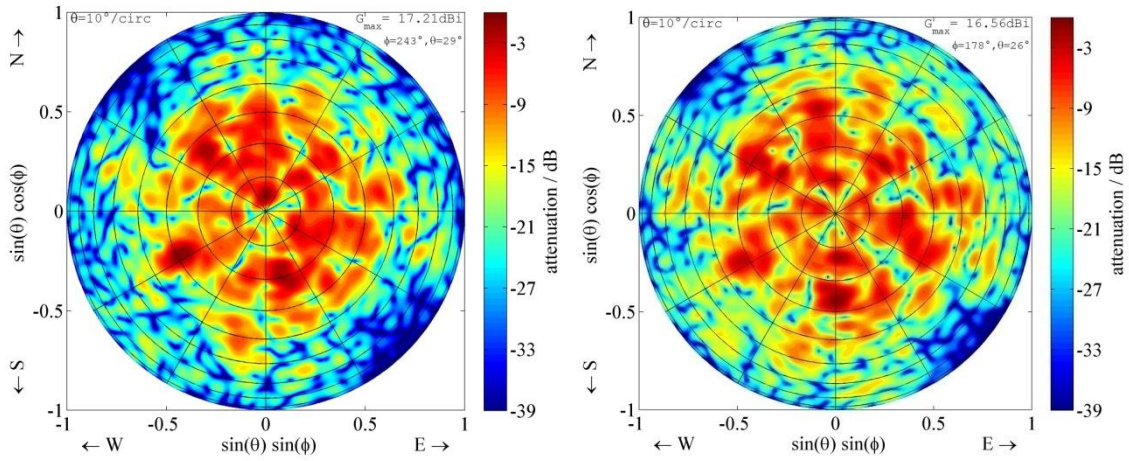
Additionally four other different configurations of the antennas feeding were calculated. Azimuth angles were the same for all of those configurations, however values of zenith angles were changed as it is shown in table 3.4. Intention of this variation of the zenith angle was to generate the maximum radiation at different positions.

		Zenith angle (θ) for configuration:			
		2	3	4	5
ring	green	20°	25°	35°	30°
	pink	25°	30°	30°	30°
	blue	30°	35°	25°	30°
	orange	35°	40°	20°	30°
	center subarray	0°	0°	0°	0°

Table 3.4. Different configurations of feeding the *4-rings* MAARSY array.

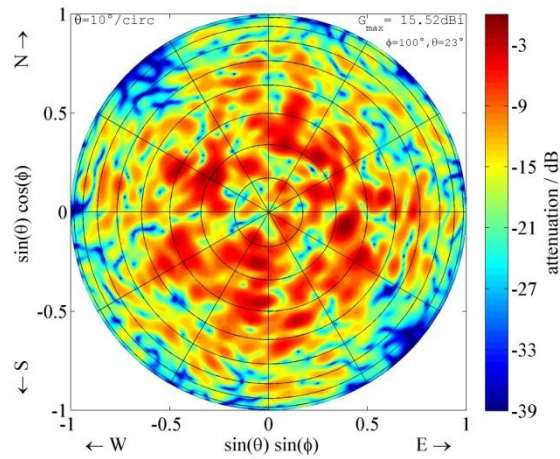
Top views of the radiation patterns of five different configurations are respectively shown in figure 3.7 (a-e).

Analyzing the radiation patterns shown in figure 3.7, it can be concluded that this way of dividing the array is not profitable. The reason of that conclusion is, that in all of the radiation patterns from figure 3.7 are a lot of regions attenuated even by 30 dB in the range between $\theta=10$ and $\theta=50$ degrees. Moreover, in figure 3.7 (c), grating lobes appeared and the power level at angles close to horizon is too high. The reason of the asymmetries in all radiation patterns discussed in this section is, that a different number of antennas are used to steer to different azimuth angles (ϕ). For example the main beams are generated by 26 antennas and are directed to $\phi=55^\circ$, while only 7 of them are directed to $\phi=69^\circ$. Therefore no further examples with the division of the array as shown in figure 3.6 have been created.

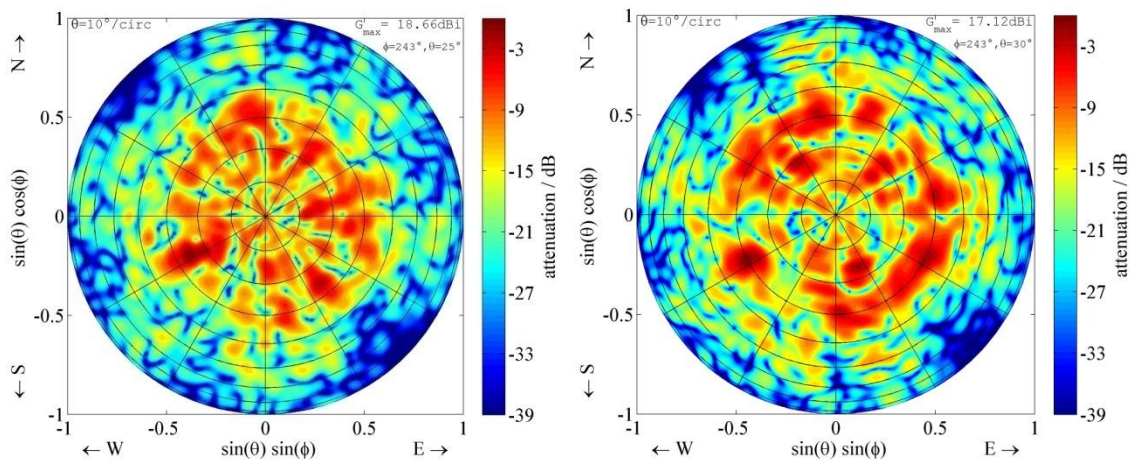


(a) configuration 1

(b) configuration 2



(c) configuration 3



(d) configuration

(e) configuration 5

Figure 3.7. Top views of radiation patterns for five ways of the antenna excitations for the 4-rings MAARSY array.

3.3. MAARSY array – groups

The next idea was to create a model in which 12 individual beams will be generated. The configuration and selection of antennas from the array can be seen in figure 3.8.

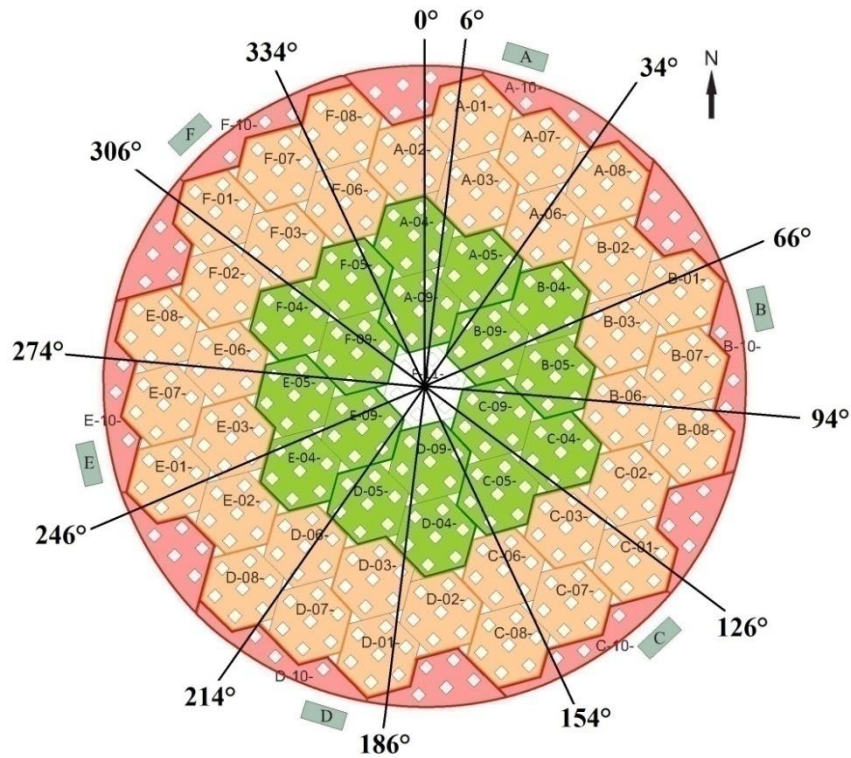


Figure 3.8. MAARSY array divided into 18 main groups consisting of 21 antennas each.

About 30 different examples were considered for this conception and a few of them are described in this section. First of them is a configuration where 426 out of 433 antennas are used. They are subdivided into 18 groups consisting of 21 antennas each completed by the most external antennas which are marked in red, as it is shown in figure 3.9. Only 7 antennas which are situated in hexagon number F-11 are not excited.

The antenna groups orange and red are used for the same zenith angle θ , however the groups marked in green have a different zenith angle (Figure 3.9 (a)). Resulting values of zenith and azimuth angles between individual antennas for the first example are demonstrated in table A.2 in the appendix.

Second example (Figure 3.9 (b)) has the same distribution of azimuth angle over the antenna groups as the first one, however zenith angles vary. Assume that different colors of groups correspond respectively to:

- green – hexagons no: A-F (04, 05, 09)
- orange – hexagons no: A-F (01, 02, 03, 06, 07, 08)
- red – hexagons no: A-F (10)

then values of θ for the second example are:

- green groups: $\theta=40^\circ$
- orange groups: $\theta=30^\circ$
- red groups: $\theta=30^\circ$

Comparison of the top views of the radiation patterns for those two examples can be observed in figure 3.10 (a, b).

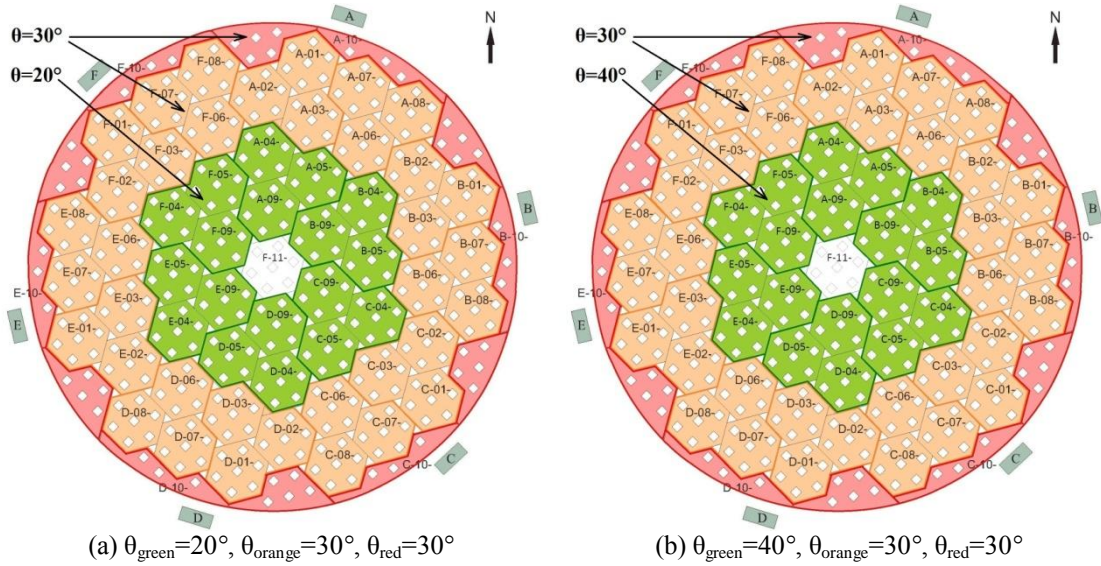


Figure 3.9. MAARSY array with *green, orange* and *red* groups of selected antennas.

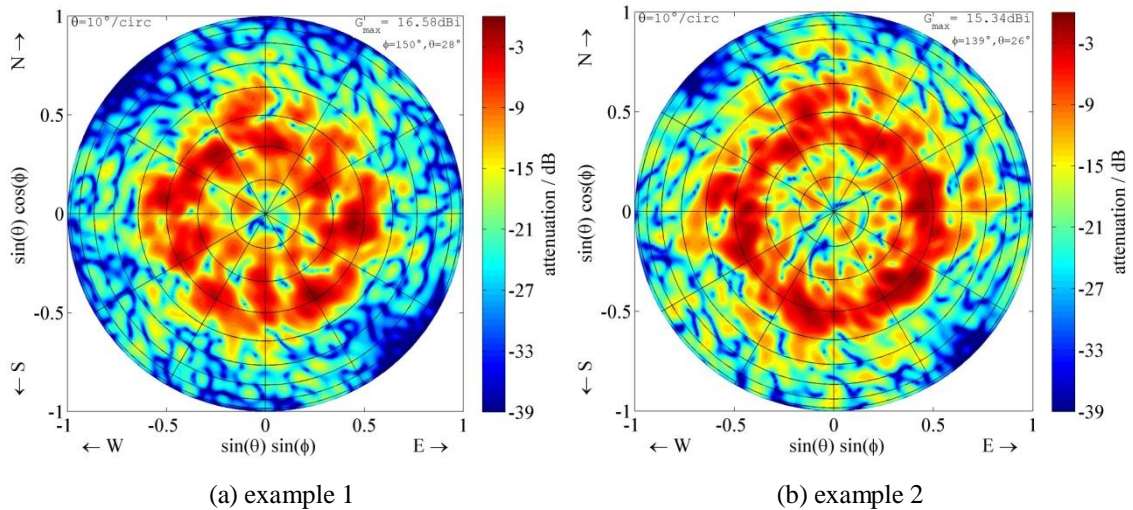


Figure 3.10. Radiation patterns for 2 instances of excitation for models shown in figure 3.9 (a, b).

The radiation patterns shown in figure 3.10 look much more promising than the ones discussed in the previous section. However there still can be seen quite large asymmetry and the radiation pattern in example 2 has too narrow beamwidth, what is not an advantage for meteor trail observations. The asymmetry is again caused by the different number of the antennas, which radiation pattern is tilted to different azimuth angles. For example main beam directed to $\phi=6^\circ$ is

generated by 47 antennas and only 24 antennas generate a beam that is directed to $\phi=34^\circ$. The cross section plots for $\phi=0^\circ$, $\phi=270^\circ$ and $\phi=315^\circ$ for those two examples can be found in the appendix as figures A.4 and A.5.

The next two models are subdivided in the same way as previously. In the first model only the orange groups are fed and in second one additionally the red groups are excited to make the entire structure more circular at the border. When power is delivered only to the orange groups the total number of fed antennas is 252, while with using also the red groups the selected amount increases to 300 antennas. Figure 3.11 (a, b) represents these two structures described above.

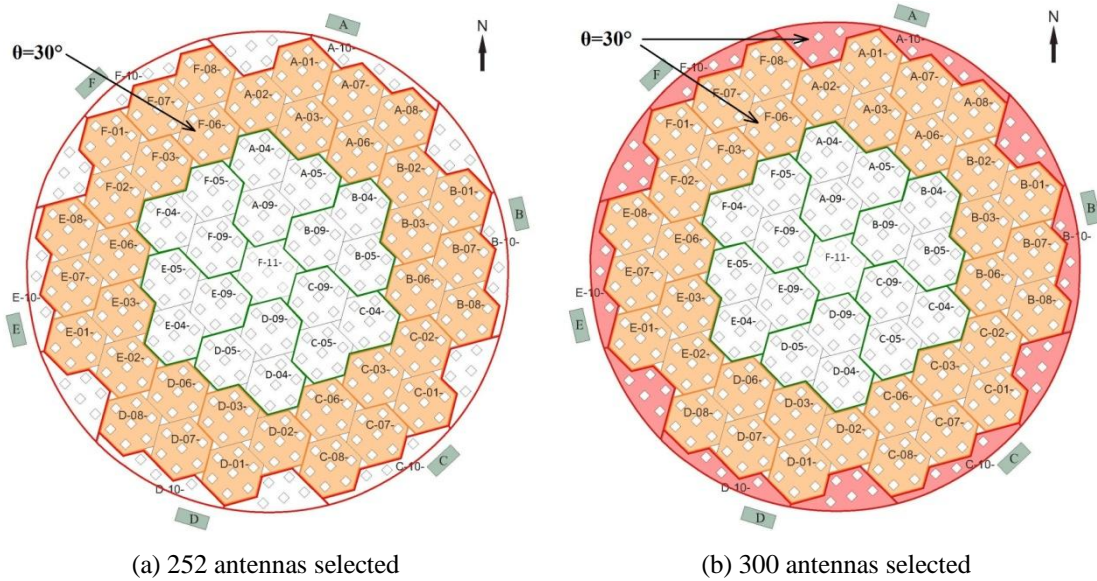


Figure 3.11. MAARSY array with the outer ring fed.

In those two examples the zenith angle for each antenna group is the same and the azimuth angles are selected in the way to get 12 beams with approximately 30° spacing between them. Exact values of those angles are shown in table A.3 and A.4 in the appendix of this thesis. The radiation patterns of those two structures are plotted in figure 3.12 (a, b).

The radiation patterns shown in figure 3.12 are much better than those generated for the earlier models shown in figure 3.10 (a, b). The ring of the maximum radiated power is now more circular inside and outside and has a more symmetrical shape. The better radiation pattern is the one in the figure 3.12 (a), because the useful beam is broader. The beam in picture (a) has not got big attenuations in range between $\theta\sim 18^\circ$ and $\theta\sim 38^\circ$, while in the picture (b) this range is comprised between $\theta\sim 20^\circ$ and $\theta\sim 35^\circ$. This difference is due to the lower number of antennas (equation 2.11) used in the case of picture (a). As it is known, the greater the number of antennas, the narrower the radiation pattern and the higher the gain are. The cross sections plots for the zenith angles $\phi=0^\circ$, $\phi=270^\circ$ and $\phi=315^\circ$ for the radiation pattern shown in figure 3.12 (a, b) can be found in the appendix as a figures A.6 and A.7.

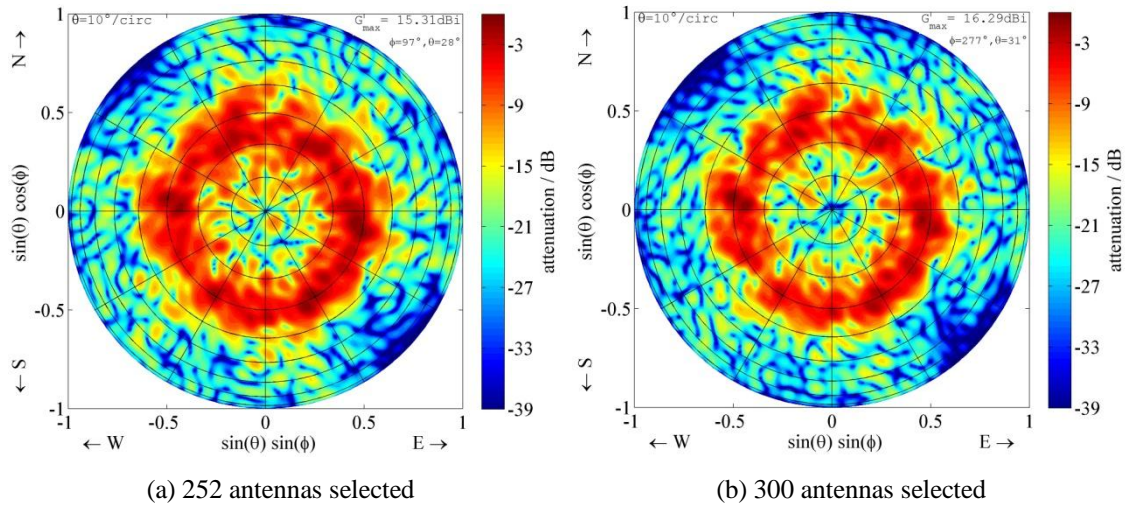


Figure 3.12. Radiation patterns for models shown in figure 3.11.

3.4. MAARSY array – 12 slices

The subsequent models were created by dividing the main array (Figure 3.5) to 12 approximately equal slices. The idea of this model have been to select antenna groups with sufficient and equal amount of array elements. With this configuration a clean pattern with adequate side lobe suppression was anticipated. Each of the slices has its own azimuth angle and in most cases the zenith angle is the same for every slice (see Figure 3.13 (a-d)). The values of azimuth angle for adjacent slices differ by 30° . In one example two values of a zenith angle of each slice were applied. Figure 3.15 shows the selection of antenna groups of the array into slices.

For this configuration also about 30 examples with different phasing of the antennas excitations and different amount of the antennas were created. Again most of them were not useful to the purpose of meteor trail observations. However examples with the most promising results are described in this section.

In the first example 426 antennas are actively used and thus each slice consists of approximately 35 antennas. This configuration can be seen in figure 3.13 (a). The antenna array shown in figure 3.13 (b) is for a smaller group of antennas where 384 of them are excited, with about 32 antennas in every slice of the structure.

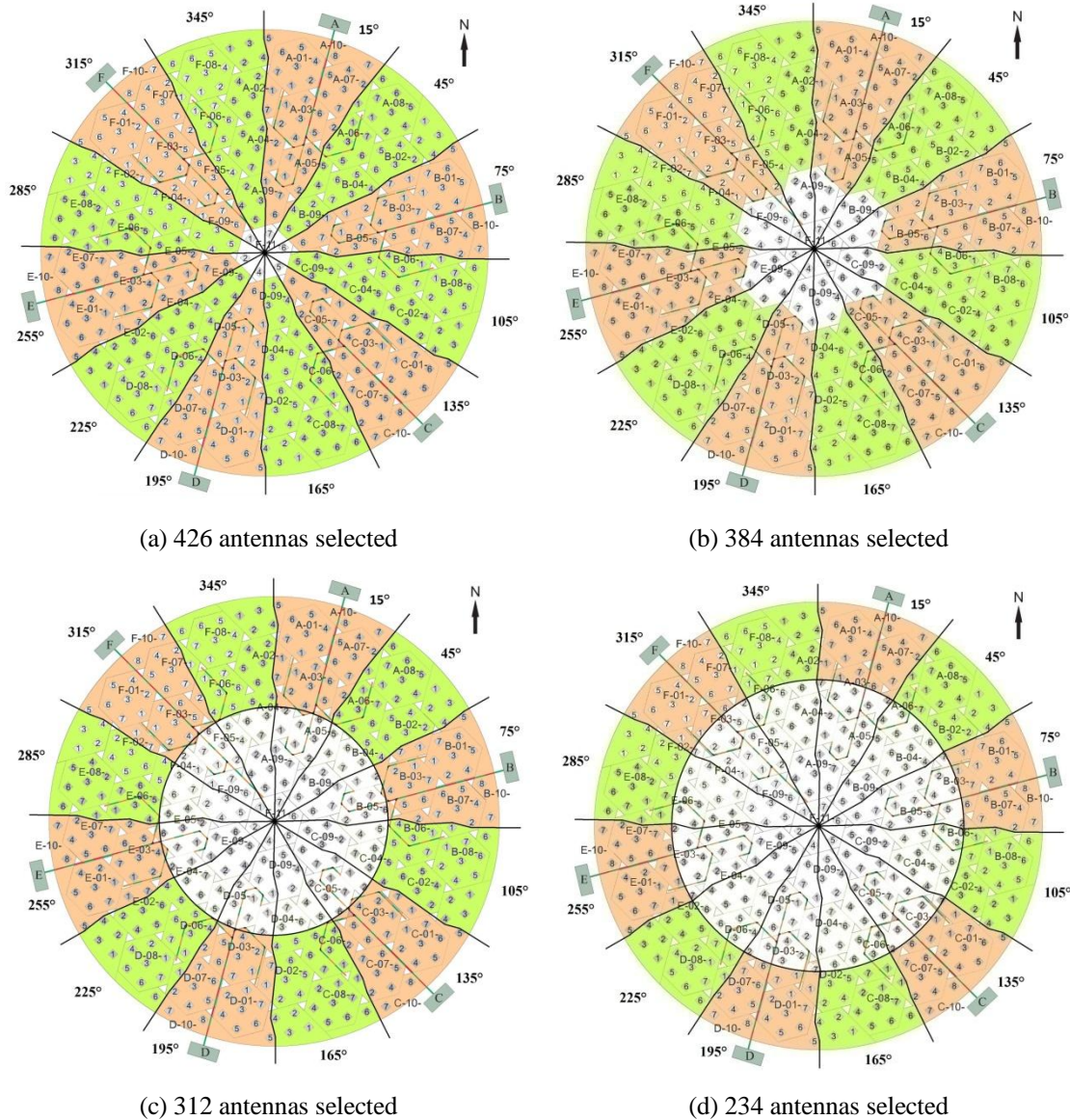


Figure 3.13. MAARSY array divided into 12 slices with the same value of a zenith angle for every used antenna.

Further attempts were considered with 312 out of 433 antennas selected (Figure 3.13 (c)). In this case 26 antennas occur in each slice. The last example in which only one off-zenith direction has been used is shown in figure 3.13 (d) where 234 antennas were excited. Therefore 19 or 20 antennas are in one slice. Slices marked in orange consist of 20 antennas and slices marked in green consist of 19 antennas. As these groups have almost the same amount of elements and are still of good quantity the resulting radiation pattern should appear useful. Tables with the chosen directions of θ and ϕ for each of the array structures described above can be found in the appendix as A.5, A.6, A.7 and A.8. Figure 3.14 (a-d) represents the radiation patterns of the array structures shown in figure 3.13 (a-d).

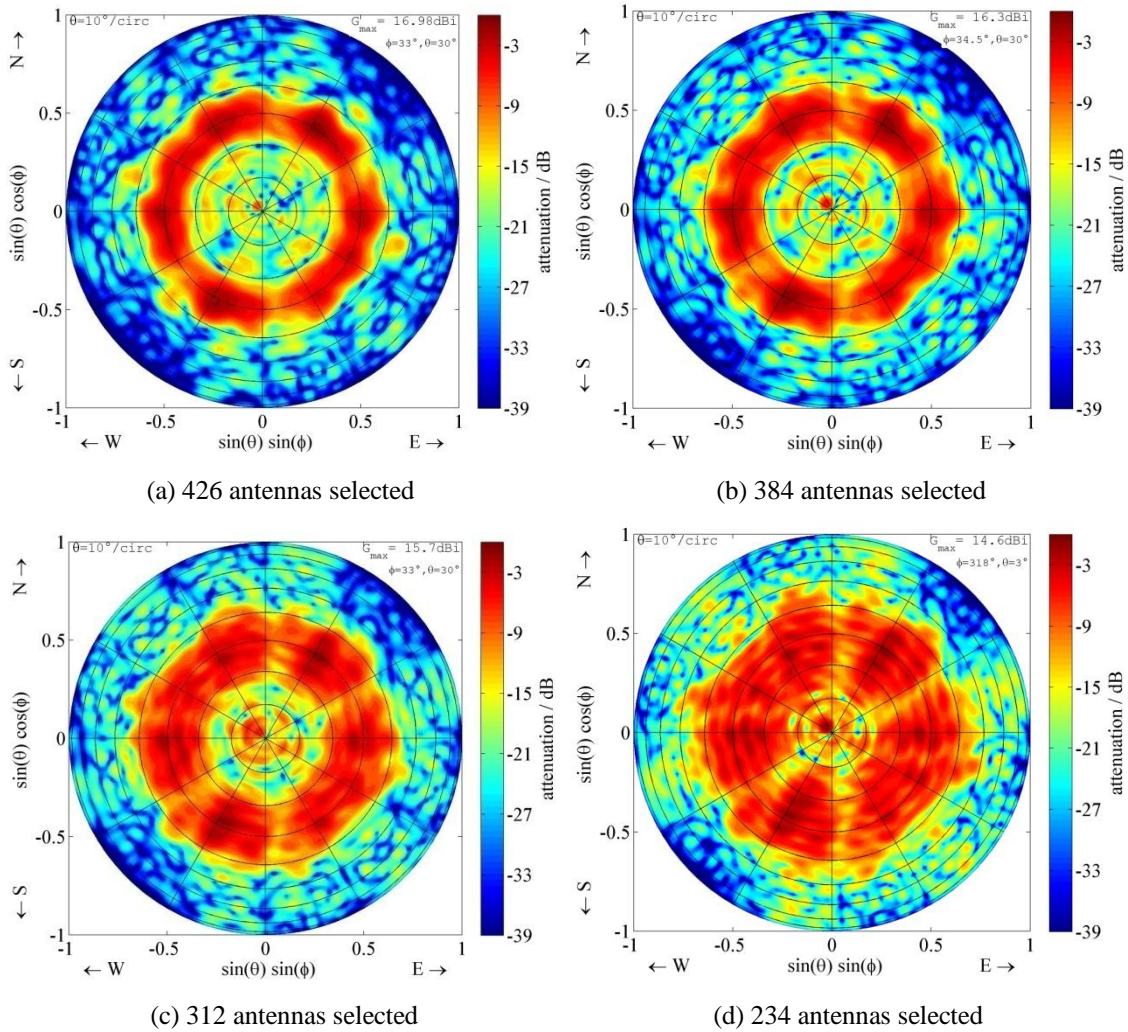


Figure 3.14. Radiation patterns for the array structures shown in figure 3.13, for $\theta=30^\circ$.

Comparing the radiation patterns shown in figure 3.14, it can be noticed that for each of them, it is circular on the outside and on the inside of the generated beam. For the example (a) the beam is very narrow, but has the biggest gain and good suppression at the horizon. The following examples (b) to (d) have a wider beam but also less maximum gain due to the lower amount of antennas used. However the differences between the gain in the radiation pattern (a) and the radiation pattern (d) are not significant. The beamwidth in the radiation pattern (a) is only about 15° , while for the example (d) the beamwidth is over 35° . The cross section plots for azimuth angles $\phi=30^\circ$, $\phi=60^\circ$ and $\phi=105^\circ$ for all of the above four examples can be found in the appendix as a figures A.8, A.9, A.10 and A.11.

The next model is also made to generate 12 main beams in different azimuth directions as it was considered before. However two different values of zenith angle were now applied within one slice. In the figure 3.15 can be seen two different colors of rings for the inner and outer ring which represent different zenith angles.

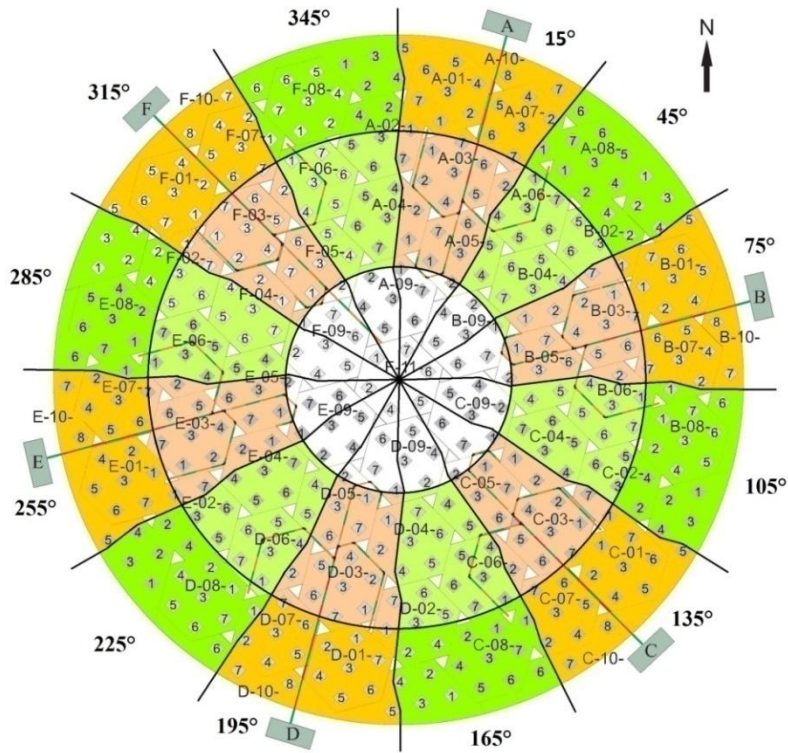
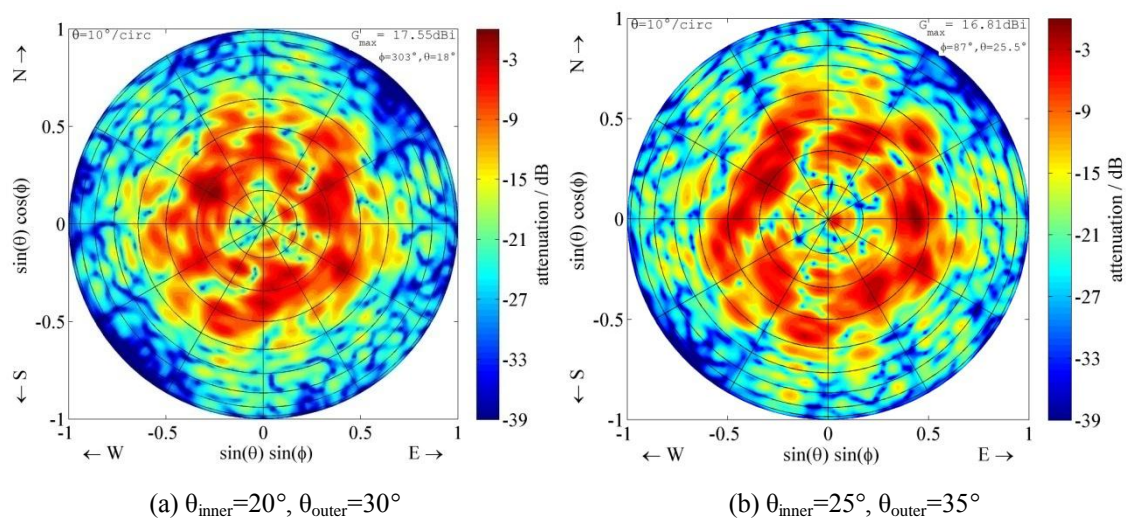


Figure 3.15. MAARSY array divided into 12 slices with two different values of zenith angle.

Two instances of this configuration will be considered. In the first of them groups of antennas which form the ring closer to the center of the array are steered to generate main beams tilted to $\theta=20^\circ$ while groups creating the external ring generate beams tilted to 30° off-zenith.

In the second attempt, the angles were increased by 5° each, therefore zenith angle of the inner ring was 25° and its value for the external ring was 35° . The exact values of zenith and azimuth angles for each antenna of those two configurations can be found in the appendix, in tables A.9 and A.10. The radiation patterns of two examples described above, are shown in figure 3.16.



(a) $\theta_{\text{inner}}=20^\circ$, $\theta_{\text{outer}}=30^\circ$

(b) $\theta_{\text{inner}}=25^\circ$, $\theta_{\text{outer}}=35^\circ$

Figure 3.16. Radiation patterns for the structures shown in figure 3.15 for different values of zenith angle.

Comparing those two radiation patterns with radiation patterns shown in figure 3.14 it can be easily seen that the previous way of feeding the antennas with using only one value of zenith angle for all of them brought far better results. The shapes of the radiation patterns now do not look like rings anymore and have a high variability of attenuation in the range where it is unwanted. Due to that dissatisfying results no further attempts of modeling this structure were realized. The cross section plots for azimuth angles $\phi=-60^\circ$, $\phi=0^\circ$ and $\phi=90^\circ$ for two examples described above can be found in the appendix as a figures A.12 and A.13.

3.5. MAARSY array – 18 slices

The next attempts were similar to these in section 3.4. The main array was subdivided into 18 slices to realize 18 main beams tilted to different azimuth angle each. The zenith angle of all slices is equal and its value is 30° . The orientation and therefore the beam direction of adjacent slices differ by 20° . The structure and its radiation pattern are shown in figure 3.17.

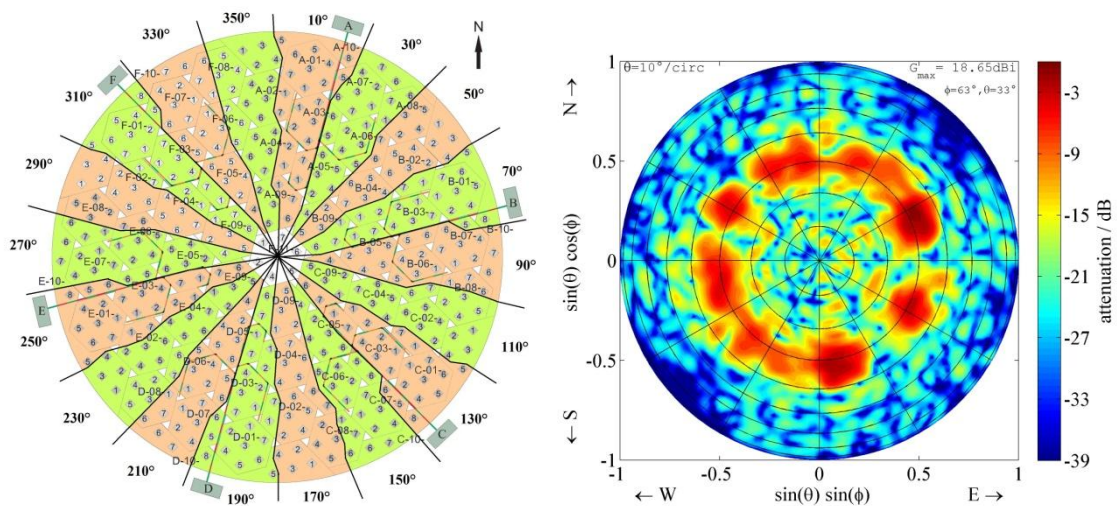


Figure 3.17. MAARSY array divided into 18 slices and its radiation pattern.

It can be seen that the radiation pattern of this structure does not look as it was expected. It is not symmetrical due to too low number of the antennas used in one slice and interaction of adjacent antenna groups. Many attempts, with different zenith angles and different numbers of the antennas were considered, but none of them brought satisfying result.

3.6. MAARSY array – 168 antennas, the actual state of the MAARSY radar

In this section the last two models are described. They are made of 168 antennas which are already connected to entire system and are used in the current MAARSY radar setup (June 2010). Figure 3.18 represents the available antennas and their transmit-receive modules.

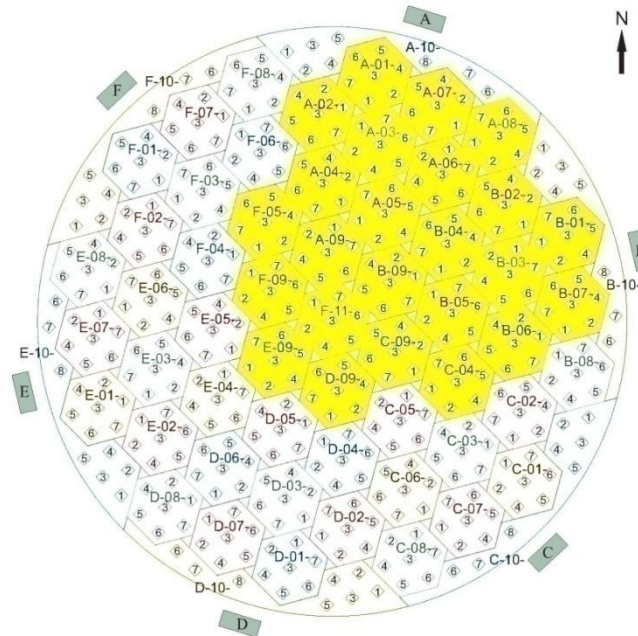


Figure 3.18. MAARSY array – 168 out of 433 antennas.

Both considered examples consist of 107 out of 168 antennas and are chosen to get a circular antenna geometry. In the first attempt those 107 antennas are divided into 6 groups consisting of about 18 antennas each. Azimuth angle of every group differ by 60° from the orientation of adjacent groups. Azimuth angle differences in the second model are 40° between adjacent groups and therefore 9 main beams are generated. Value of the zenith angle is 30° and it is equal for every group of antennas in both examples. Accurate values of azimuth and zenith angles can be found in the appendix as tables A.11 and A.12. Figure 3.19 (a, b) represents the described examples. Antennas marked in yellow in figure 3.19 are not actively used.

Figure 3.20 shows the radiation patterns for the two structures described earlier in this section. Comparing the plots shown in figure 3.20 it can be noticed that the one on the left hand side (Figure 3.20 (a)) has a more symmetrical shape at the borders and the power level close to the horizon is lower than in the figure 3.20 (b). In figure (a) the attenuation is significant for the azimuth angles $\phi=120^\circ$ and $\phi=0^\circ$. However the width of the attenuation at these points is acceptable with less than 10° .

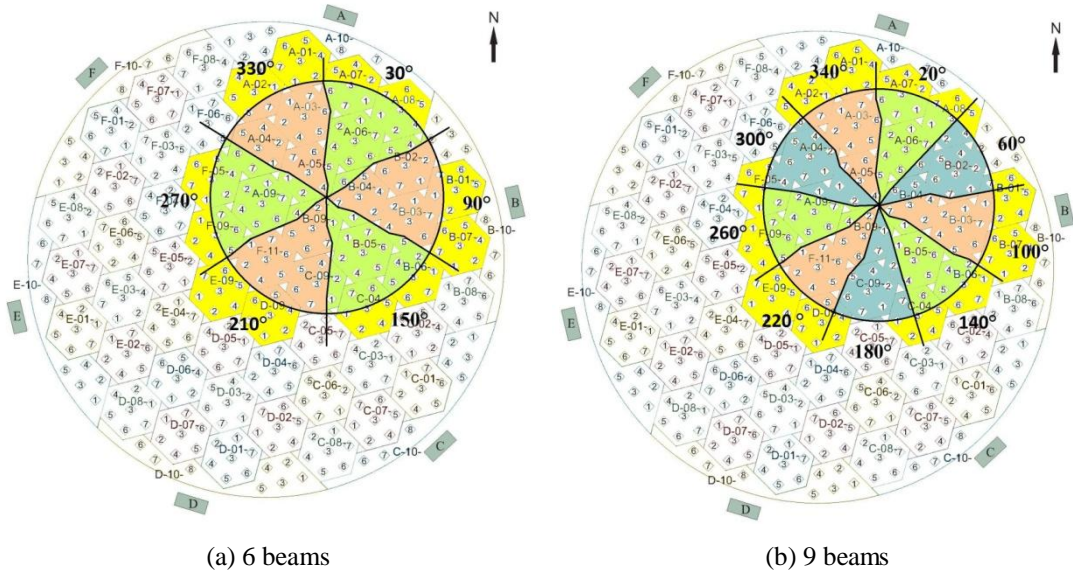


Figure 3.19. MAARSY array - 107 out of 168 antennas used.

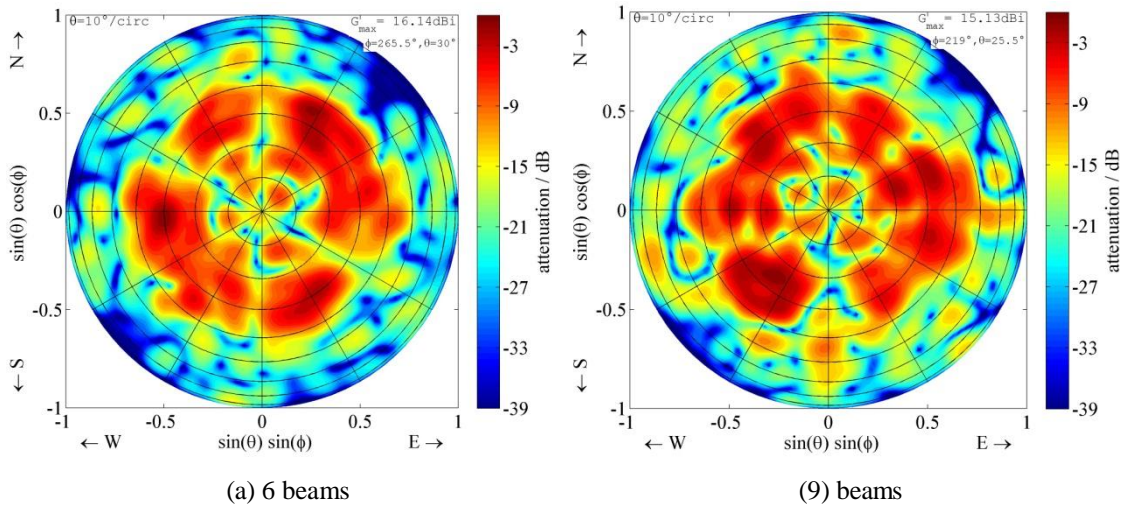


Figure 3.20. Radiation patterns for the structures shown in figure 3.19.

Results obtained from those currently active antennas are obviously not as good as those obtained with the complete MAARSY array. However the radiation pattern shown in figure 3.20 (a) is satisfactory enough to use this configuration for meteor trails observations until more antennas with their transceiver modules will be connected to the system. The cross section plots for azimuth angles $\phi=0^\circ$, $\phi=30^\circ$ and $\phi=120^\circ$ for those two examples of the currently assembled system can be found in the appendix as figures A.14 and A.15.

Chapter 4

Summary

Within the chapter 3 different examples of antenna arrays were described and analyzed. The objective of all models was to obtain a radiation pattern in the form of a so called "donut beam" which is useful for meteor trail observations. In the first models the intention has been to generate a rather small model to prove the general functionality of phased antenna arrays. Furthermore this structure has been studied to verify the generation of off-broadside radiation maxima. Especially in the beginning of this work it has been advantageous to handle with rather small and simple models which could have been calculated very fast. The latter models were created for the MAARSY array and its idea was to generate several individual maxima in the radiation pattern. Each of the maxima was generated by a specific group of antennas. A resultant donut beam is composed of those individual maxima and it can be also called as a multi beam approach.

The first attempts described in section 3.1 of this thesis were for a structure of 64 antennas arranged to an eight arms star array. Results obtained in this point were not satisfactory. Especially for the configuration with all antennas arranged parallel to each other which has been illustrated in figure 3.3. The example where the antennas are arranged perpendicular to the arms of the star structure (Figure 3.1) brought more promising results. However in contrast to that all antennas in the MAARSY array are aligned parallel to each other and therefore no further models of this configuration were studied as the results were disappointing.

Within the next sections models with the MAARSY array (Figure 3.5) were performed. In the first attempt to generate a donut beam the whole antenna array was divided into 4 rings (Figure 3.6) and each of the rings had its maximum of radiation to an individual zenith angle. Azimuth directions for all antennas can be found in table A1. Models were examined for various values of the zenith angle for each of the rings. Unfortunately the results were far different from the shape of the donut beam. The reason of this was that in each azimuthal direction a different amount of antennas were used. The exact description of these models can be found in the section 3.2.

Another idea was to generate 12 major beams and point them in 12 different directions (section 3.3). For this purpose the complete antenna array was divided into 12 or 18 groups containing 21 antennas each and additionally 12 groups of 3 or 5 antennas (Figure 3.8). The azimuth directions of the groups can be seen respectively in figure 3.8 and in table A.2. Attempts in this section have been examined for the structures consisting of 426, 300 or 252 antennas. Figure 3.11 shows which groups of antennas were selected for the models containing 300 and 252

antennas. The radiation patterns obtained in section 3.3 had a more symmetrical shape than radiation patterns for the structures in section 3.2. The most promising result (Figure 3.12 (a)) has been achieved with a structure containing 252 antennas. Its shape was close to a donut, but its beamwidth was not yet sufficient.

Subsequent models (section 3.4) were also created to generate 12 major beams. However, the chosen groups of antennas were formed by another method as it is shown in figure 3.13. The azimuth angles of the adjacent slices differed by 30 degrees. In section 3.4 examples were also examined with different number of antennas selected (426, 384, 312 and 234). The zenith angle for all models of this type was 30°. The radiation pattern of each of the four configurations with different number of antennas had a shape of a donut beam with different beamwidths (Figure 3.14). The following examples containing a smaller number of active antennas (a to d) had a wider beamwidth but lower gain.

Another example that was considered in section 3.4 was the structure where two different values of the zenith angle for each slice were applied (Figure 3.15). In that case the shape of the radiation pattern (Figure 3.16) was significantly different from the shape of the so called donut beam and has thus been considered as being not useful for meteor trail observations.

The next models (section 3.5) were considered for the structure created by dividing the MAARSY array into 18 pieces (Figure 3.17) and generating 18 major beams. Azimuth angles for each of the adjacent slices differ by 20 degrees. The obtained result was not satisfactory (Figure 3.17) and therefore no more instances of this structure were examined.

The last two models were created for the currently available and connected 168 out of 433 antennas (Figure 3.18). Both of those models consist of 107 antennas which are selected to achieve a circular aperture (Figure 3.19). The first example was to generate 6 main beams and in the second example nine beams were generated. The radiation pattern is more symmetric for the structure divided into 6 groups what can be seen in figure 3.20. The precise description of those two examples can be found in section 3.6.

Comparing the radiation patterns of all created models it can be concluded that the best for meteor trail observations is the radiation pattern in figure 3.14 (d). It is obtained for a structure created by dividing the complete array into 12 pieces and therefore selecting 234 out of 433 antennas. The useful part of the radiation pattern for this structure is symmetrical and it has a broad beamwidth. The gain yield from this selection of active antennas is satisfactory and is therefore proposed to be applied in the MAARSY VHF radar.

References

- [Bal05] Balanis, C. A.: *Antenna Theory*. Third Edition. John Wiley & Sons 2005.
- [Bem73] Bem D. J.: *Anteny i rozchodzenie się fal radiowych*. Wydawnictwa Naukowo-Techniczne. Warszawa 1973.
- [BP81] Burke G. J.; Poggio A. J.: *Numerical Electromagnetic Code (NEC) – Method Of Moments*. Part I. Lawrence Livermore Laboratory 1981.
- [Ceb99] Cebik L. B.: *Basic Antenna Modeling: A Hands-On Tutorial*. L. B. Cebik 1999.
- [Han09] Hansen R. C.: *Phased Array Antennas*. Second Edition. John Wiley & Sons 2009.
- [Joh93] Johnson R. C.: *Antenna Engineering Handbook*. Third edition. McGraw-Hill, 1993.
- [LSRR10] Latteck R.; Singer W.; Rapp, M.; Renkwitz T.: *MAARSY – The new MST radar on Andøya/Norway*. Geophysical Research Abstracts Vol. 12, 2010. EGU General Assembly 2010.
- [Mai94] Mailloux R. J.: *Phased Array Antenna Handbook*. Artech House London 1994.
- [NS98] Nittany Scientific, Inc.: *GNEC-4. User's Manual. Antenna Analysis Software. Version 1.1*. Nittany Scientific, Inc. 1998.
- [Orf04] Orfanidis S. J.: *Electromagnetic Waves & Antennas*. S. J. Orfanidis 2004.
- [Pie93] Pieniak J.: *Anteny Telewizyjne i Radiowe*. Wydawnictwa Komunikacji i Łączności. Warszawa 1993.
- [Ren08] Renkwitz T.: *Analysis an Optimisation of Medium Gain X-Yagi Antennas for the EISCAT_3D 237.5 MHz Incoherent Scatter Radar Active Array*. Master-Thesis 2008.
- [RMOK82] Rudge A. W.; Milne K.; Olver A. D.; Knight P.: *The Handbook of Antenna Design*. Volume I. Peter Peregrinus Ltd. 1982.
- [Sch07] Schöch A.: *Thermal structure and gravity waves in the Arctic middle atmosphere above ALOMAR (69.3° N, 16.0° E)*. Ph.D. – Thesis 2007.
- [SMO⁺06] Sarkar T. K.; Mailloux R. J.; Oliner A. A.; Salazar-Palma M.; Sengupta D. L.: *History of Wireless*. John Wiley & Sons 2006. P. 462-466.
- [Stu81] Stutzman W. L.: *Antenna Theory and Design*. John Wiley & Sons 1981.
- [Szo01] Szóstka J.: *Fale i Anteny*. Wydawnictwa Komunikacji i Łączności. Warszawa 2001.
- [Zie01] Zieniutycz W.: *Anteny. Podstawy polowe*. Wydawnictwa Komunikacji i Łączności. Warszawa 2001.

Appendix

Figures and tables

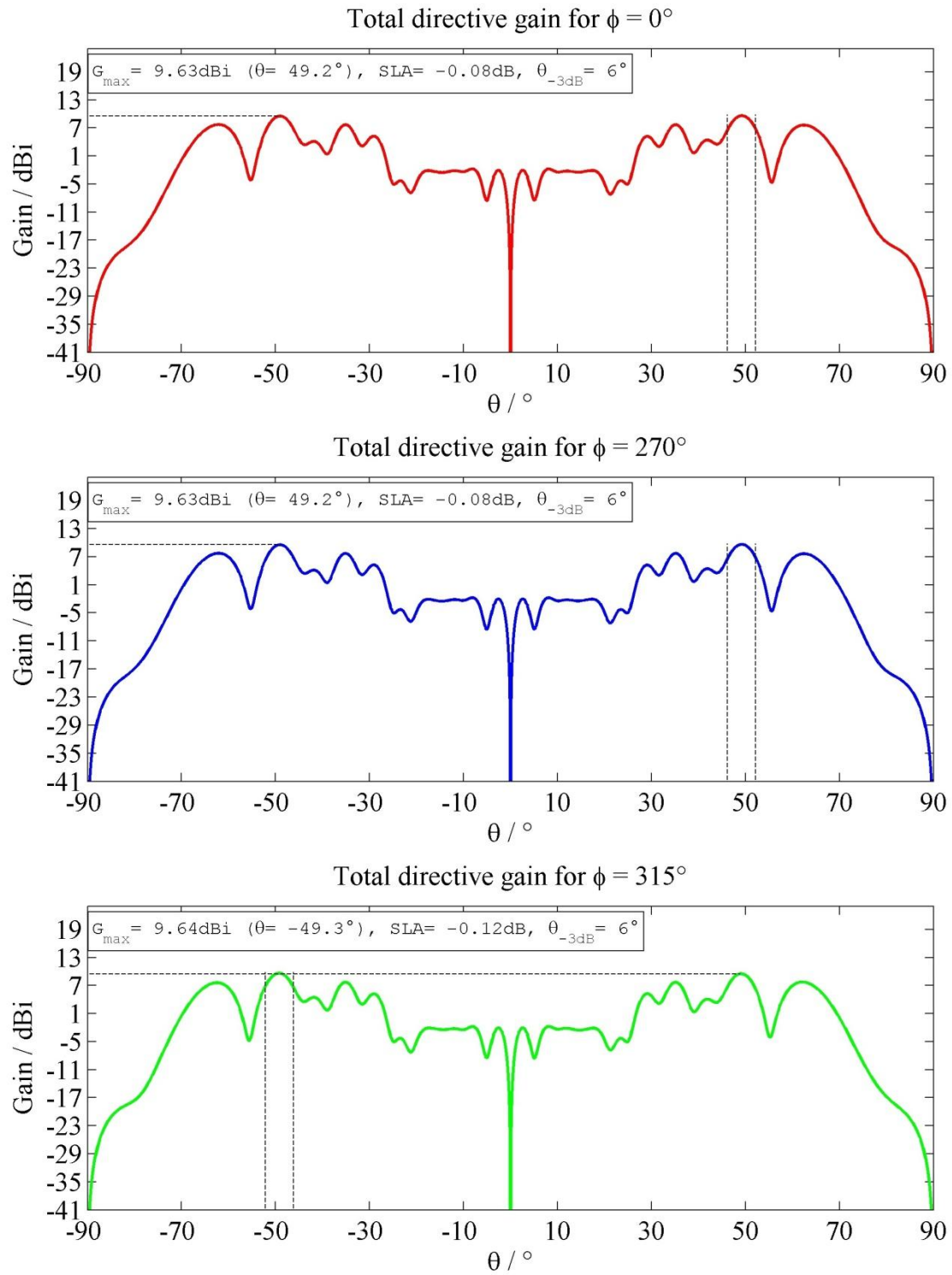


Figure A.1. Cross section plots for a 64-antenna star structure – antennas aligned perpendicular to arms.

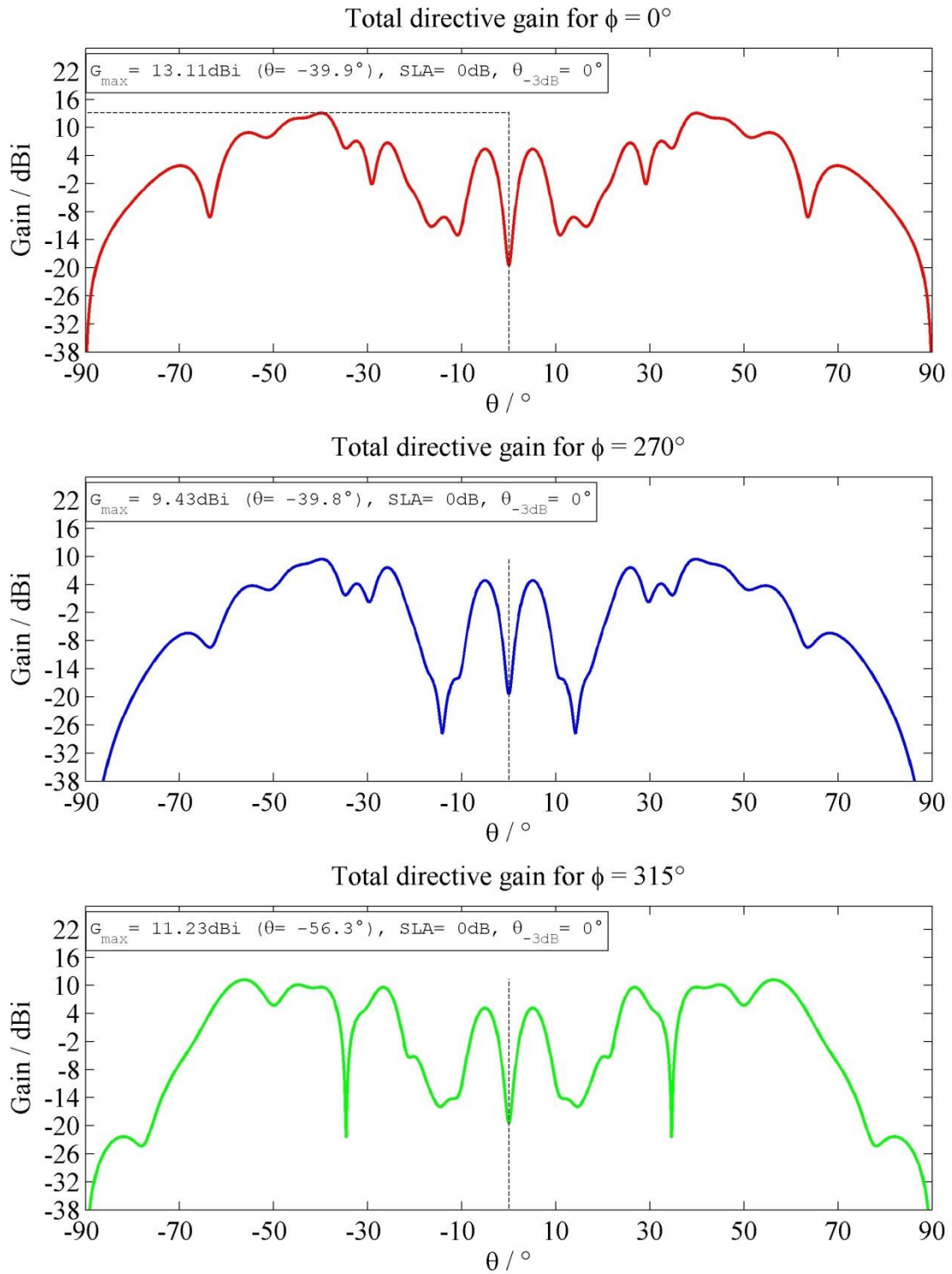


Figure A.2. Cross section plots for a 64-antenna star structure – example 2a (feeding with equal phasing in each arm).

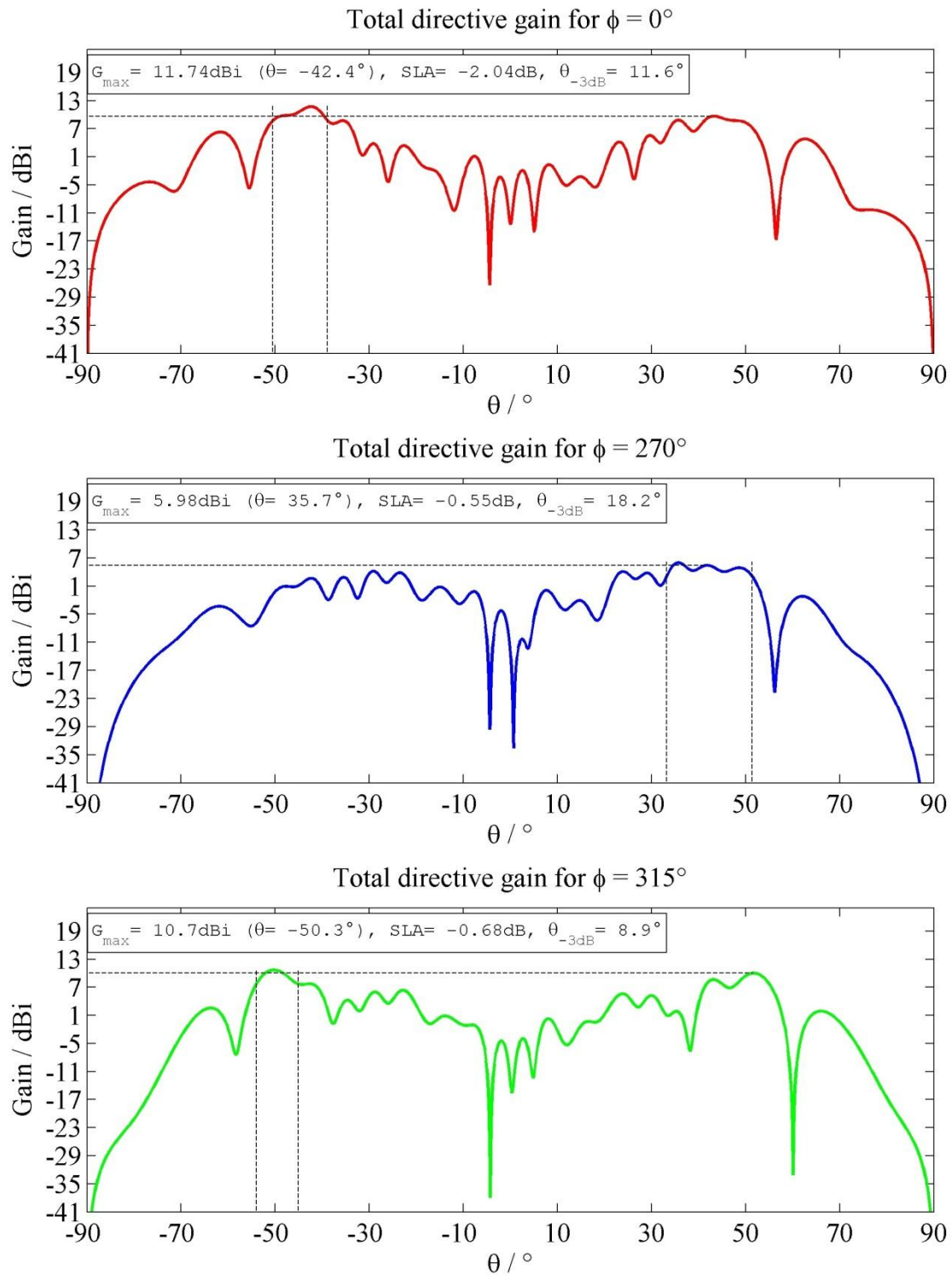


Figure A.3. Cross section plots for a 64-antenna star structure – example 2b (feeding with different phasing in each arm).

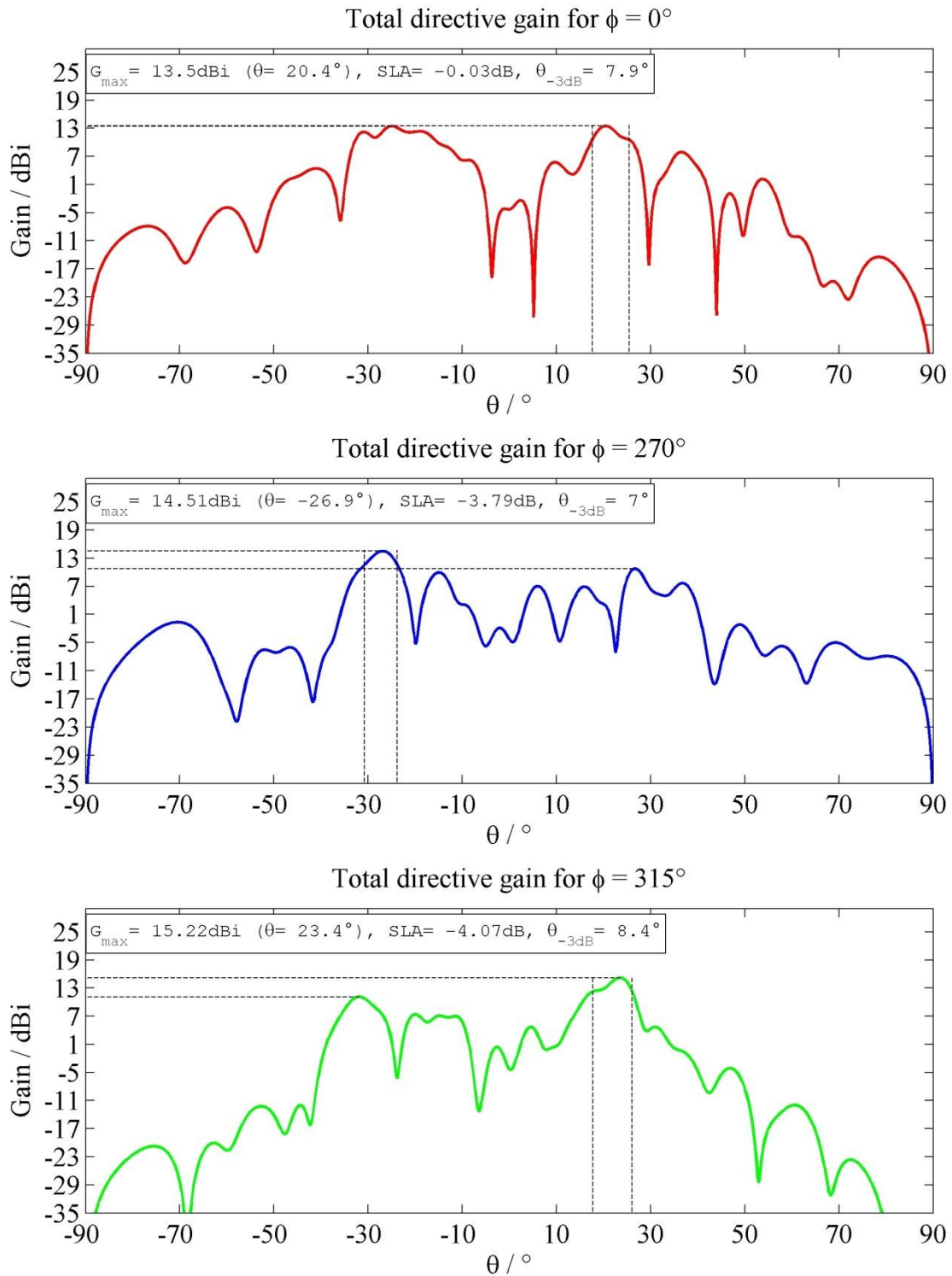


Figure A.4. Cross section plots for the radiation pattern for the MAARSY array divided into groups and 426 antennas selected – example 1.

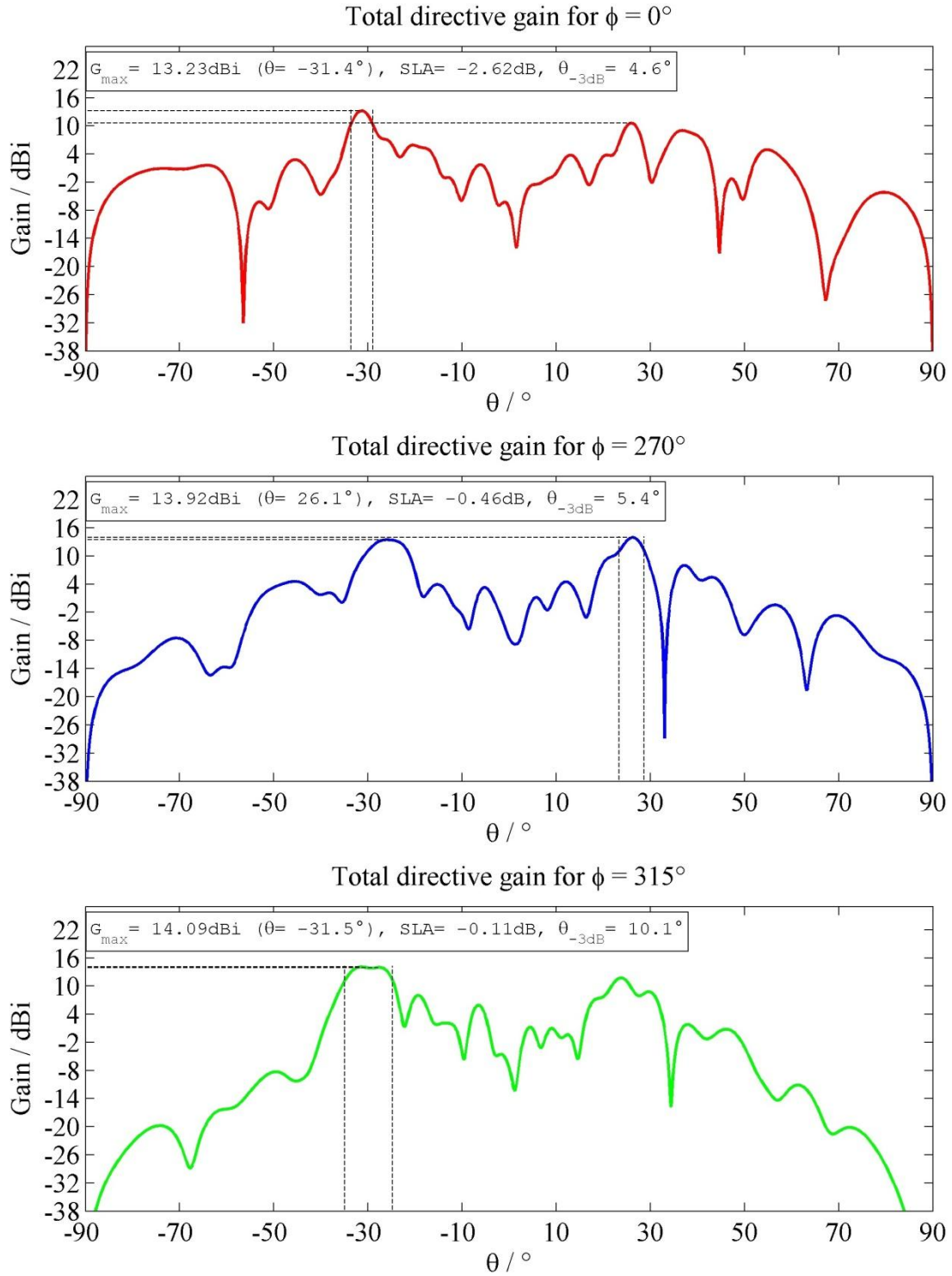


Figure A.5. Cross section plots for the radiation pattern for the MAARSY array divided into groups and 426 antennas selected – example 2.

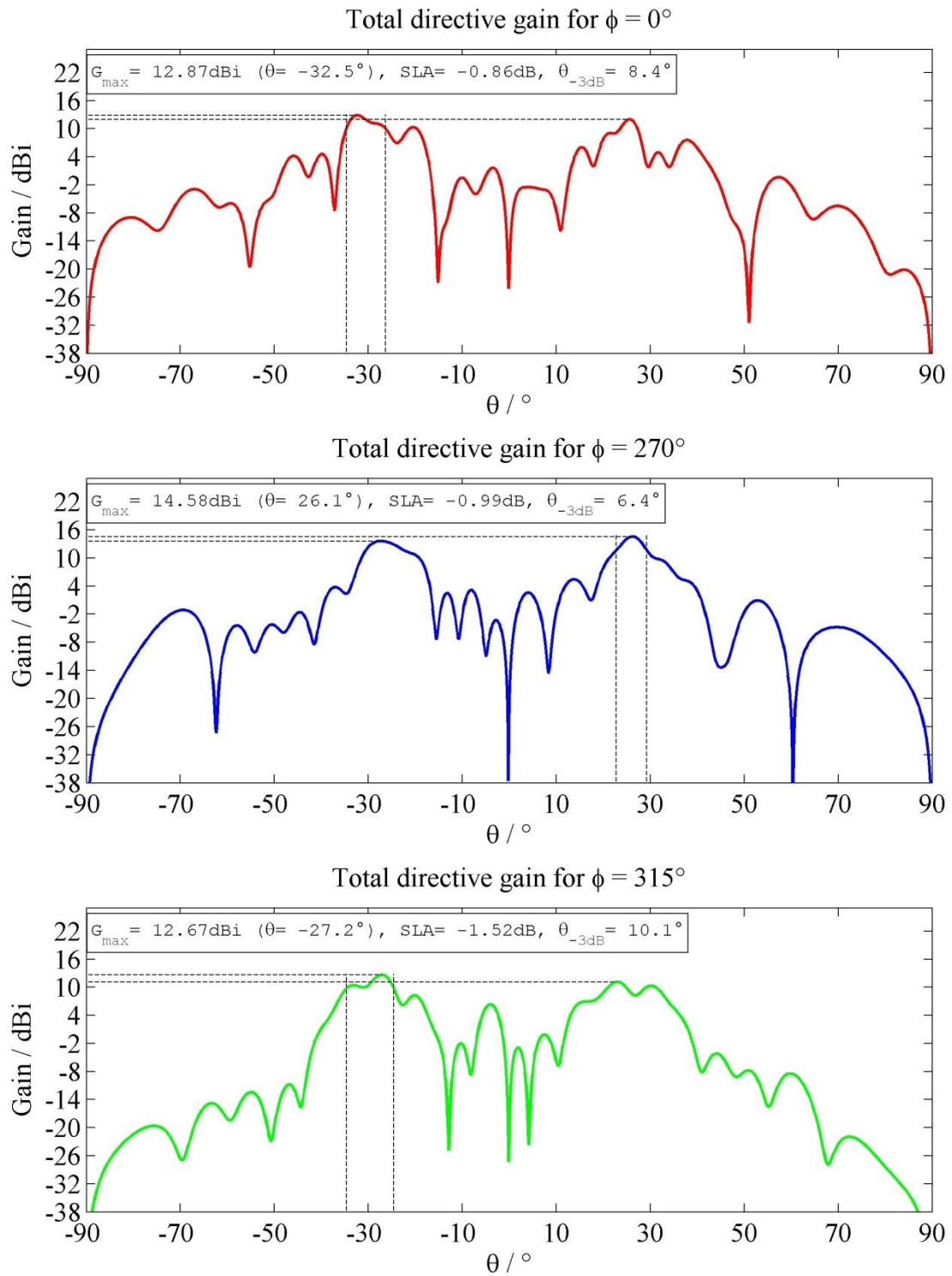


Figure A.6. Cross section plots for the radiation pattern for the MAARSY array divided into groups and 252 antennas selected.

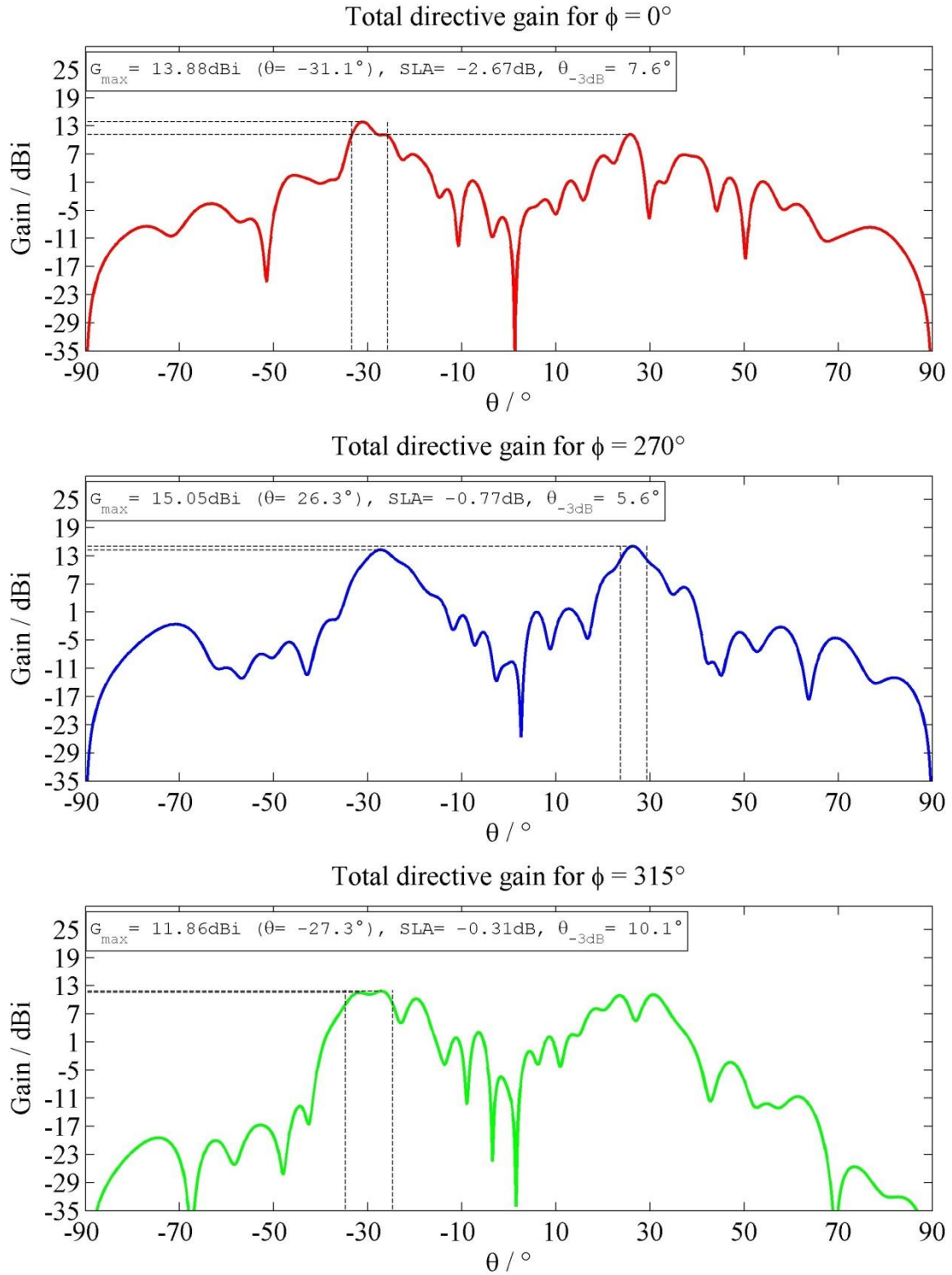


Figure A.7. Cross section plots for the radiation pattern the MAARSY array divided into groups and 300 antennas selected.

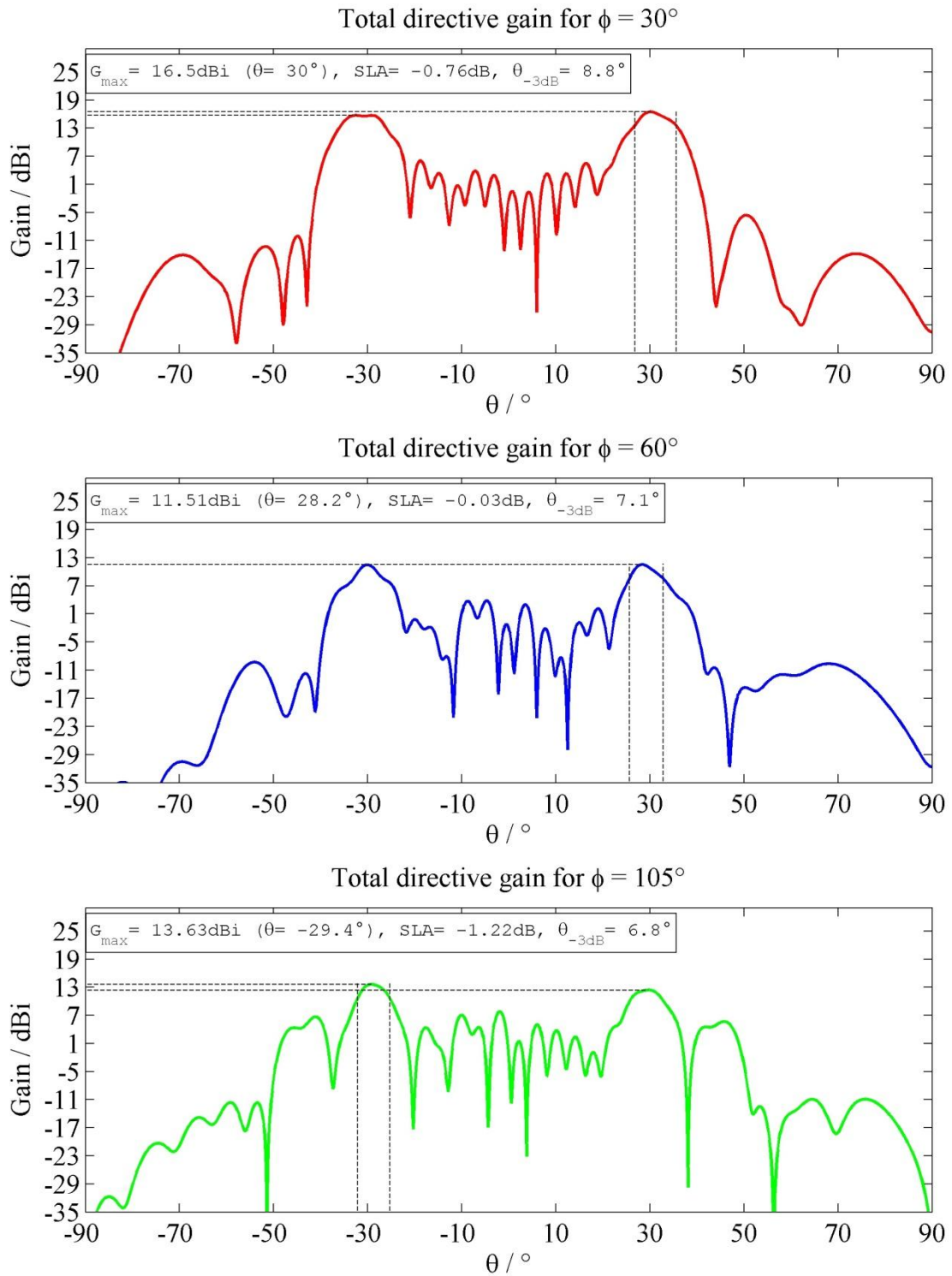


Figure A.8. Cross section plots for the radiation pattern the MAARSY array divided into 12 slices and 426 antennas selected.

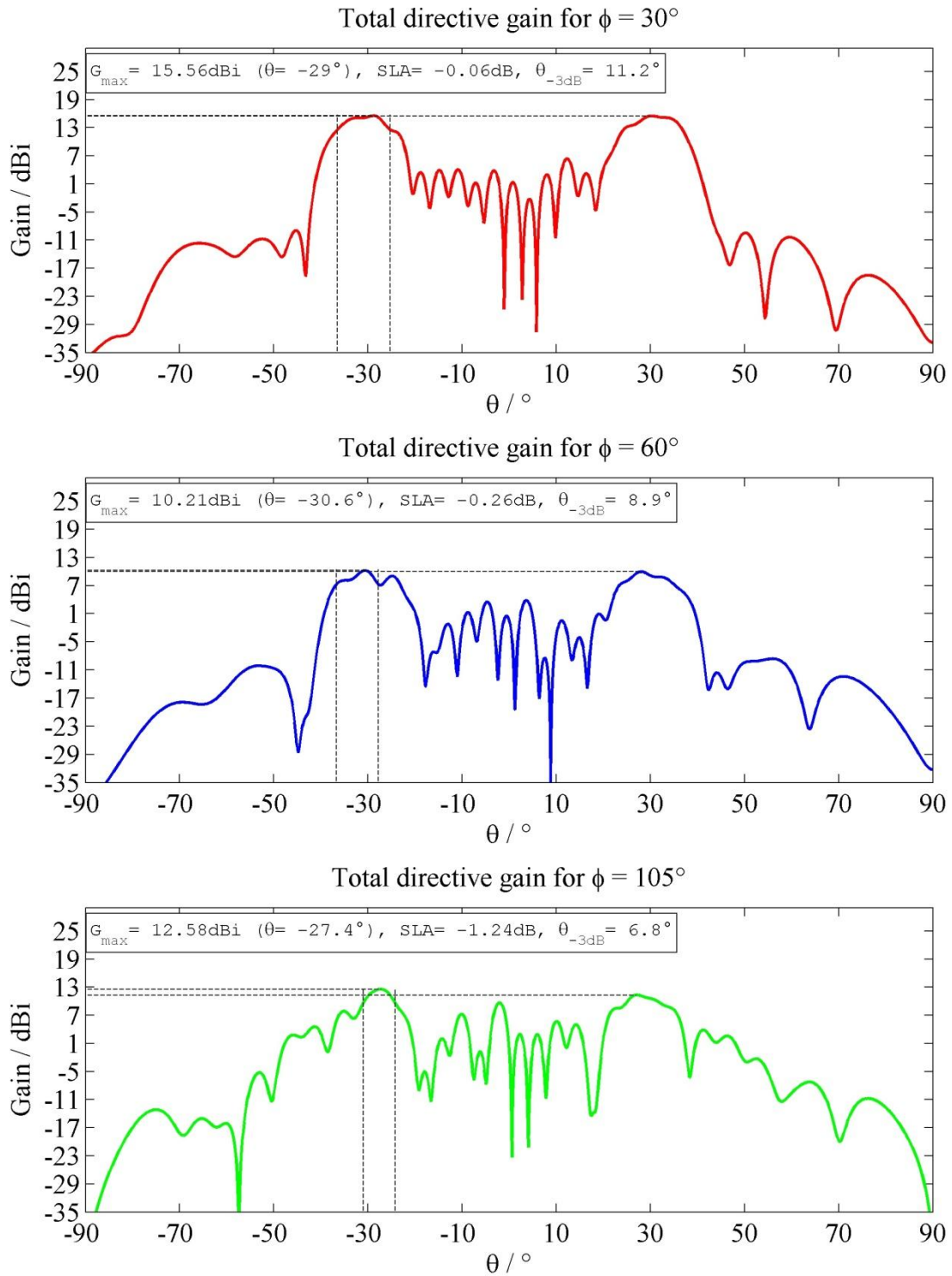


Figure A.9. Cross section plots for the radiation pattern the MAARSY array divided into 12 slices and 384 antennas selected.

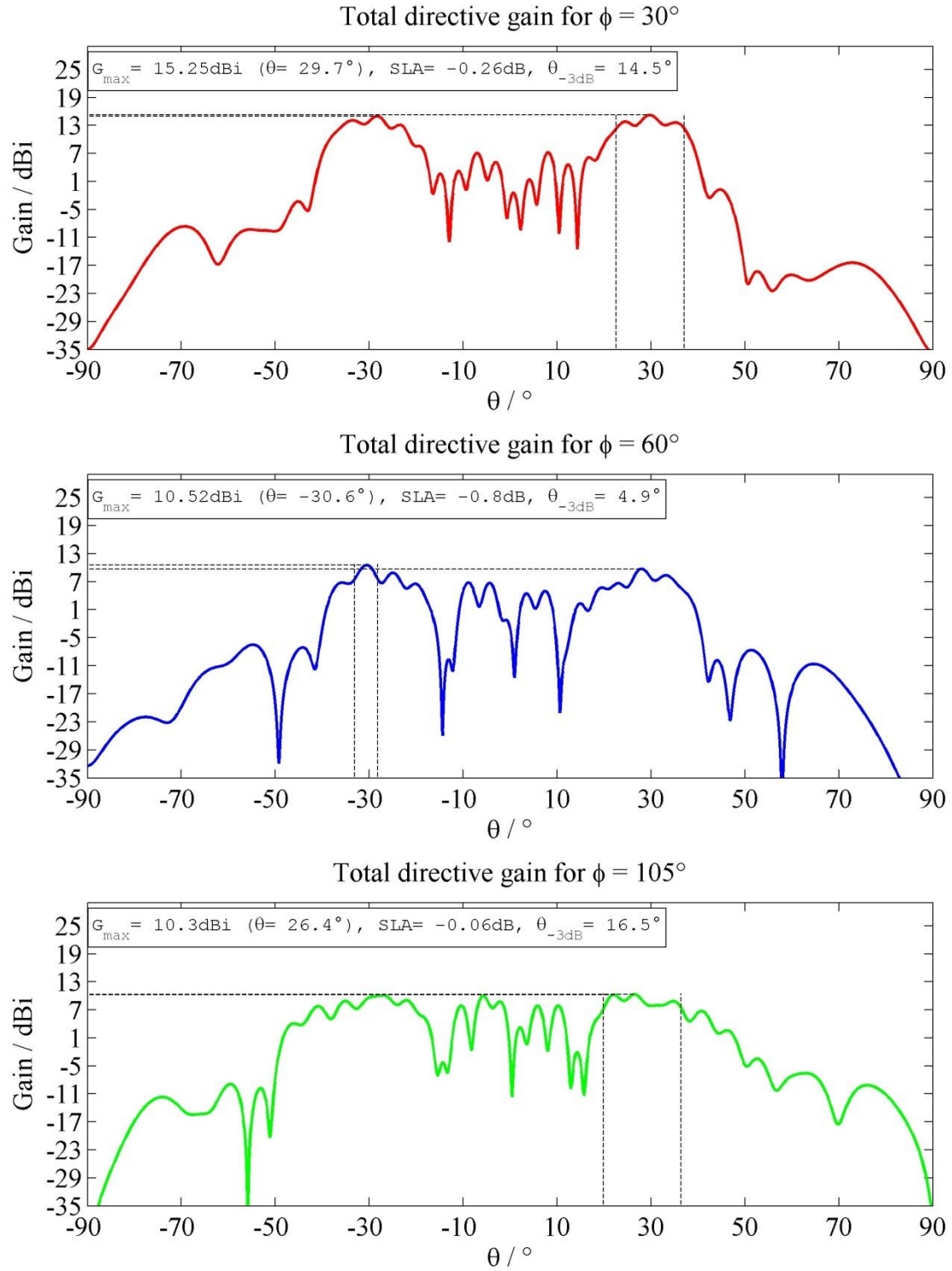


Figure A.10. Cross section plots for the radiation pattern the MAARSY array divided into 12 slices and 312 antennas selected.

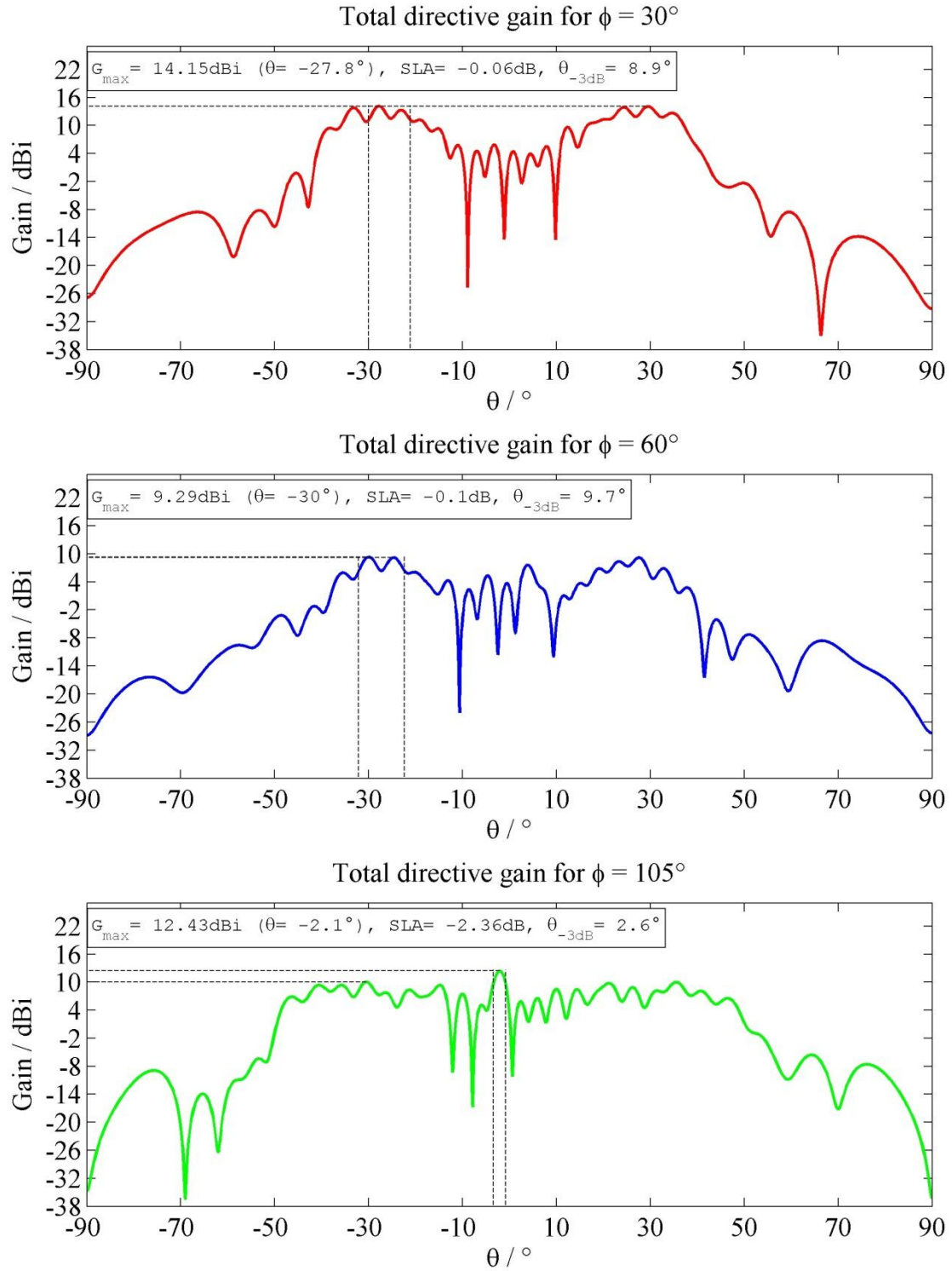


Figure A.11. Cross section plots for the radiation pattern the MAARSY array divided into 12 slices and 234 antennas selected.

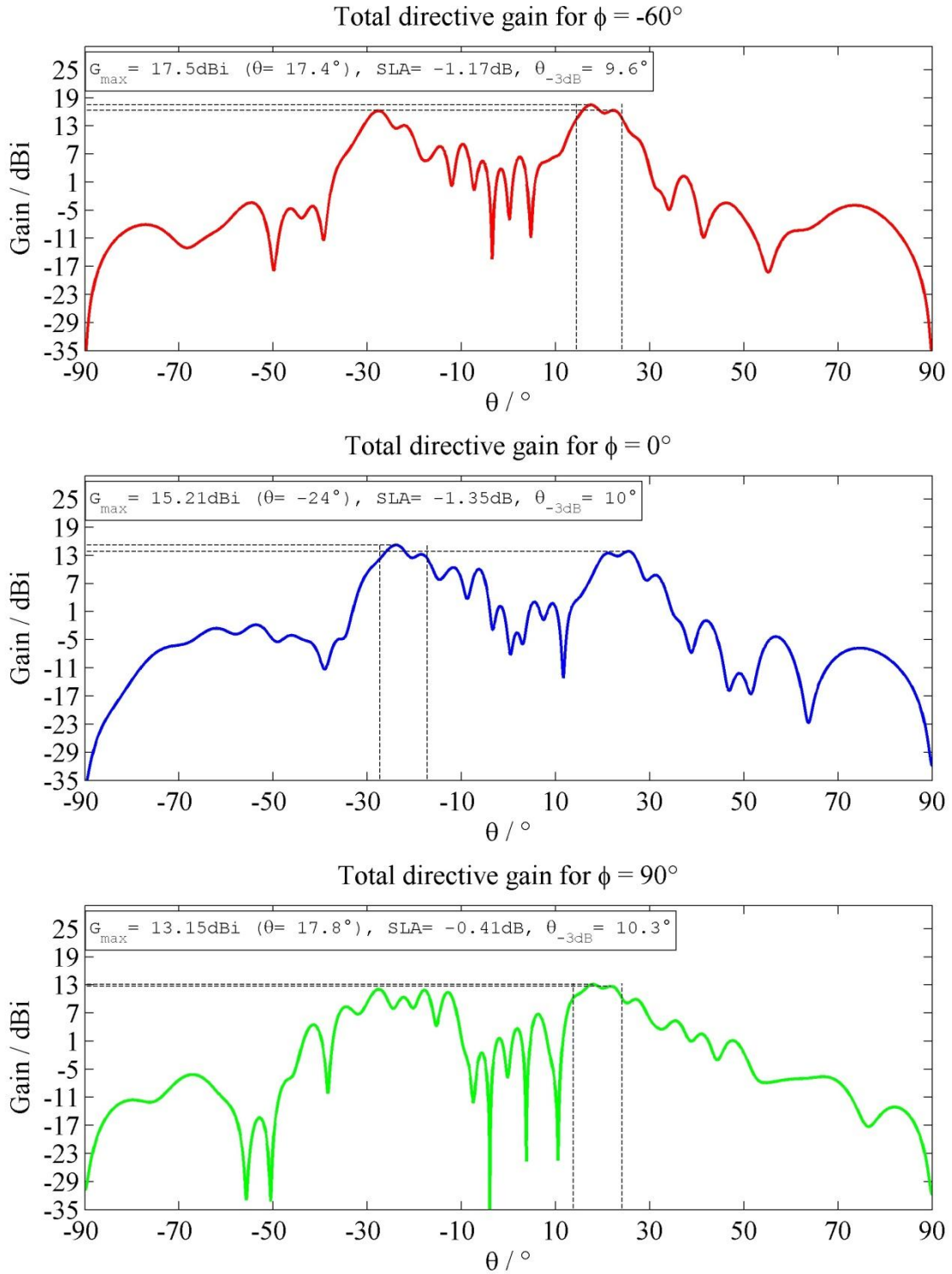


Figure A.12. Cross section plots for the radiation pattern the MAARSY array divided into 12 slices and 2 values of a zenith angle in each slice applied – instance 1.

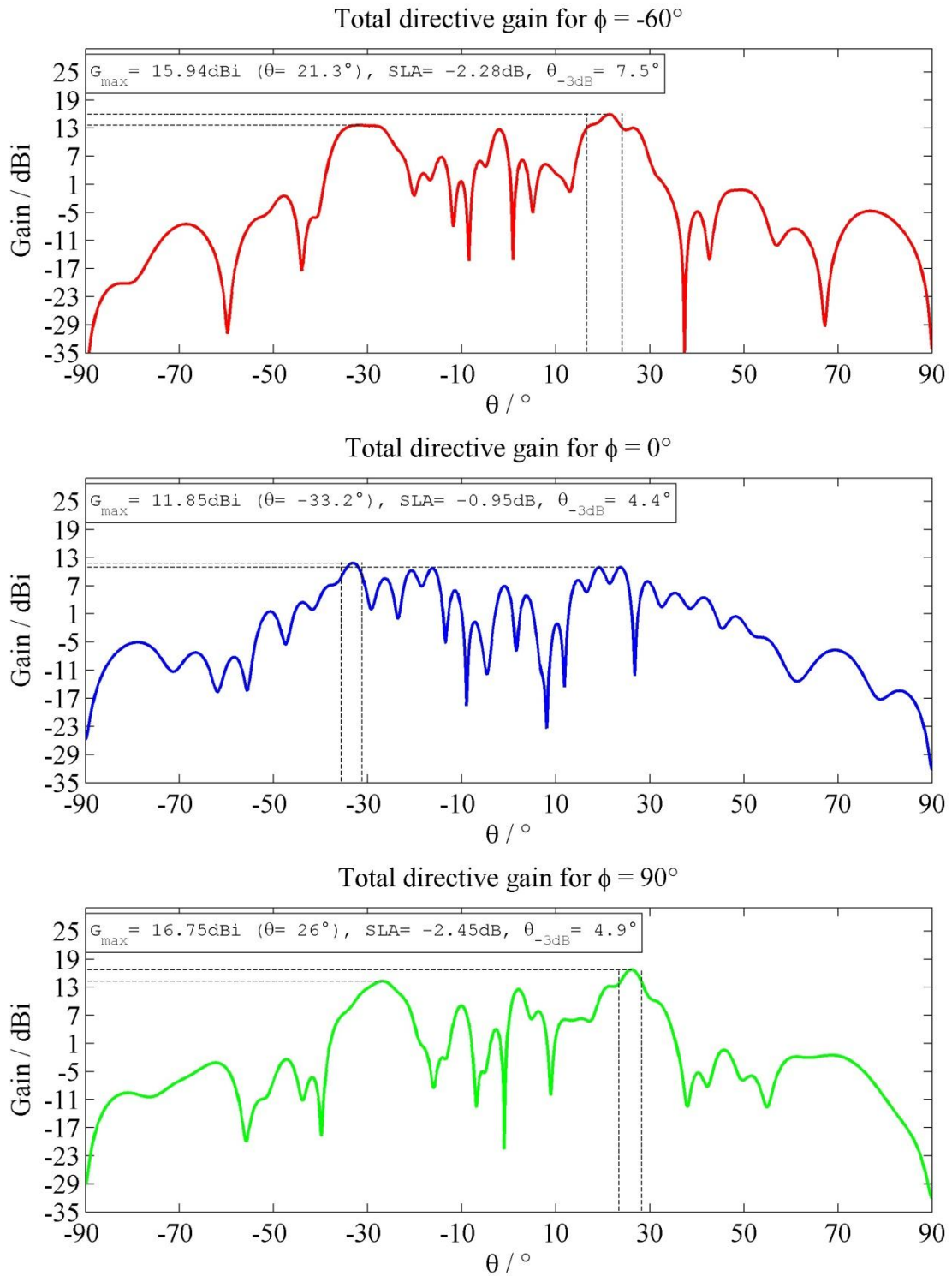


Figure A.13. Cross section plots for the radiation pattern the MAARSY array divided into 12 slices and 2 values of a zenith angle in each slice applied – instance 2.

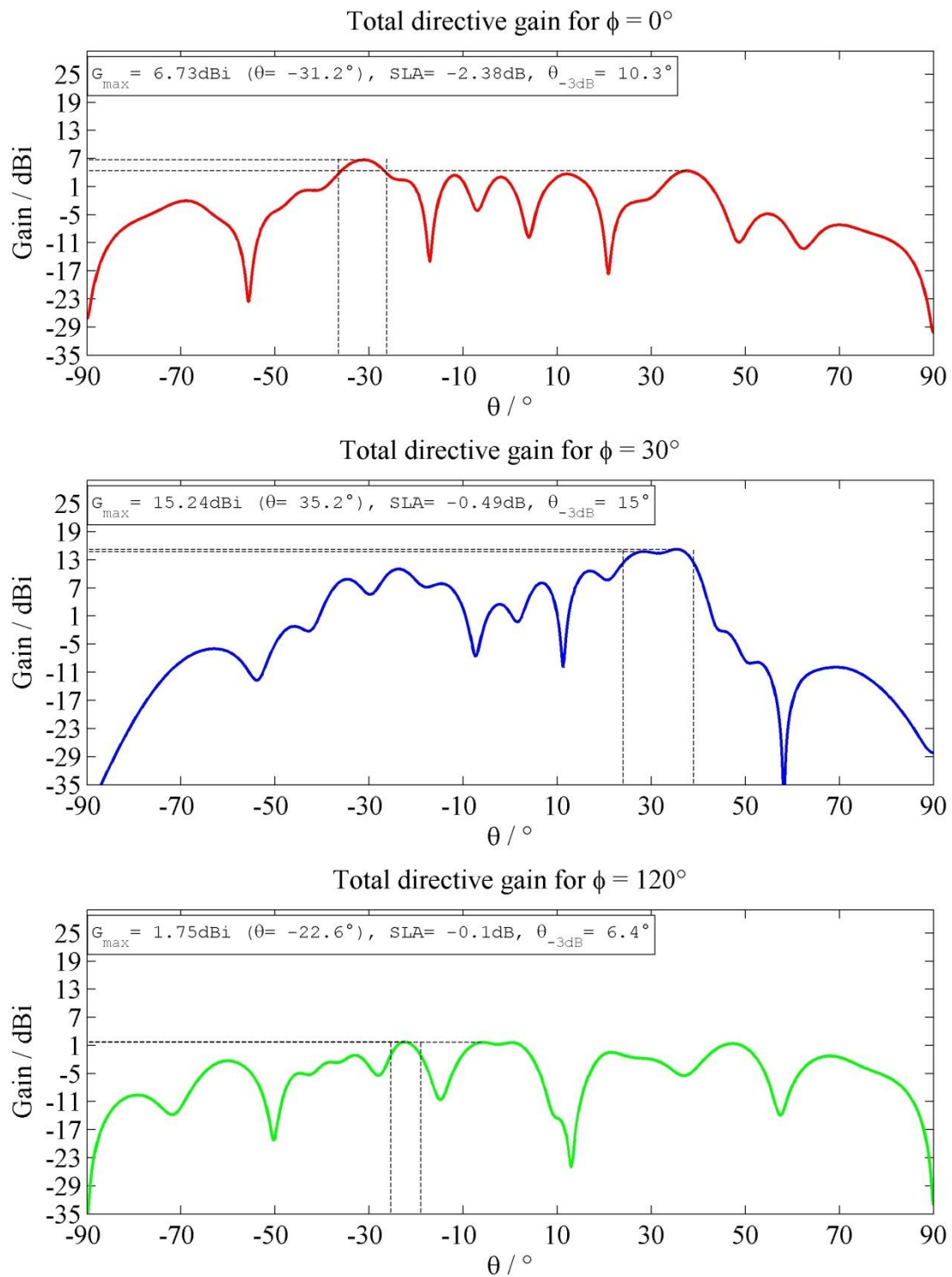


Figure A.14. Cross section plots for the radiation pattern for the actual state of the MAARSY radar with 6 main beams generated.

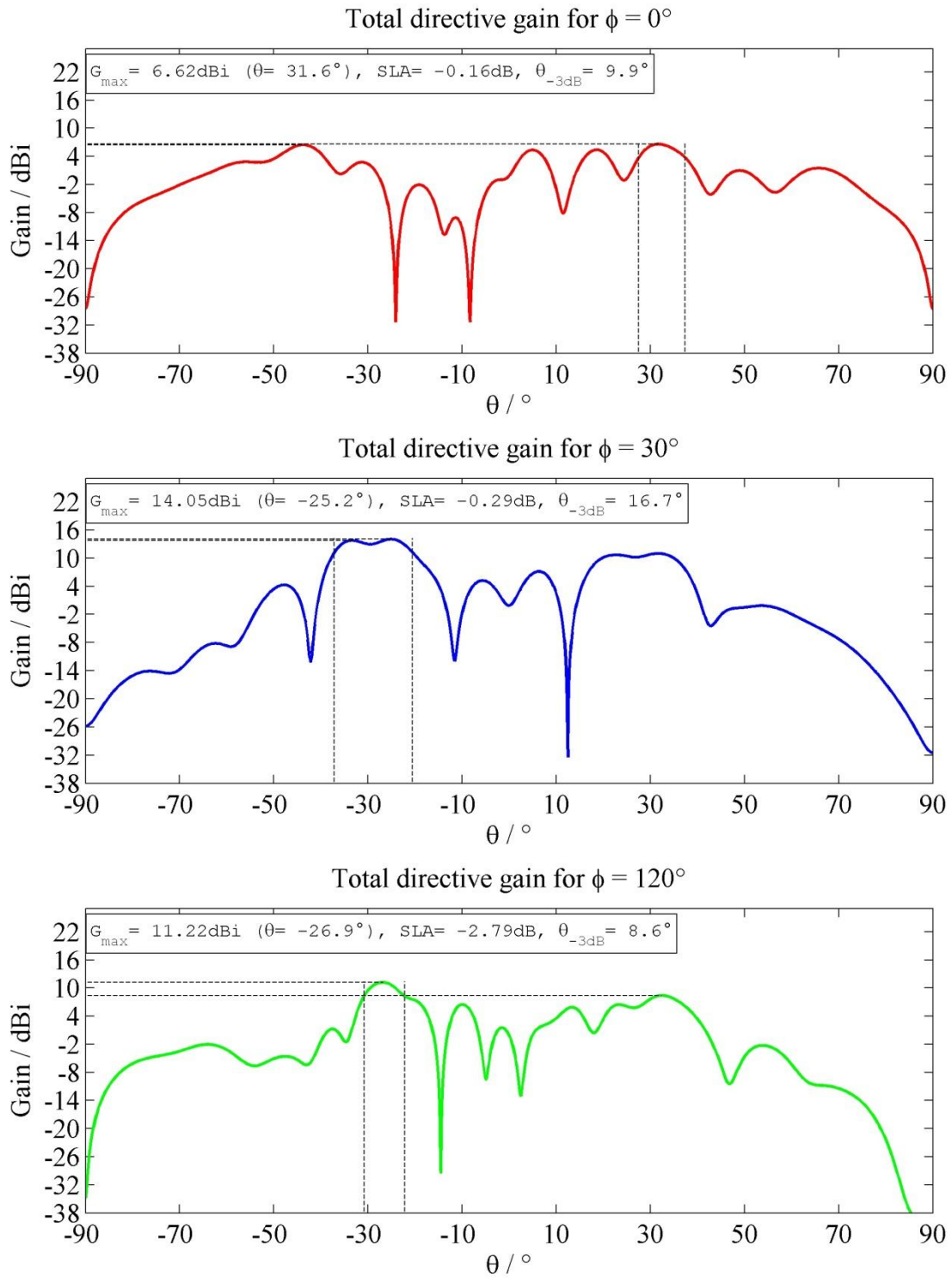


Figure A.15. Cross section plots for the radiation pattern for the actual state of the MAARSY radar with 9 main beams generated.

Subarray (antenna)	θ°	ϕ°	Subarray (antenna)	θ°	ϕ°
A-01- (1-7)	30°	9°	D-01- (1-7)	30°	189°
A-02- (1-7)	25°	355°	D-02- (1-7)	25°	175°
A-03- (1-7)	25°	14°	D-03- (1-7)	25°	194°
A-04- (1-7)	20°	355°	D-04- (1-7)	20°	175°
A-05- (1-7)	20°	25°	D-05- (1-7)	20°	205°
A-06- (1-7)	25°	36°	D-06- (1-7)	25°	216°
A-07- (1-7)	30°	25°	D-07- (1-7)	30°	205°
A-08- (1-7)	30°	41°	D-08- (1-7)	30°	221°
A-09- (1-7)	15°	355°	D-09- (1-7)	15°	175°
A-10- (1-5)	30°	355°	D-10- (1-5)	30°	175°
A-10- (6)	30°	41°	D-10- (6)	30°	221°
A-10- (7-8)	30°	25°	D-10- (7-8)	30°	205°
B-01- (1-7)	30°	69°	E-01- (1-7)	30°	249°
B-02- (1-7)	25°	55°	E-02- (1-7)	25°	235°
B-03- (1-7)	25°	74°	E-03- (1-7)	25°	254°
B-04- (1-7)	20°	55°	E-04- (1-7)	20°	235°
B-05- (1-7)	20°	85°	E-05- (1-7)	20°	265°
B-06- (1-7)	25°	96°	E-06- (1-7)	25°	275°
B-07- (1-7)	30°	85°	E-07- (1-7)	30°	265°
B-08- (1-7)	30°	101°	E-08- (1-7)	30°	281°
B-09- (1-7)	15°	55°	E-09- (1-7)	15°	235°
B-10- (1-5)	30°	55°	E-10- (1-5)	30°	235°
B-10- (6)	30°	101°	E-10- (6)	30°	281°
B-10- (7-8)	30°	85°	E-10- (7-8)	30°	265°
C-01- (1-7)	30°	129°	F-01- (1-7)	30°	309°
C-02- (1-7)	25°	115°	F-02- (1-7)	25°	295°
C-03- (1-7)	25°	133°	F-03- (1-7)	25°	314°
C-04- (1-7)	20°	115°	F-04- (1-7)	20°	295°
C-05- (1-7)	20°	145°	F-05- (1-7)	20°	325°
C-06- (1-7)	25°	155°	F-06- (1-7)	25°	336°
C-07- (1-7)	30°	145°	F-07- (1-7)	30°	325°
C-08- (1-7)	30°	161°	F-08- (1-7)	30°	341°
C-09- (1-7)	15°	115°	F-09- (1-7)	15°	295°
C-10- (1-5)	30°	115°	F-10- (1-5)	30°	295°
C-10- (6)	30°	161°	F-10- (6)	30°	341°
C-10- (7-8)	30°	145°	F-10- (7-8)	30°	325°
-----	-----	-----	F-11- (1-7)	0°	0°

Table A.1. Zenith (θ) and azimuth (ϕ) angles for the structure shown in figure 3.6 – configuration 1.

Subarray (antenna)	θ°	ϕ°	Subarray (antenna)	θ°	ϕ°
A-01- (1-7)	30°	6°	D-01- (1-7)	30°	186°
A-02- (1-7)	30°	6°	D-02- (1-7)	30°	186°
A-03- (1-7)	30°	6°	D-03- (1-7)	30°	186°
A-04- (1-7)	20°	6°	D-04- (1-7)	20°	186°
A-05- (1-7)	20°	6°	D-05- (1-7)	20°	186°
A-06- (1-7)	30°	34°	D-06- (1-7)	30°	214°
A-07- (1-7)	30°	34°	D-07- (1-7)	30°	214°
A-08- (1-7)	30°	34°	D-08- (1-7)	30°	214°
A-09- (1-7)	20°	6°	D-09- (1-7)	20°	186°
A-10- (1-5)	30°	6°	D-10- (1-5)	30°	186°
A-10- (6-8)	30°	34°	D-10- (6-8)	30°	214°
B-01- (1-7)	30°	66°	E-01- (1-7)	30°	246°
B-02- (1-7)	30°	66°	E-02- (1-7)	30°	246°
B-03- (1-7)	30°	66°	E-03- (1-7)	30°	246°
B-04- (1-7)	20°	66°	E-04- (1-7)	20°	246°
B-05- (1-7)	20°	66°	E-05- (1-7)	20°	246°
B-06- (1-7)	30°	94°	E-06- (1-7)	30°	274°
B-07- (1-7)	30°	94°	E-07- (1-7)	30°	274°
B-08- (1-7)	30°	94°	E-08- (1-7)	30°	274°
B-09- (1-7)	20°	66°	E-09- (1-7)	20°	246°
B-10- (1-5)	30°	66°	E-10- (1-5)	30°	246°
B-10- (6-8)	30°	94°	E-10- (6-8)	30°	274°
C-01- (1-7)	30°	126°	F-01- (1-7)	30°	306°
C-02- (1-7)	30°	126°	F-02- (1-7)	30°	306°
C-03- (1-7)	30°	126°	F-03- (1-7)	30°	306°
C-04- (1-7)	20°	126°	F-04- (1-7)	20°	306°
C-05- (1-7)	20°	126°	F-05- (1-7)	20°	306°
C-06- (1-7)	30°	154°	F-06- (1-7)	30°	334°
C-07- (1-7)	30°	154°	F-07- (1-7)	30°	334°
C-08- (1-7)	30°	154°	F-08- (1-7)	30°	334°
C-09- (1-7)	20°	126°	F-09- (1-7)	20°	306°
C-10- (1-5)	30°	126°	F-10- (1-5)	30°	306°
C-10- (6-8)	30°	154°	F-10- (6-8)	30°	334°

Table A.2. Zenith (θ) and azimuth (ϕ) angles for the array consisting of 426 antennas for the generation of 12 beams – example 1.

Subarray (antenna)	θ°	ϕ°	Subarray (antenna)	θ°	ϕ°
A-01- (1-7)	30°	6°	D-01- (1-7)	30°	186°
A-02- (1-7)	30°	6°	D-02- (1-7)	30°	186°
A-03- (1-7)	30°	6°	D-03- (1-7)	30°	186°
A-06- (1-7)	30°	34°	D-06- (1-7)	30°	214°
A-07- (1-7)	30°	34°	D-07- (1-7)	30°	214°
A-08- (1-7)	30°	34°	D-08- (1-7)	30°	214°
B-01- (1-7)	30°	66°	E-01- (1-7)	30°	246°
B-02- (1-7)	30°	66°	E-02- (1-7)	30°	246°
B-03- (1-7)	30°	66°	E-03- (1-7)	30°	246°
B-06- (1-7)	30°	94°	E-06- (1-7)	30°	274°
B-07- (1-7)	30°	94°	E-07- (1-7)	30°	274°
B-08- (1-7)	30°	94°	E-08- (1-7)	30°	274°
C-01- (1-7)	30°	126°	F-01- (1-7)	30°	306°
C-02- (1-7)	30°	126°	F-02- (1-7)	30°	306°
C-03- (1-7)	30°	126°	F-03- (1-7)	30°	306°
C-06- (1-7)	30°	154°	F-06- (1-7)	30°	334°
C-07- (1-7)	30°	154°	F-07- (1-7)	30°	334°
C-08- (1-7)	30°	154°	F-08- (1-7)	30°	334°

Table A.3. Zenith (θ) and azimuth (ϕ) angles for the array consisting of 252 antennas for the generation of 12 beams.

Subarray (antenna)	θ°	ϕ°	Subarray (antenna)	θ°	ϕ°
A-01- (1-7)	30°	6°	D-01- (1-7)	30°	186°
A-02- (1-7)	30°	6°	D-02- (1-7)	30°	186°
A-03- (1-7)	30°	6°	D-03- (1-7)	30°	186°
A-06- (1-7)	30°	34°	D-06- (1-7)	30°	214°
A-07- (1-7)	30°	34°	D-07- (1-7)	30°	214°
A-08- (1-7)	30°	34°	D-08- (1-7)	30°	214°
A-10- (1-5)	30°	6°	D-10- (1-5)	30°	186°
A-10- (6-8)	30°	34°	D-10- (6-8)	30°	214°
B-01- (1-7)	30°	66°	E-01- (1-7)	30°	246°
B-02- (1-7)	30°	66°	E-02- (1-7)	30°	246°
B-03- (1-7)	30°	66°	E-03- (1-7)	30°	246°
B-06- (1-7)	30°	94°	E-06- (1-7)	30°	274°
B-07- (1-7)	30°	94°	E-07- (1-7)	30°	274°
B-08- (1-7)	30°	94°	E-08- (1-7)	30°	274°
B-10- (1-5)	30°	66°	E-10- (1-5)	30°	246°
B-10- (6-8)	30°	94°	E-10- (6-8)	30°	274°
C-01- (1-7)	30°	126°	F-01- (1-7)	30°	306°
C-02- (1-7)	30°	126°	F-02- (1-7)	30°	306°
C-03- (1-7)	30°	126°	F-03- (1-7)	30°	306°
C-06- (1-7)	30°	154°	F-06- (1-7)	30°	334°
C-07- (1-7)	30°	154°	F-07- (1-7)	30°	334°
C-08- (1-7)	30°	154°	F-08- (1-7)	30°	334°
C-10- (1-5)	30°	126°	F-10- (1-5)	30°	306°
C-10- (6-8)	30°	154°	F-10- (6-8)	30°	334°

Table A.4. Zenith (θ) and azimuth (ϕ) angles for the array consisting of 300 antennas for the generation of 12 beams.

Subarray (antenna)	θ°	ϕ°	Subarray (antenna)	θ°	ϕ°
A-01- (1-7)	30°	15°	D-01- (1-7)	30°	195°
A-02- (1, 7)	30°	15°	D-02- (1, 7)	30°	195°
A-02- (2-6)	30°	345°	D-02- (2-6)	30°	165°
A-03- (1-7)	30°	15°	D-03- (1-7)	30°	195°
A-04- (1, 2)	30°	15°	D-04- (1, 2)	30°	195°
A-04- (3-7)	30°	345°	D-04- (3-7)	30°	165°
A-05- (1, 2, 3, 6, 7)	30°	15°	D-05- (1, 2, 3, 6, 7)	30°	195°
A-05- (4, 5)	30°	45°	D-05- (4, 5)	30°	225°
A-06- (1, 3-7)	30°	45°	D-06- (1, 3-7)	30°	225°
A-06- (2)	30°	15°	D-06- (2)	30°	195°
A-07- (1)	30°	45°	D-07- (1)	30°	225°
A-07- (2-7)	30°	15°	D-07- (2-7)	30°	195°
A-08- (1-7)	30°	45°	D-08- (1-7)	30°	225°
A-09- (1, 6, 7)	30°	15°	D-09- (1, 6, 7)	30°	195°
A-09- (2-5)	30°	345°	D-09- (2-5)	30°	165°
A-10- (1-4)	30°	345°	D-10- (1-4)	30°	165°
A-10- (5, 7, 8)	30°	15°	D-10- (5, 7, 8)	30°	195°
A-10- (6)	30°	45°	D-10- (6)	30°	225°
B-01- (1-7)	30°	75°	E-01- (1-7)	30°	255°
B-02- (1, 7)	30°	75°	E-02- (1, 7)	30°	255°
B-02- (2-6)	30°	45°	E-02- (2-6)	30°	225°
B-03- (1-7)	30°	75°	E-03- (1-7)	30°	255°
B-04- (1, 2)	30°	75°	E-04- (1, 2)	30°	255°
B-04- (3-7)	30°	45°	E-04- (3-7)	30°	225°
B-05- (1, 2, 3, 6, 7)	30°	75°	E-05- (1, 2, 3, 6, 7)	30°	255°
B-05- (4, 5)	30°	105°	E-05- (4, 5)	30°	285°
B-06- (1, 3-7)	30°	105°	E-06- (1, 3-7)	30°	285°
B-06- (2)	30°	75°	E-06- (2)	30°	255°
B-07- (1)	30°	105°	E-07- (1)	30°	285°
B-07- (2-7)	30°	75°	E-07- (2-7)	30°	255°
B-08- (1-7)	30°	105°	E-08- (1-7)	30°	285°
B-09- (1, 6, 7)	30°	75°	E-09- (1, 6, 7)	30°	255°
B-09- (2-5)	30°	45°	E-09- (2-5)	30°	225°
B-10- (1-4)	30°	45°	E-10- (1-4)	30°	225°
B-10- (5, 7, 8)	30°	75°	E-10- (5, 7, 8)	30°	255°
B-10- (6)	30°	105°	E-10- (6)	30°	285°
C-01- (1-7)	30°	135°	F-01- (1-7)	30°	315°
C-02- (1, 7)	30°	135°	F-02- (1, 7)	30°	315°
C-02- (2-6)	30°	105°	F-02- (2-6)	30°	285°
C-03- (1-7)	30°	135°	F-03- (1-7)	30°	315°
C-04- (1, 2)	30°	135°	F-04- (1, 2)	30°	315°
C-04- (3-7)	30°	105°	F-04- (3-7)	30°	285°
C-05- (1, 2, 3, 6, 7)	30°	135°	F-05- (1, 2, 3, 6, 7)	30°	315°
C-05- (4, 5)	30°	165°	F-05- (4, 5)	30°	345°
C-06- (1, 3- 7)	30°	165°	F-06- (1, 3-7)	30°	345°
C-06- (2)	30°	135°	F-06- (2)	30°	315°
C-07- (1)	30°	165°	F-07- (1)	30°	345°
C-07- (2-7)	30°	135°	F-07- (2-7)	30°	315°
C-08- (1-7)	30°	165°	F-08- (1-7)	30°	345°
C-09- (1, 6, 7)	30°	135°	F-09- (1, 6, 7)	30°	315°
C-09- (2-5)	30°	105°	F-09- (2-5)	30°	315°
C-10- (1-4)	30°	105°	F-10- (1-4)	30°	315°
C-10- (5, 7, 8)	30°	135°	F-10- (5, 7, 8)	30°	315°
C-10- (6)	30°	165°	F-10- (6)	30°	345°

Table A.5. Zenith (θ) and azimuth (ϕ) angles for the MAARSY array divided into 12 slices and 426 antennas selected.

Subarray (antenna)	θ°	ϕ°	Subarray (antenna)	θ°	ϕ°
A-01- (1-7)	30°	15°	D-01- (1-7)	30°	195°
A-02- (1, 7)	30°	15°	D-02- (1, 7)	30°	195°
A-02- (2-6)	30°	345°	D-02- (2-6)	30°	165°
A-03- (1-7)	30°	15°	D-03- (1-7)	30°	195°
A-04- (1, 2)	30°	15°	D-04- (1, 2)	30°	195°
A-04- (3-7)	30°	345°	D-04- (3-7)	30°	165°
A-05- (1, 2, 3, 6, 7)	30°	15°	D-05- (1, 2, 3, 6, 7)	30°	195°
A-05- (4, 5)	30°	45°	D-05- (4, 5)	30°	225°
A-06- (1, 3-7)	30°	45°	D-06- (1, 3-7)	30°	225°
A-06- (2)	30°	15°	D-06- (2)	30°	195°
A-07- (1)	30°	45°	D-07- (1)	30°	225°
A-07- (2-7)	30°	15°	D-07- (2-7)	30°	195°
A-08- (1-7)	30°	45°	D-08- (1-7)	30°	225°
A-10- (1-4)	30°	345°	D-10- (1-4)	30°	165°
A-10- (5, 7, 8)	30°	15°	D-10- (5, 7, 8)	30°	195°
A-10- (6)	30°	45°	D-10- (6)	30°	225°
B-01- (1-7)	30°	75°	E-01- (1-7)	30°	255°
B-02- (1, 7)	30°	75°	E-02- (1, 7)	30°	255°
B-02- (2-6)	30°	45°	E-02- (2-6)	30°	225°
B-03- (1-7)	30°	75°	E-03- (1-7)	30°	255°
B-04- (1, 2)	30°	75°	E-04- (1, 2)	30°	255°
B-04- (3-7)	30°	45°	E-04- (3-7)	30°	225°
B-05- (1, 2, 3, 6, 7)	30°	75°	E-05- (1, 2, 3, 6, 7)	30°	255°
B-05- (4, 5)	30°	105°	E-05- (4, 5)	30°	285°
B-06- (1, 3-7)	30°	105°	E-06- (1, 3-7)	30°	285°
B-06- (2)	30°	75°	E-06- (2)	30°	255°
B-07- (1)	30°	105°	E-07- (1)	30°	285°
B-07- (2-7)	30°	75°	E-07- (2-7)	30°	255°
B-08- (1-7)	30°	105°	E-08- (1-7)	30°	285°
B-10- (1-4)	30°	45°	E-10- (1-4)	30°	225°
B-10- (5, 7, 8)	30°	75°	E-10- (5, 7, 8)	30°	255°
B-10- (6)	30°	105°	E-10- (6)	30°	285°
C-01- (1-7)	30°	135°	F-01- (1-7)	30°	315°
C-02- (1, 7)	30°	135°	F-02- (1, 7)	30°	315°
C-02- (2-6)	30°	105°	F-02- (2-6)	30°	285°
C-03- (1-7)	30°	135°	F-03- (1-7)	30°	315°
C-04- (1, 2)	30°	135°	F-04- (1, 2)	30°	315°
C-04- (3-7)	30°	105°	F-04- (3-7)	30°	285°
C-05- (1, 2, 3, 6, 7)	30°	135°	F-05- (1, 2, 3, 6, 7)	30°	315°
C-05- (4, 5)	30°	165°	F-05- (4, 5)	30°	345°
C-06- (1, 3- 7)	30°	165°	F-06- (1, 3-7)	30°	345°
C-06- (2)	30°	135°	F-06- (2)	30°	315°
C-07- (1)	30°	165°	F-07- (1)	30°	345°
C-07- (2-7)	30°	135°	F-07- (2-7)	30°	315°
C-08- (1-7)	30°	165°	F-08- (1-7)	30°	345°
C-10- (1-4)	30°	105°	F-10- (1-4)	30°	315°
C-10- (5, 7, 8)	30°	135°	F-10- (5, 7, 8)	30°	315°
C-10- (6)	30°	165°	F-10- (6)	30°	345°

Table A.6. Zenith (θ) and azimuth (ϕ) angles for the MAARSY array divided into 12 slices and 384 antennas selected.

Subarray (antenna)	θ°	ϕ°	Subarray (antenna)	θ°	ϕ°
A-01- (1-7)	30°	15°	D-01- (1-7)	30°	195°
A-02- (1, 7)	30°	15°	D-02- (1, 7)	30°	195°
A-02- (2-6)	30°	345°	D-02- (2-6)	30°	165°
A-03- (1-7)	30°	15°	D-03- (1-7)	30°	195°
A-04- (4, 5)	30°	345°	D-04- (4, 5)	30°	165°
A-06- (1, 3-7)	30°	45°	D-06- (1, 3-7)	30°	225°
A-06- (2)	30°	15°	D-06- (2)	30°	195°
A-07- (1)	30°	45°	D-07- (1)	30°	225°
A-07- (2-7)	30°	15°	D-07- (2-7)	30°	195°
A-08- (1-7)	30°	45°	D-08- (1-7)	30°	225°
A-10- (1-4)	30°	345°	D-10- (1-4)	30°	165°
A-10- (5, 7, 8)	30°	15°	D-10- (5, 7, 8)	30°	195°
A-10- (6)	30°	45°	D-10- (6)	30°	225°
B-01- (1-7)	30°	75°	E-01- (1-7)	30°	255°
B-02- (1, 7)	30°	75°	E-02- (1, 7)	30°	255°
B-02- (2-6)	30°	45°	E-02- (2-6)	30°	225°
B-03- (1-7)	30°	75°	E-03- (1-7)	30°	255°
B-04- (4, 5)	30°	45°	E-04- (4, 5)	30°	225°
B-06- (1, 3-7)	30°	105°	E-06- (1, 3-7)	30°	285°
B-06- (2)	30°	75°	E-06- (2)	30°	255°
B-07- (1)	30°	105°	E-07- (1)	30°	285°
B-07- (2-7)	30°	75°	E-07- (2-7)	30°	255°
B-08- (1-7)	30°	105°	E-08- (1-7)	30°	285°
B-10- (1-4)	30°	45°	E-10- (1-4)	30°	225°
B-10- (5, 7, 8)	30°	75°	E-10- (5, 7, 8)	30°	255°
B-10- (6)	30°	105°	E-10- (6)	30°	285°
C-01- (1-7)	30°	135°	F-01- (1-7)	30°	315°
C-02- (1, 7)	30°	135°	F-02- (1, 7)	30°	315°
C-02- (2-6)	30°	105°	F-02- (2-6)	30°	285°
C-03- (1-7)	30°	135°	F-03- (1-7)	30°	315°
C-04- (4, 5)	30°	105°	F-04- (4, 5)	30°	285°
C-06- (1, 3- 7)	30°	165°	F-06- (1, 3-7)	30°	345°
C-06- (2)	30°	135°	F-06- (2)	30°	315°
C-07- (1)	30°	165°	F-07- (1)	30°	345°
C-07- (2-7)	30°	135°	F-07- (2-7)	30°	315°
C-08- (1-7)	30°	165°	F-08- (1-7)	30°	345°
C-10- (1-4)	30°	105°	F-10- (1-4)	30°	315°
C-10- (5, 7, 8)	30°	135°	F-10- (5, 7, 8)	30°	315°
C-10- (6)	30°	165°	F-10- (6)	30°	345°

Table A.7. Zenith (θ) and azimuth (ϕ) angles for the MAARSY array divided into 12 slices and 312 antennas selected.

Subarray (antenna)	θ°	ϕ°	Subarray (antenna)	θ°	ϕ°
A-01- (1-7)	30°	15°	D-01- (1-7)	30°	195°
A-02- (1)	30°	15°	D-02- (1)	30°	195°
A-02- (2-5)	30°	345°	D-02- (2-5)	30°	165°
A-03- (1, 6, 7)	30°	15°	D-03- (1, 6, 7)	30°	195°
A-06- (1, 7)	30°	45°	D-06- (1, 7)	30°	225°
A-07- (1)	30°	45°	D-07- (1)	30°	225°
A-07- (2-7)	30°	15°	D-07- (2-7)	30°	195°
A-08- (1-7)	30°	45°	D-08- (1-7)	30°	225°
A-10- (1-4)	30°	345°	D-10- (1-4)	30°	165°
A-10- (5, 7, 8)	30°	15°	D-10- (5, 7, 8)	30°	195°
A-10- (6)	30°	45°	D-10- (6)	30°	225°
B-01- (1-7)	30°	75°	E-01- (1-7)	30°	255°
B-02- (1)	30°	75°	E-02- (1)	30°	255°
B-02- (2-5)	30°	45°	E-02- (2-5)	30°	225°
B-03- (1, 6, 7)	30°	75°	E-03- (1, 6, 7)	30°	255°
B-06- (1, 7)	30°	105°	E-06- (1, 7)	30°	285°
B-07- (1)	30°	105°	E-07- (1)	30°	285°
B-07- (2-7)	30°	75°	E-07- (2-7)	30°	255°
B-08- (1-7)	30°	105°	E-08- (1-7)	30°	285°
B-10- (1-4)	30°	45°	E-10- (1-4)	30°	225°
B-10- (5, 7, 8)	30°	75°	E-10- (5, 7, 8)	30°	255°
B-10- (6)	30°	105°	E-10- (6)	30°	285°
C-01- (1-7)	30°	135°	F-01- (1-7)	30°	315°
C-02- (1)	30°	135°	F-02- (1)	30°	315°
C-02- (2-5)	30°	105°	F-02- (2-5)	30°	285°
C-03- (1, 6, 7)	30°	135°	F-03- (1, 6, 7)	30°	315°
C-06- (1, 7)	30°	165°	F-06- (1, 7)	30°	345°
C-07- (1)	30°	165°	F-07- (1)	30°	345°
C-07- (2-7)	30°	135°	F-07- (2-7)	30°	315°
C-08- (1-7)	30°	165°	F-08- (1-7)	30°	345°
C-10- (1-4)	30°	105°	F-10- (1-4)	30°	315°
C-10- (5, 7, 8)	30°	135°	F-10- (5, 7, 8)	30°	315°
C-10- (6)	30°	165°	F-10- (6)	30°	345°

Table A.8. Zenith (θ) and azimuth (ϕ) angles for the MAARSY array divided into 12 slices and 234 antennas selected.

Subarray (antenna)	θ°	ϕ°	Subarray (antenna)	θ°	ϕ°
A-01- (1-7)	30°	15°	D-01- (1-7)	30°	195°
A-02- (1)	30°	15°	D-02- (1)	30°	195°
A-02- (2, 4)	30°	345°	D-02- (2, 4)	30°	165°
A-02- (3, 5, 6)	20°	345°	D-02- (3, 5, 6)	20°	165°
A-02- (7)	20°	15°	D-02- (7)	20°	195°
A-03- (1-7)	20°	15°	D-03- (1-7)	20°	195°
A-04- (1, 2)	20°	15°	D-04- (1, 2)	20°	195°
A-04- (3-7)	20°	345°	D-04- (3-7)	20°	165°
A-05- (1, 2, 3, 6, 7)	20°	15°	D-05- (1, 2, 3, 6, 7)	20°	195°
A-05- (4, 5)	20°	45°	D-05- (4, 5)	20°	225°
A-06- (1, 3-7)	20°	45°	D-06- (1, 3-7)	20°	225°
A-06- (2)	20°	15°	D-06- (2)	20°	195°
A-07- (1)	30°	45°	D-07- (1)	30°	225°
A-07- (2-7)	30°	15°	D-07- (2-7)	30°	195°
A-08- (1-7)	30°	45°	D-08- (1-7)	30°	225°
A-10- (1-4)	30°	345°	D-10- (1-4)	30°	165°
A-10- (5, 7, 8)	30°	15°	D-10- (5, 7, 8)	30°	195°
A-10- (6)	30°	45°	D-10- (6)	30°	225°
B-01- (1-7)	30°	75°	E-01- (1-7)	30°	255°
B-02- (1)	30°	75°	E-02- (1)	30°	255°
B-02- (2, 4)	30°	45°	E-02- (2, 4)	30°	225°
B-02- (3, 5, 6)	20°	45°	E-02- (3, 5, 6)	20°	225°
B-02- (7)	20°	75°	E-02- (7)	20°	255°
B-03- (1-7)	20°	75°	E-03- (1-7)	20°	255°
B-04- (1, 2)	20°	75°	E-04- (1, 2)	20°	255°
B-04- (3-7)	20°	45°	E-04- (3-7)	20°	225°
B-05- (1, 2, 3, 6, 7)	20°	75°	E-05- (1, 2, 3, 6, 7)	20°	255°
B-05- (4, 5)	20°	105°	E-05- (4, 5)	20°	285°
B-06- (1, 3-7)	20°	105°	E-06- (1, 3-7)	20°	285°
B-06- (2)	20°	75°	E-06- (2)	20°	255°
B-07- (1)	30°	105°	E-07- (1)	30°	285°
B-07- (2-7)	30°	75°	E-07- (2-7)	30°	255°
B-08- (1-7)	30°	105°	E-08- (1-7)	30°	285°
B-10- (1-4)	30°	45°	E-10- (1-4)	30°	225°
B-10- (5, 7, 8)	30°	75°	E-10- (5, 7, 8)	30°	255°
B-10- (6)	30°	105°	E-10- (6)	30°	285°
C-01- (1-7)	30°	135°	F-01- (1-7)	30°	315°
C-02- (1)	30°	135°	F-02- (1)	30°	315°
C-02- (2, 4)	30°	105°	F-02- (2, 4)	30°	285°
C-02- (3, 5, 6)	20°	105°	F-02- (3, 5, 6)	20°	285°
C-02- (7)	20°	135°	F-02- (7)	20°	315°
C-03- (1-7)	20°	135°	F-03- (1-7)	20°	315°
C-04- (1, 2)	20°	135°	F-04- (1, 2)	20°	315°
C-04- (3-7)	20°	105°	F-04- (3-7)	20°	285°
C-05- (1, 2, 3, 6, 7)	20°	135°	F-05- (1, 2, 3, 6, 7)	20°	315°
C-05- (4, 5)	20°	165°	F-05- (4, 5)	20°	345°
C-06- (1, 3- 7)	20°	165°	F-06- (1, 3-7)	20°	345°
C-06- (2)	20°	135°	F-06- (2)	20°	315°
C-07- (1)	30°	165°	F-07- (1)	30°	345°
C-07- (2-7)	30°	135°	F-07- (2-7)	30°	315°
C-08- (1-7)	30°	165°	F-08- (1-7)	30°	345°
C-10- (1-4)	30°	105°	F-10- (1-4)	30°	315°
C-10- (5, 7, 8)	30°	135°	F-10- (5, 7, 8)	30°	315°
C-10- (6)	30°	165°	F-10- (6)	30°	345°

Table A.9. Zenith (θ) and azimuth (ϕ) angles for the MAARSY array divided into 12 slices and 2 values of a zenith angle ($\theta_{\text{inner}}=20^\circ$, $\theta_{\text{outer}}=30^\circ$) in each slice applied.

Subarray (antenna)	θ°	ϕ°	Subarray (antenna)	θ°	ϕ°
A-01- (1-7)	35°	15°	D-01- (1-7)	35°	195°
A-02- (1)	35°	15°	D-02- (1)	35°	195°
A-02- (2, 4)	35°	345°	D-02- (2, 4)	35°	165°
A-02- (3, 5, 6)	25°	345°	D-02- (3, 5, 6)	25°	165°
A-02- (7)	25°	15°	D-02- (7)	25°	195°
A-03- (1-7)	25°	15°	D-03- (1-7)	25°	195°
A-04- (1, 2)	25°	15°	D-04- (1, 2)	25°	195°
A-04- (3-7)	25°	345°	D-04- (3-7)	25°	165°
A-05- (1, 2, 3, 6, 7)	25°	15°	D-05- (1, 2, 3, 6, 7)	25°	195°
A-05- (4, 5)	25°	45°	D-05- (4, 5)	25°	225°
A-06- (1, 3-7)	25°	45°	D-06- (1, 3-7)	25°	225°
A-06- (2)	25°	15°	D-06- (2)	25°	195°
A-07- (1)	35°	45°	D-07- (1)	35°	225°
A-07- (2-7)	35°	15°	D-07- (2-7)	35°	195°
A-08- (1-7)	35°	45°	D-08- (1-7)	35°	225°
A-10- (1-4)	35°	345°	D-10- (1-4)	35°	165°
A-10- (5, 7, 8)	35°	15°	D-10- (5, 7, 8)	35°	195°
A-10- (6)	35°	45°	D-10- (6)	35°	225°
B-01- (1-7)	35°	75°	E-01- (1-7)	35°	255°
B-02- (1)	35°	75°	E-02- (1)	35°	255°
B-02- (2, 4)	35°	45°	E-02- (2, 4)	35°	225°
B-02- (3, 5, 6)	25°	45°	E-02- (3, 5, 6)	25°	225°
B-02- (7)	25°	75°	E-02- (7)	25°	255°
B-03- (1-7)	25°	75°	E-03- (1-7)	25°	255°
B-04- (1, 2)	25°	75°	E-04- (1, 2)	25°	255°
B-04- (3-7)	25°	45°	E-04- (3-7)	25°	225°
B-05- (1, 2, 3, 6, 7)	25°	75°	E-05- (1, 2, 3, 6, 7)	25°	255°
B-05- (4, 5)	25°	105°	E-05- (4, 5)	25°	285°
B-06- (1, 3-7)	25°	105°	E-06- (1, 3-7)	25°	285°
B-06- (2)	25°	75°	E-06- (2)	25°	255°
B-07- (1)	35°	105°	E-07- (1)	35°	285°
B-07- (2-7)	35°	75°	E-07- (2-7)	35°	255°
B-08- (1-7)	35°	105°	E-08- (1-7)	35°	285°
B-10- (1-4)	35°	45°	E-10- (1-4)	35°	225°
B-10- (5, 7, 8)	35°	75°	E-10- (5, 7, 8)	35°	255°
B-10- (6)	35°	105°	E-10- (6)	35°	285°
C-01- (1-7)	35°	135°	F-01- (1-7)	35°	315°
C-02- (1)	35°	135°	F-02- (1)	35°	315°
C-02- (2, 4)	35°	105°	F-02- (2, 4)	35°	285°
C-02- (3, 5, 6)	25°	105°	F-02- (3, 5, 6)	25°	285°
C-02- (7)	25°	135°	F-02- (7)	25°	315°
C-03- (1-7)	25°	135°	F-03- (1-7)	25°	315°
C-04- (1, 2)	25°	135°	F-04- (1, 2)	25°	315°
C-04- (3-7)	25°	105°	F-04- (3-7)	25°	285°
C-05- (1, 2, 3, 6, 7)	25°	135°	F-05- (1, 2, 3, 6, 7)	25°	315°
C-05- (4, 5)	25°	165°	F-05- (4, 5)	25°	345°
C-06- (1, 3-7)	25°	165°	F-06- (1, 3-7)	25°	345°
C-06- (2)	25°	135°	F-06- (2)	25°	315°
C-07- (1)	35°	165°	F-07- (1)	35°	345°
C-07- (2-7)	35°	135°	F-07- (2-7)	35°	315°
C-08- (1-7)	35°	165°	F-08- (1-7)	35°	345°
C-10- (1-4)	35°	105°	F-10- (1-4)	35°	315°
C-10- (5, 7, 8)	35°	135°	F-10- (5, 7, 8)	35°	315°
C-10- (6)	35°	165°	F-10- (6)	35°	345°

Table A.10. Zenith (θ) and azimuth (ϕ) angles for the MAARSY array divided into 12 slices and 2 values of a zenith angle ($\theta_{\text{inner}}=25^\circ$, $\theta_{\text{outer}}=35^\circ$) in each slice applied.

Subarray (antenna)	θ°	ϕ°	Subarray (antenna)	θ°	ϕ°
A-02- (6, 7)	30°	330°	B-04- (1)	30°	150°
A-03- (1-7)	30°	330°	B-04- (2, 3, 4, 5, 7)	30°	90°
A-04- (1-5)	30°	330°	B-04- (6)	30°	30°
A-04- (6, 7)	30°	270°	B-05- (1-7)	30°	150°
A-05- (1, 2)	30°	270°	B-06- (2, 4, 5)	30°	150°
A-05- (3, 4, 6, 7)	30°	330°	B-09- (1)	30°	150°
A-05- (5)	30°	30°	B-09- (2, 3, 5, 6, 7)	30°	210°
A-06- (1-7)	30°	30°	B-09- (4)	30°	270°
A-07- (1, 3, 6, 7)	30°	30°	C-04- (6, 7)	30°	150°
A-08- (1-4)	30°	30°	C-09- (1, 2)	30°	150°
A-09- (1-7)	30°	270°	C-09- (3-7)	30°	210°
B-01- (1, 7)	30°	90°	D-09- (5)	30°	210°
B-02- (1, 2, 3, 6, 7)	30°	90°	F-05- (2, 4)	30°	270°
B-02- (4, 5)	30°	30°	F-09- (5-7)	30°	270°
B-03- (1, 2, 3, 4, 6, 7)	30°	90°	F-11- (1-7)	30°	210°
B-03- (5)	30°	150°	-----	-----	-----

Table A.11. Zenith (θ) and azimuth (ϕ) angles for the actual state of the MAARSY radar with 6 main beams generated.

Subarray (antenna)	θ°	ϕ°	Subarray (antenna)	θ°	ϕ°
A-02- (6)	30°	300°	B-04- (1)	30°	140°
A-02- (7)	30°	340°	B-04- (2, 3, 4, 7)	30°	100°
A-03- (1-7)	30°	340°	B-04- (5, 6)	30°	60°
A-04- (1-7)	30°	300°	B-05- (1, 3, 4, 5, 6, 7)	30°	140°
A-05- (1, 2)	30°	300°	B-05- (2)	30°	180°
A-05- (3, 4, 6, 7)	30°	340°	B-06- (2, 4, 5)	30°	140°
A-05- (5)	30°	20°	B-09- (1, 7)	30°	180°
A-06- (1, 2, 3, 4, 5, 7)	30°	20°	B-09- (2, 3, 5, 6)	30°	220°
A-06- (6)	30°	60°	B-09- (4)	30°	260°
A-07- (1, 3, 6, 7)	30°	20°	C-04- (6)	30°	140°
A-08- (1, 3)	30°	20°	C-04- (7)	30°	180°
A-08- (2, 4)	30°	60°	C-09- (1-7)	30°	180°
A-09- (1)	30°	300°	D-09- (5)	30°	220°
A-09- (2-7)	30°	260°	F-05- (2)	30°	260°
B-01- (1)	30°	100°	F-05- (4)	30°	300°
B-01- (7)	30°	60°	F-09- (5-7)	30°	260°
B-02- (1-7)	30°	60°	F-11- (1-7)	30°	220°
B-03- (1-7)	30°	100°	-----	-----	-----

Table A.12. Zenith (θ) and azimuth (ϕ) angles for the actual state of the MAARSY radar with 9 main beams generated.

Acknowledgements

At first I wish to thank M.Sc.-Ing. Toralf Renkwitz from the Leibniz-Institute of Atmospheric Physics e.V. at University of Rostock (IAP) under whose supervision this work was written, for his assistance and many fruitful suggestions about various aspects of this thesis, for many conversations and devoted time.

Not less thanks are spread to the other supervisors of this thesis: Dr inż. Krzysztof Oprzędkiewicz (SHVS Tarnów), Prof. Dr.-Ing. habil. Andreas Ahrens (HS Wismar) and Dr.-Ing. Ralph Latteck (IAP) for all their contribution.

Furthermore my thanks are directed to Professors, Doctors and Masters from the State Higher Vocational School in Tarnów, who have been teaching me for the last four years, for passing me the priceless knowledge on.

Great thanks to the people from the IAP who contributed to a possibility of having my practice in this Institute and for providing me this interesting and challenging subject for my Diploma thesis and giving me the opportunity to take part in such an amazing project as the extension of the MAARSY radar to a meteor observation mode.

Additionally I wish to thank people who made my participation in the student exchange program possible, especially the heads of International Offices of Tarnów and Wismar Universities: Dr inż. Agnieszka Lisowska-Lis and Mrs Korinna Stubbe.

Special thank goes to Dr Gabriele Sauerbier for her valuable advices and coordination of student exchange program.

Last but not least of course special thanks to my family and my girlfriend for their permanent support.

Declaration of Authorship

I certify that the presented work is, to the best of my knowledge and belief, original and the result of my own investigations, except as acknowledged and has not been submitted, either in part or whole, for a degree at any University.

Kühlungsborn, 18th June 2010

Rafał Gancarz